Distribution Agreement

In presenting this thesis or dissertation as a partial fulfillment of the requirements for an advanced degree from Emory University, I hereby grant to Emory University and its agents the non-exclusive license to archive, make accessible, and display my thesis or dissertation in whole or in part in all forms of media, now or hereafter known, including display on the world wide web. I understand that I may select some access restrictions as part of the online submission of this thesis or dissertation. I retain all ownership rights to the copyright of the thesis or dissertation. I also retain the right to use in future works (such as articles or books) all or part of this thesis or dissertation.

Signature: _____ _____

Ailing Yu Date

Developing Transition Metal Catalysts that Incorporate Redox-Active Ligand Frameworks for Sustainable Catalysis

By

Ailing Yu
Doctor of Philosophy

Chemistry

_____

Cora E. MacBeth, Ph.D.
Advisor

_____

Craig L. Hill, Ph.D.
Committee Member

_____

Vincent Conticello, Ph.D.
Committee Member

Accepted

_____

Kimberly Jacob Arriola, Ph.D, MPH
Dean of the James T. Laney School of Graduate Studies

_____

Date

Developing Transition Metal Catalysts that Incorporate Redox-Active Ligand Frameworks for Sustainable Catalysis

By

Ailing Yu
B.S., Lanzhou University, 2018

Advisor: Cora E. MacBeth, Ph.D.

An abstract of
A dissertation submitted to the Faculty of the
James T. Laney School of Graduate Studies of Emory University
in partial fulfillment of the requirements for the degree of
Doctor of Philosophy
in Chemistry
2023

Abstract

Developing Transition Metal Catalysts that Incorporate Redox-Active Ligand Frameworks for Sustainable Catalysis

By

Ailing Yu

Transition metal catalysis has been an essential pillar of modern organic synthesis. Traditionally, the primary focus has been on using expensive noble metal catalysts since they tend to undergo multi-electron transformations. Recently, the more sustainable first-row transition metal catalysts attracted wide attention with the development of redox-active ligands that can function as electron reservoirs to facilitate multi-electron reactions.

We aim to develop sustainable catalysts that incorporate redox-active ligands with first-row transition metals and use dioxygen as the green oxidant for environmentally benign chemical transformations. In Chapter 2, the design, syntheses, and characterizations of two novel redox-active ligands will be described. These ligands contain a multi-dentate nitrogenous moiety and catechol moieties, allowing more coordinative versatility and electronic tunability of corresponding metal complexes. The catalytic properties of the two resulting Cu complexes, a cobalt cluster, and an iron cluster were investigated by X-ray crystallography, cyclic voltammetry, and UV-vis spectroscopy. Chapter 3 discusses the design, syntheses, and characterizations of terminal alkyne modified redox-active ligands for application in flow chemistry. Cobalt complexes with these newly synthesized ligands were obtained and used in cyclic voltammetry studies, UV-vis spectroscopy, O-atom transfer reaction, and aerobic hydrazone oxidation.

Developing Transition Metal Catalysts that Incorporate Redox-Active Ligand Frameworks for Sustainable Catalysis

By

Ailing Yu
B.S., Lanzhou University, 2018

Advisor: Cora E. MacBeth, Ph.D.

A dissertation submitted to the Faculty of the
James T. Laney School of Graduate Studies of Emory University
in partial fulfillment of the requirements for the degree of
Doctor of Philosophy
in Chemistry
2023

Acknowledgments

Throughout my five years at Emory University, I am deeply grateful for the help, support, and care from my advisor, professors, lab mates, friends, and family members. They have been my pillars of strength, guiding me through challenging times and cheering for each milestone achieved.

First and foremost, I extend my heartfelt appreciation to my advisor, Dr. Cora MacBeth. Her guidance, encouragement, and support have been instrumental in shaping my academic journey and personal growth. I am immensely thankful for her generous sharing of research expertise, life and career experiences, which have contributed significantly to my development. I would also like to thank my committee members, Dr. Craig Hill, and Dr. Vincent Conticello, for their invaluable feedback and suggestions during my graduate journey. In addition, I would like to thank Dr. John Bacsa for his help in solving all the X-ray crystal structures in my Ph.D. studies. His efforts and patience in solving the disordered systems are greatly appreciated.

My journey would not have been as fulfilling without the support of my lab mates and friends from the MacBeth Group: Dr. Dan Liu, Dr. Elaine Liu, Annabel Zhang, Yiran Zhang, Vico Wang, and Joseph Kim. It is my pleasure to work with these wonderful individuals, and I enjoyed our time together both in and outside the lab. Dr. Dan Liu and Dr. Elaine Liu mentored me when I first joined the group in 2018, and I want to thank them for their mentorship which has left a lasting positive impact on me. I extend my best wishes to Annabel Zhang, Yiran Zhang, Vico Wang, and Joseph Kim as they continue their future journeys. Their contributions to my Ph.D. experience have been invaluable.

I am also grateful to my colleagues outside of the MacBeth group. Many thanks to Dr. Michael Hollerbach and Ethan Heyboer from Dr. Simon Blakey's group and Jasper Luo and Ziyi Chen from Dr. Huw Davies' group, for their assistance with auto column operations.

To my friends at Emory University who may not have been directly involved in my research projects—Ruoxing Li, Yiting Zhang, Ting Cheng, Sheng He, Zhicheng Yang, Kristin Shimabukuro, Duc Ly, and many more —I extend my heartfelt thanks for their support throughout my Ph.D. journey. To my friends outside of Emory University, Shuhan Yang and Siping Zhang, I am deeply grateful for having them as my friends. Their care and support helped me stay positive, persevering, and courageous throughout my Ph.D. journey.

Last but not least, I want to thank my family members, who always provided me with unconditional mental and physical support. Although I have not been able to meet them in person for the past five years due to the pandemic, I know they are always there for me. I am deeply grateful for their continuous support. My journey towards earning a Ph.D. would not have been possible without them.

Table of Contents

List of Figures

List of Schemes

List of Tables

1. Chapter 1: History and Introduction of Redox-Active Ligands and Their Role in Facilitating Chemical Reactions with First-Row Transition Metals

Introduction

Metal-based catalysis is an integral aspect of modern life. For example, the Harbor-Bosch process made ammonia fertilizer widely available, which significantly advanced modern agriculture. This method achieved large-scale ammonia production through artificial nitrogen fixation using hydrogen and nitrogen gas and an iron catalyst. Another example of metal-based catalysis in our daily life is the catalytic converters for automobiles. This device converts toxic gas and pollutants including hydrocarbons, carbon monoxide, and nitrogen oxides into less harmful pollutants through reduction and oxidation reactions catalyzed by palladium, platinum, or rhodium. The utilization of catalysts can help facilitate these desirable chemical transformations. However, traditional catalyst design often utilize expensive noble metals such as second and third-row transition metals.[1] For example, Pd-catalyzed cross-coupling reactions have been widely used in industrial applications to synthesize potential or existing drug candidates.[2] While powerful, catalysis using these noble transition metals comes with several limitations, including limited natural abundance, high cost, and specific toxicity. These limitations of noble transition metal catalysts have led to an extensive search for more sustainable, cost-effective catalysts.

First-row transition metals present a promising alternative for being less expensive, more earth-abundant, and environmentally benign. These properties have led to an increase in the number of researchers trying to incorporate first-row transition metals in catalyst design.

Despite these attractive properties, one limitation in these systems is that the first-row transition metal complexes tend to undergo one-electron redox events rather than the two-electron processes necessary for various synthetically relevant catalytic conversions, including oxidative addition, reductive elimination, and atom transfer reactions. Fortunately, nature has provided one possible solution by incorporating redox-active ligands with first-row transition metals for the successful catalysis of multi-electron reactions. Inspired by nature, researchers have focused on developing first-row transition metal complexes that incorporate redox-active ligands to facilitate multi-electron reactions. This approach imparts noble-metal characters to more abundant, less toxic first-row transition metals such as Fe, Co, Ni, Cu, and Zn in the multi-electron reactions.[1]

Redox-active ligands in nature

The power of incorporating redox-active moieties with first-row transition metals has long been demonstrated in nature. Because many important biological transformations are multi-electron processes, redox-active moieties have been incorporated with cheap, earth-abundant first-row transition metals to facilitate such redox events. Some biological enzymes such as galactose oxidase, ribonucleotide reductase, cytochrome *c* oxidase, glyoxal oxidase, and catechol dioxygenase incorporate first-row transition metal catalysts supported by redox-active ligands. Facilitated by these redox-active ligands, these enzymes can achieve multi-electron reactions by distributing redox-events over multiple redox-active centers.

Galactose oxidase (GO) is a copper-containing enzyme that catalyzes the oxidation of primary alcohols to the corresponding aldehydes.[3] At its core, GO contains a novel redox-active site comprised of a copper ion coordinated with four amino acid residues, including

two histidines, two tyrosines, and a solvent molecule which can later be replaced by the substrate.[4] GO can exist in three distinct oxidation states: (a) Cu(II) coordinated with a tyrosyl radical, which is the catalytically active species, (b) Cu(II) with a tyrosine, (c) Cu(I) with a tyrosine.[5] Extensive spectroscopic and X-ray crystal studies suggested a proposed mechanism for the two-electron oxidation reaction as shown in Scheme 1-1.[6-8] The free radical on Tyr272 in the copper active site is stabilized through delocalization by the aromatic ring of the tyrosine and the cross-linked cysteine sulfur. This tyrosine 272 residue functions as the redox-active ligand in GO enzyme and facilitates the electron transfer during the oxidation reaction, allowing the conversion of galactose to galactose-1-aldehyde.

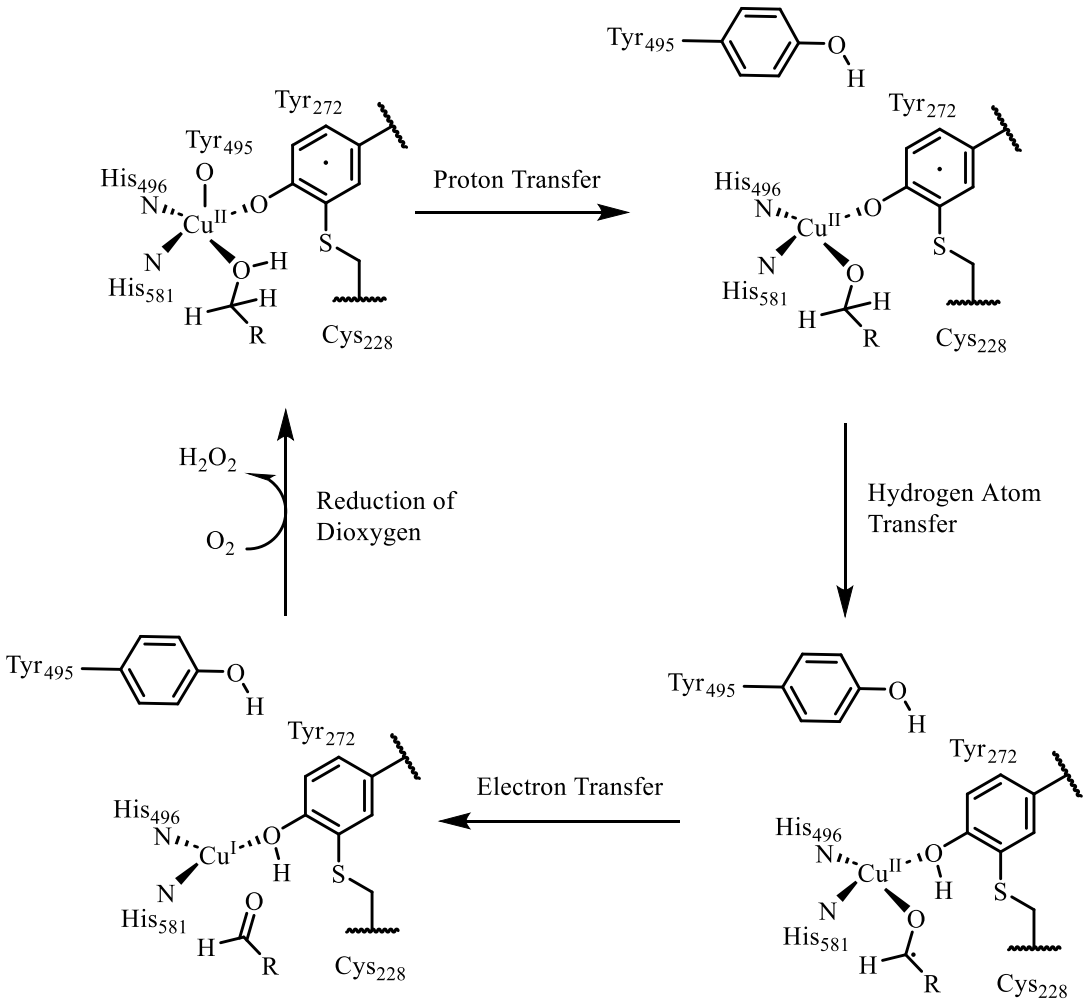

Scheme 1-1. Mechanism proposed for galactose oxidase catalyzed oxidation reaction.[6-8]

Ribonucleotide reductase found in humans and bacteria utilizes a diiron-tyrosyl radical cofactor to promote multi-electron reactions at the first-row transition metal site (Figure 1-1). Ribonucleotide reductase (RNR) is essential for the conversion of ribonucleotides into deoxyribonucleotides, the building blocks of DNA (Scheme 1-2).[9] Studies showed that the tyrosyl radical is critical for the enzymatic activities and is stabilized by an adjacent binuclear iron center.[9,10]

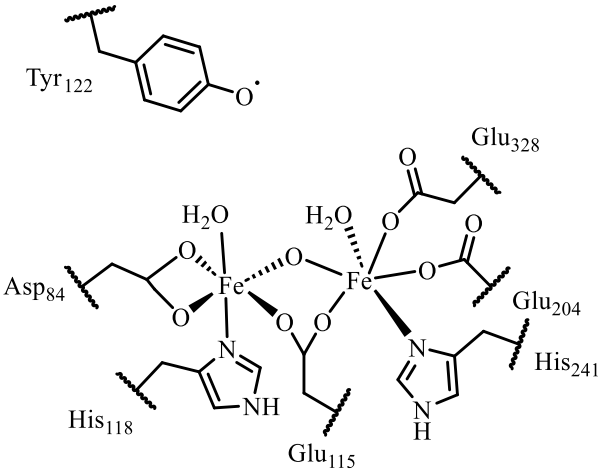

Figure 1-1. Ribonucleotide reductase.

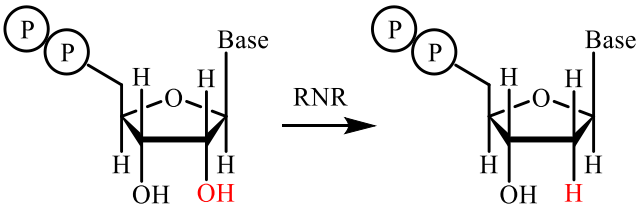

ribonucleotide deoxyribonucleotide

Scheme 1-2. Ribonucleotide reductase catalyzed reduction of ribonucleotide to deoxyribonucleotide.

Another example of enzyme that incorporates redox-active ligand with first row transition metal is cytochrome *c* oxidase (C*c*O). Cytochrome *c* oxidase is a key respiratory enzyme that reduces oxygen to water and stores the energy released from the reaction with a bimetallic Cu-Fe system in the active site (Figure 1-2).[11-13] The porphyrin ligand in the C*c*O

enzyme helps facilitate multi-electron reactions at its first-row transition metal center. The extensive π-network in the porphyrin ligand allows the delocalization of the electrons and thus stabilizes the ligand radical.[14,15]

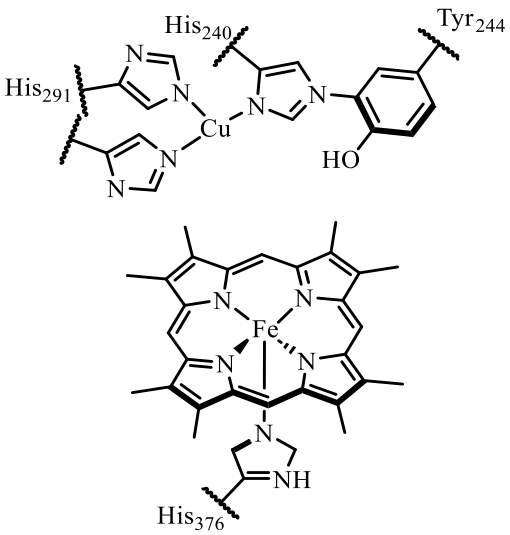

Figure 1-2. Cytochrome *c* oxidase.

The redox-active moieties in these enzymes help store and mediate electron transfer as well as promote multi-electron catalytic reactions. Inspired by these naturally occurring enzymes, researchers have been developing redox-active ligand systems to advance first-row transition metals in multi-electron catalysis.

Development of redox-active ligands

The concept of redox innocent and non-innocent ligands was first introduced by Jørgensen in 1966.[16] Redox non-innocent or redox-active ligands can accept or donate electrons and actively participate in electron transfer reactions, thus having received special attention. In the system where the metal center is coordinated with a redox-active ligand, the frontier molecular orbitals, HOMO (highest occupied molecular orbitals) and LUMO (lowest unoccupied molecular orbitals) of the metal center, are similar in energy to the frontier

molecular orbitals of the ligand to which they coordinate. This similarity in energy allows the electron transfer to not only occur solely on the ligands or metal centers, but synergistically between the redox-active ligands and the metal centers as well. The redox-active ligands coordinated with first-row transition metals function as electron reservoirs and allow more possible redox events in the metal complexes, thus expanding their utilization in multi-electron catalysis. The incorporation of redox-active ligands in the metal complexes is a powerful strategy to overcome the inherent electronic limitation of first-row transition metals for multi-electron catalysis. Therefore, the development of redox-active ligands and their metal complexes for catalysis was and continues to be the focus of many research efforts. [17-22]

Dithiolene ligands

The initial studies of redox-active ligands trace back to more than half a century ago. In 1962, Schrauzer and Mayweg first synthesized complex **1-1** by reacting nickel sulfides with diphenylacetylene.[23] They reported that only one signal was observed in the proton magnetic resonance spectrum, suggesting a square planar geometry around the nickel center. The charge of the nickel complex **1-1** and dithiobenzil ligand **1-2** are both zero, suggesting a formal Ni^0 oxidation state; however, magnetic measurements and spectroscopic evidence suggested a Ni^{II} center.[23] This in turn, implies that each ligand **1-2** was reduced by one electron, forming the Ni^{II} neutral complex.[24]

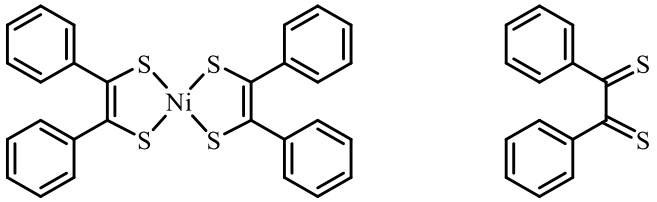

1-1 **1-2**

Figure 1-3. Nickel complex **1-1** and dithiobenzil ligand **1-2.**

In 1962, the Gray group synthesized and studied a series of complexes M^{2+}, which coordinated to modified dithiolene ligands (maleonitriledithiolate ligands).[25] The bis-ligated complexes $M(MNT)_2^{2-}$ (M= Ni^{II}, Cu^{II}, Co^{II}, Pd^{II}, Pt^{II}) were found to be in square planar geometry as supported by X-ray powder diffractometry and magnetic susceptibility measurements. In the following year, the Gray group reported another series of complexes M^{+}, with toluene 3,4-dithiolate ligand coordination.[26] The magnetic susceptibility data and electronic spectra suggested that the complexes are planar and are composed of metal centers with +1 oxidation state and two dithiolate mono-radical anion moieties.[26]

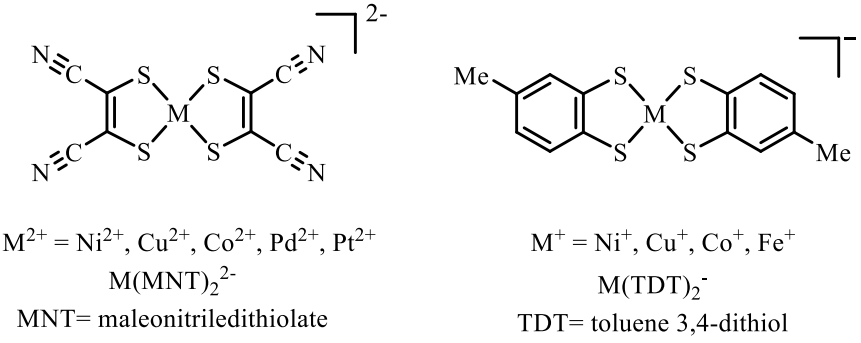

M^{2+} = Ni^{2+}, Cu^{2+}, Co^{2+}, Pd^{2+}, Pt^{2+}
$M(MNT)_2^{2-}$
MNT= maleonitriledithiolate

M^{+} = Ni^{+}, Cu^{+}, Co^{+}, Fe^{+}
$M(TDT)_2^{-}$
TDT= toluene 3,4-dithiol

Figure 1-4. Two series of dithiolene complexes synthesized by the Gray group.

To further investigate the possible redox events in the complexes with dithiolene ligands, Davison *et al.* prepared a series of neutral complexes with dithiolene ligands, and their corresponding one-electron and two-electron reduction products were generated through electron-transfer reactions by polarography.[27] Through the studies regarding the structural, spectroscopic and electronic properties of dithiolene metal complexes, it was concluded that the redox chemistry could happen solely on the ligand, leaving the oxidation state of metal centers unchanged.[24,28] The research regarding the dithiolene complexes set the stage for the development of redox-active ligand incorporated metal complexes in multi-electron reactions.

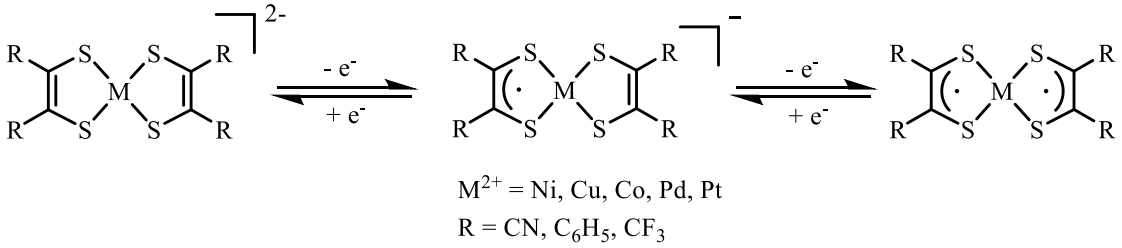

Scheme 1-3. Dithiolene complexes in three different oxidation states.

Catecholate ligands—the oxygen analogs

With the report of dithiolene ligands functioning as electron reservoirs in redox events involving metal centers, increasing interests were devoted to the development of redox-active ligands with dithiolene analogs. The *ortho*-benzoquinones (catecholate) systems, the oxygen analogs of dithiolene ligands, have received extensive attention.[29] Similar to dithiolene ligands, catecholate ligands have three potential oxidation states as shown in scheme **1-4**. The catecholate $[Cat]^{2-}$ ligand can undergo one-electron oxidation to form semiquinone $[SQ]^{-}$ ligand or undergo two-electron oxidation to form benzoquinone [BQ] ligand. The electronic tunability of the catecholate ligands provide three possible coordination modes with the metal centers (Scheme 1-4 (b)).

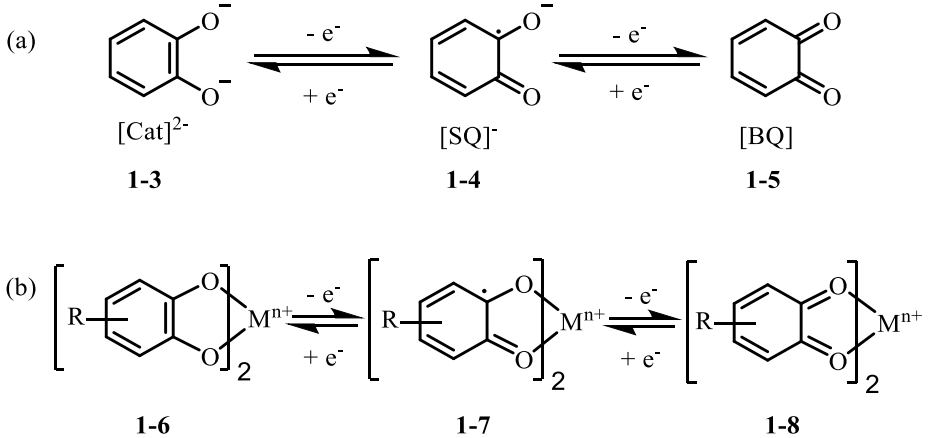

Scheme 1-4. (a) Schematic representation of three oxidation states of catecholate ligands (b) three possible binding modes of catecholate ligands involved metal complexes.

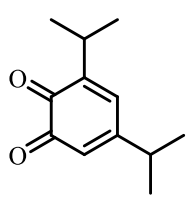

3,5-di-*t*-butylbenzoquinone

1-9

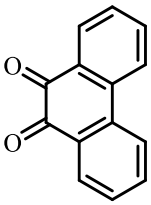

9,10-phenanthrenequinone

1-10

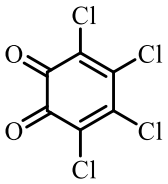

tetrachloro-1,2-benzoquinone

1-11

Figure 1-5. Three developed catecholate redox-active ligands.

Many initial studies were carried out using three catecholate ligands in their various oxidation states: 3,5-di-*t*-butylbenzoquinone, 9,10-phenanthrenequinone and tetrachloro-1,2-benzoquinone (Figure 1-5). In 1966, Holm and coworkers reported the syntheses and characterizations of a series of bis(catecholato) complexes where metal centers are Co^{II}, Ni^{II}, Cu^{II} or Zn^{II}.[30] However, this study was not able to confirm the oxidation states of the metals and ligands. In 1978, the Hendrickson group studied the structural and magnetic properties of neutral tris(semiquinone) complexes prepared with Fe and Cr (Figure 1-6).[31] The tris-chelated iron complexes had an octahedral geometry and the Mössbauer parameters suggested ferric Fe^{III} ion.[29] The magnetic moment studies assigned a S=1 ground state which aligned well with a S=5/2 metal ion interacting with three S=1/2 semiquinone ligands, affirming the $Fe^{III}(R\text{-}SQ)_3$ assignment. In the case of Cr^{III} metal ion, the spin state of the metal is 3/2. The complexes Cr^{III} $(R\text{-}SQ)_3$ were found to be diamagnetic at all temperatures, thus affirming the assignment of Cr^{III} coordinating with three S=1/2 semiquinones.

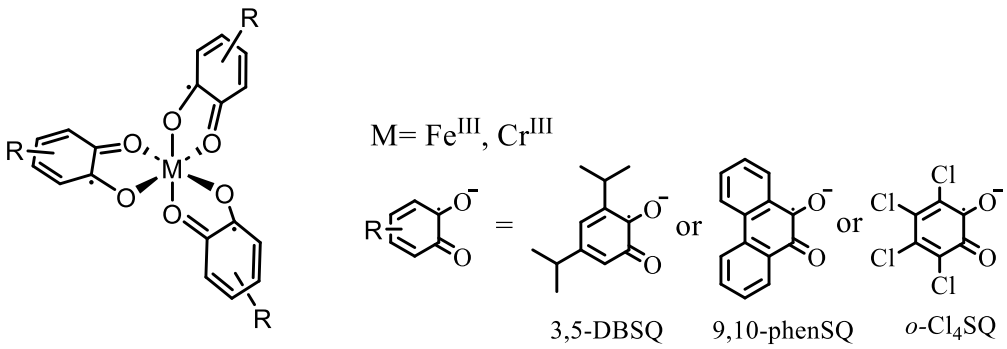

Figure 1-6. $M(SQ)_3$ complexes prepared by the Hendrickson group.

Diimine and amidophenolate ligands—the nitrogen analogs

To expand the scope of redox-active ligands, the nitrogen analogs were synthesized and explored. Diimine and amidophenolate ligand systems were developed and both exhibit similar redox properties to catecholate ligands, where three oxidation states are possible.

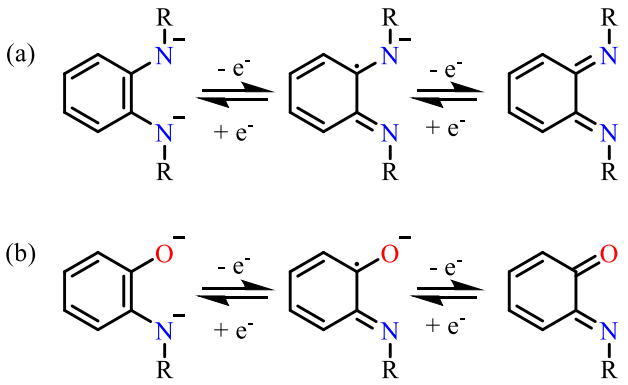

Figure 1-7. Three possible oxidation states of (a) diimine, (b) amidophenolate ligand.

The first diimine complex was synthesized in 1927 by Feigl and Fürth. A violet complex $Ni[C_6H_4(NH)_2]_2$ formed upon mixing Ni^{2+} and *o*-phenylenediamine in aqueous ammonia.[32] Later in 1965 and 1966, Holm and coworkers synthesized a series of $[M{-}N_4]^z$ complexes as parallel work to their catecholate/ semiquinone/ quinone studies.[33,34] The metals studied were Pd, Pt, Co, Ni and $[M{-}N_4]^z$ complexes were proposed to have formal charge z= -2, -1, 0, +1, +2. However, spectroscopic and magnetic data cannot be used to unambiguously assign the oxidation states of metals and ligands at that time. It was not until 2001 that the

electronic structures of these complexes with radical involved diimine ligands were carefully studied by Wieghardt and co-workers.[35] They reported that the diamagnetic square planar complexes of Ni^{II}, Pd^{II}, and Pt^{II} of the type $[M{-}O_4]$, $[M{-}N_4]$, and $[M{-}O_2N_2]$ contain two *o*-semiquinonato radical ligands, and the observed singlet ground state is due to intramolecular antiferromagnetic coupling of the radicals in the ligand system (Figure 1-8). An example of their study regarding the select bond lengths of complexes with amidophenolate ligand in three different oxidation state is shown in Figure 1-9.[36]

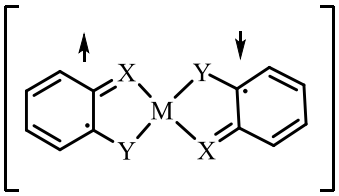

Singlet groud state

(X, Y)= (NH,NH); (NH,O); (O,O), (S,S)

M= Ni^{II}, Pd^{II}, Pt^{II}

Figure 1-8. Electronic structure of $[M{-}O_4]$, $[M{-}N_4]$, and $[M{-}O_2N_2]$ reported by Wieghardt and co-workers.

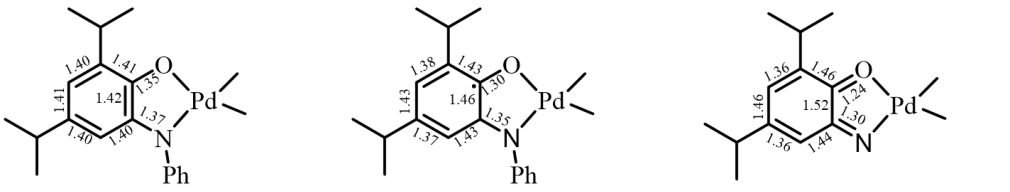

amidophenolate (2-) amidobenzoquinone (0)

amidobenzosemiquinonate (1-)

Figure 1-9. Select bond lengths of complexes with amidophenolate ligand in three different oxidation states.

The 2,2'-bipyridine (bpy) ligand derived from diimine ligand was discovered at the end of nineteenth century[37] and has become one of the most explored chelating systems in coordination chemistry.[38] 2,2'-bipyridine has a similar extensive π-network as dithiolene, catecholate and diimine ligands, and therefore can also facilitate redox events.

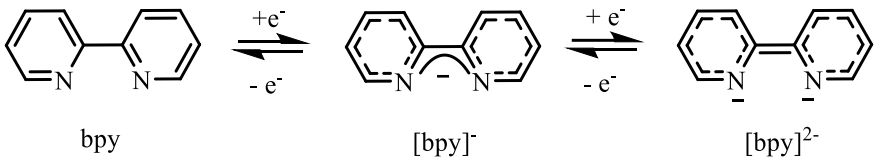

Scheme 1-5. Three possible oxidation states of 2,2'-bipyridine ligand.

In 1928, magenetochemical investigations were first applied to the metal complex with 2,2'-bibyridine ligand, $[Fe(bpy)_3](SO_4)$, which was determined to be a diamagnetic low spin Fe^{II} complex.[39,40] Since then, extensive studies have been done with focus on utilizing the bidentate 2,2'-bibyridine ligands to form metal complexes[40] and metallosupramolecular complexes.[41-43] With the advancing of spectroscopic technologies, researchers were able to determine and characterize the structure of these complexes. However, their redox-activities were not reported until early 2000.[44-46] The Wieghardt group first performed a density functional theoretical (DFT) study to provide guidance on the assignment of the oxidation level of bpy ligand in the complexes.[47] In later years, they performed detailed electronic structure studies on a number of tris-2,2'-bipyridine complexes $M[bpy_3]^n$ of V, Fe, Ru, Ti, Cr, Mo and Mn.[48-53] Discussions of analogous complexes $M[tby_2]^n$, which has 2,2:6,2-terpyridine ligands were also included in their reports (Scheme 1-6). The inclusion of reduced mono-radical anions was confirmed in the monoanion metal complexes such as $Fe[bpy_3]^{1-}$.

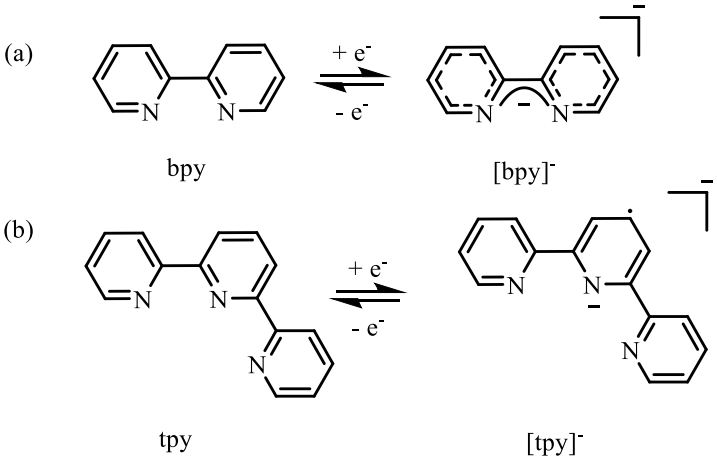

Scheme 1-6. Neutral and mono-radical anions of (a) 2,2'-bipyridine and (b) 2,2:6,2-terpyridine.

Iminopyridine ligands

Iminopyridine ligands are one of the most widely used ligands due to their ease of synthesis and capability of coordinating with a wide variety of metals. In addition, change of functionalities on the pyridyl or aryl rings can modulate the steric and electronic properties of the ligands. Wieghardt and co-workers reported the syntheses and characterizations of a series of bis(α-iminopyridine)metal complexes with the first-row transition metal ions (Cr, Mn, Fe, Co, Ni, and Zn) in 2008.[54] In principle, the α-iminopyridine ligand can exist in three different oxidation states as shown in Scheme 1-7. Wieghardt and co-workers reported that the neutral bis(α-iminopyridine)metal complexes comprise a divalent metal ion and two mono-anionic ligand radicals as supported by physical measurements including X-ray crystallography, magnetic susceptibility measurements, cyclic voltammetry, UV-vis spectroscopy, NMR, EPR, and Mössbauer spectroscopy, as well as density functional theoretical (DFT) calculations. In addition, the unpaired spins at the ligands and metal center were shown to be antiferromagnetically coupled.[54] Detailed investigations on the one-electron oxidized cationic series suggested ligand-centered oxidation, resulting in mostly mixed-valent complexes, wherein the two ligands have formally different redox states, $(L)^0$ and $(L\bullet)^-$. Different electronic structures were observed due to the nature of the metal linker: the ligand radical was fully delocalized in the cationic Fe and Co complexes, while localized in Zn, Cr, and Mn complexes.

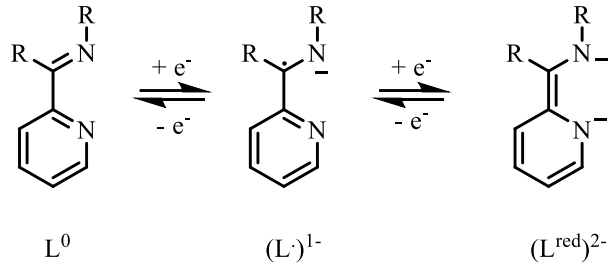

Scheme 1-7. Three possible oxidation states of α-iminopyridine.

In addition to α-iminopyridine ligands, Wieghardt and co-workers also contributed significantly to the coordination chemistry of bis(imino)pyridine ligands.[55,56] A study on the model complex (^{i}PrPDI)$FeCl_2$ revealed that it consisted of a high-spin ferrous center ligated by a neutral bis(imino)pyridine ligand.[56] The single-electron reduction product, (^{i}PrPDI)FeCl, was still with a high-spin ferrous center (S=2), but was also antiferromagnetically coupled to the radical (S=1/2) in the reduced ligand, resulting in experimentally observed S=3/2 ground state. Continued single-electron reduction preserved the ferrous center and generated a bis(imino)pyriidine diradical. These results demonstrated that sequential redox events happened on the conjugated π-system of the bis(imino)pyridine ligands, rather than on the metal center.

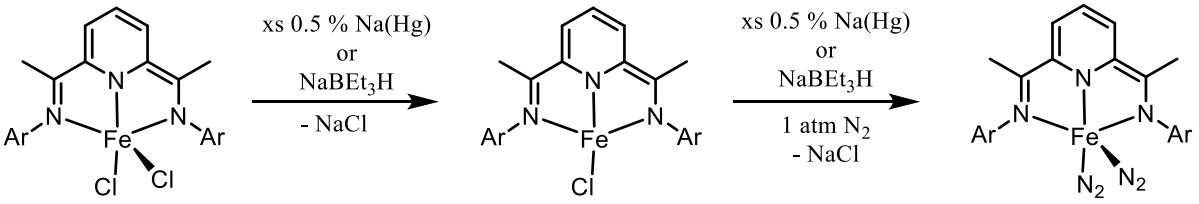

Scheme 1-8. Reduction of (^{i}PrPDI)$FeCl_2$.

Other imine based ligands

Porphyrin is a naturally occurring redox-active ligand that is a component of hemoproteins, whose functions include carrying oxygen in the bloodstream. Porphyrin can

act as a tetradentate ligand, and the extensive π-network allows its redox-active property. Dipyrrin, which can be seen as 'half-porphyrin'[57], has similar electronic, geometrical, and structural parameters with the porphyrin ligand and can facilitate multi-electron events at the metal center.[58-61] In 2009, the Betley group developed a dipyrrin ferrous complex that can catalyze intramolecular C−H amination.[61] In the same year, the Betley group also performed structural and electronic studies on a series of transition metal complexes (Mn, Fe, Co, Ni, Cu, Zn) of the dipyrrin ligand. A two-electron oxidation pathway, which was entirely ligand-based, was detected through differential pulse voltammetry.[60] Other studied nitrogenous redox-active ligands include pathalocyanine[62-65] and 9,10-phenanthrenediimine (Figure 1-10).[66-69] One common feature of these redox-active ligands is the existence of extensive π-network which can function as electron reservoir and facilitate redox events when coordinated with metals.

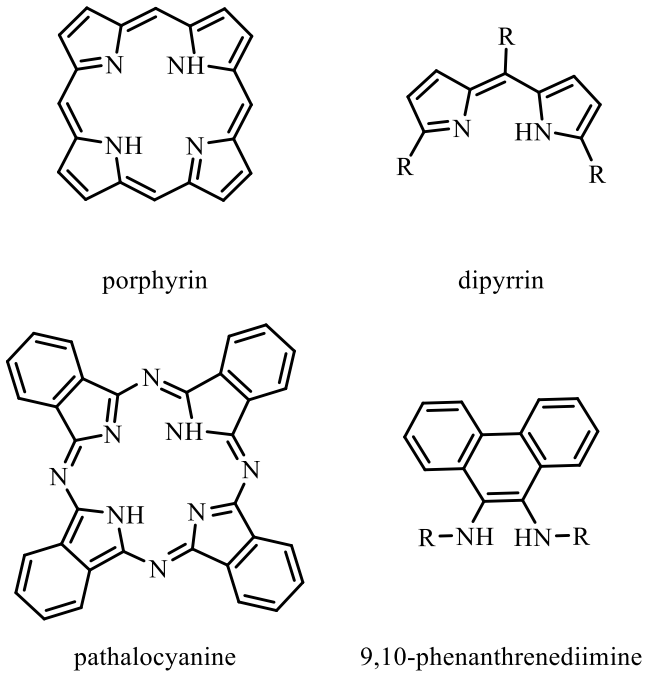

Figure 1-10. Examples of other imine based redox-active ligands.

In 2008, Hu *et. al*, developed a new amidobis(amine) pincer type ligand as shown in Figure 1-11.[70] Studies showed that the nickel compound incorporating this ligand can promote cross coupling of nonactivated alkyl halides.[71,72]

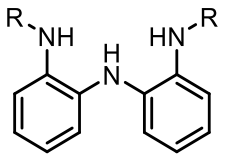

Figure 1-11. Amidobis(amine) pincer type ligand.

Phenol-containing ligands

Inspired by the discovery of tyrosyl radicals in the active site of enzymes that naturally catalyze multi-electron reactions, researchers have been developing phenol containing redox-active ligands that could form phenoxyl radicals. In some cases, 2,6-di-*tert*-butylphenol moiety was installed to the original ligand system,[73,74] allowing the formation of relatively stable phenoxyl radical upon oxidation.

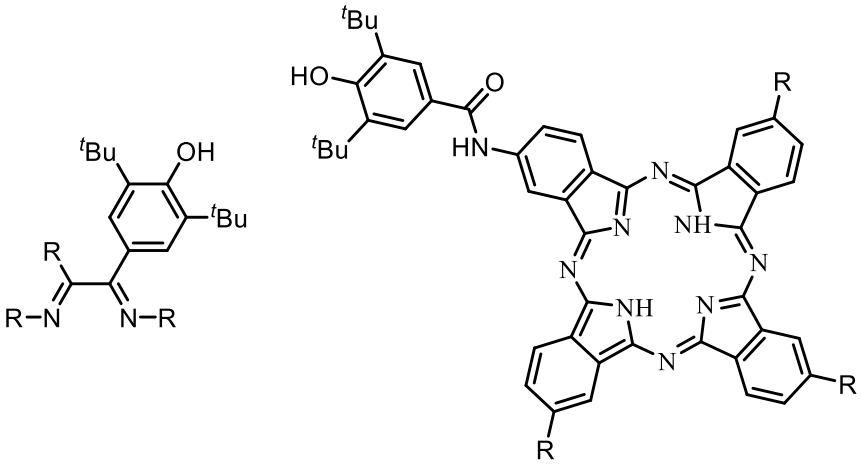

1-12 **1-13**

Figure 1-12. Examples of ligand system involving 2,6-di-*tert*-butylphenol moiety.

Some other examples of phenol containing redox-active ligands include salphen ligands **1-14**,[75-79] bis(phenol)amine ligands **1-15**,[80-85] and *o*-mercaptophenol ligands **1-16**.[86-89]

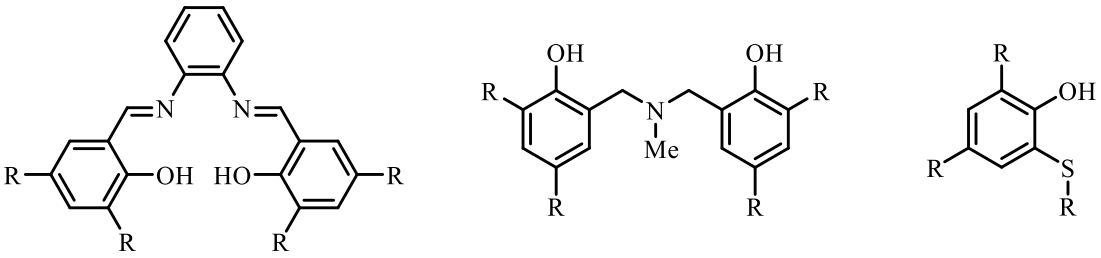

1-14 **1-15** **1-16**

Figure 1-13. Examples of phenol containing redox-active ligands.

Applications of redox-active ligands in catalysis

Conventionally, in the metal complex with redox-inactive ligands, the redox events originate on the metal center while the coordinated ligands remain spectators. Whereas for complexes with redox-active ligands, redox events can happen on the metal center or ligand scaffold or even both in the metal complexes with redox-active ligands, offering better multi-electron catalysis by first-row transition metals which usually prefer single-electron redox events. However, the involvement of redox-active ligands in the system made the assignment of oxidation state on the metal center more difficult. Consequently, researchers over the years have been focusing on investigating the structure-bonding correlation and understanding the electronic and magnetic properties of the redox-active ligands and their complexes.

Only recently, with advances in the mechanistic elucidation of metallo-enzymatic reactions that include redox-active ligand participation, research interests have shifted to utilizing redox-active ligand-metal cooperative system for catalysis. Redox-active ligands not only can offer coordination and steric control to the metal centers, but also function as electron reservoirs and/or participate in the reactions, thus facilitating the multi-electron catalysis at first-row transition metals.

Carbon–Carbon bond formation

Carbon–carbon bond formation has consistently been a key area of interest in synthetic chemistry. Generally, these reactions proceed through the mechanism of oxidative addition/reductive elimination, which often involve two-electron transfer mechanisms. As a result, several noble transition metal catalysts including the well-known palladium catalysts for cross-coupling reactions were developed. However, with higher demand for chemical products and rapid depletion of natural resources, scientists have been searching for more

cost-effective and eco-friendly alternatives to replace the expensive noble transition metal catalysts. First-row transition metals with redox-active ligands have become popular in sustainable catalyst design. First-row transition metals are more earth-abundant and less toxic, and their preference for single-electron events can be altered by incorporating redox-active ligands that serve as electron reservoirs to facilitate multi-electron events. With the help of redox-active ligands, the multi-electron redox events can happen either synergistically at the metal center and ligand system or purely at the ligand, thus avoiding unfavorable intermediates with high oxidation states of metal centers.

In 2006, Chirik and co-workers developed a bis(imino)-pyridine-coordinate Fe^{II}-dinitrogen catalyst **1-17** for [2π+2π] cycloadditions.[90] The proposed mechanism started with a reaction between the catalyst **1-17** and the diene substrate. The diene substrate was π-coordinated to the metal through ligand exchange and formed the intermediate **1-18**. Both **1-17** and **1-18** contained a ferrous ion center with a two-electron-reduced bis(imino)-pyridine ligand radical. Intermediate **1-19** formed in equilibrium with **1-18**. The C–C coupling product was then formed through reductive elimination with the regeneration of the catalyst **1-17**. The ligand-centered redox events in the catalytic cycle allowed the oxidation state of the iron center remained unchanged, thus avoiding the unfavorable oxidized Fe^{IV} species (Scheme 1-9).[18,90]

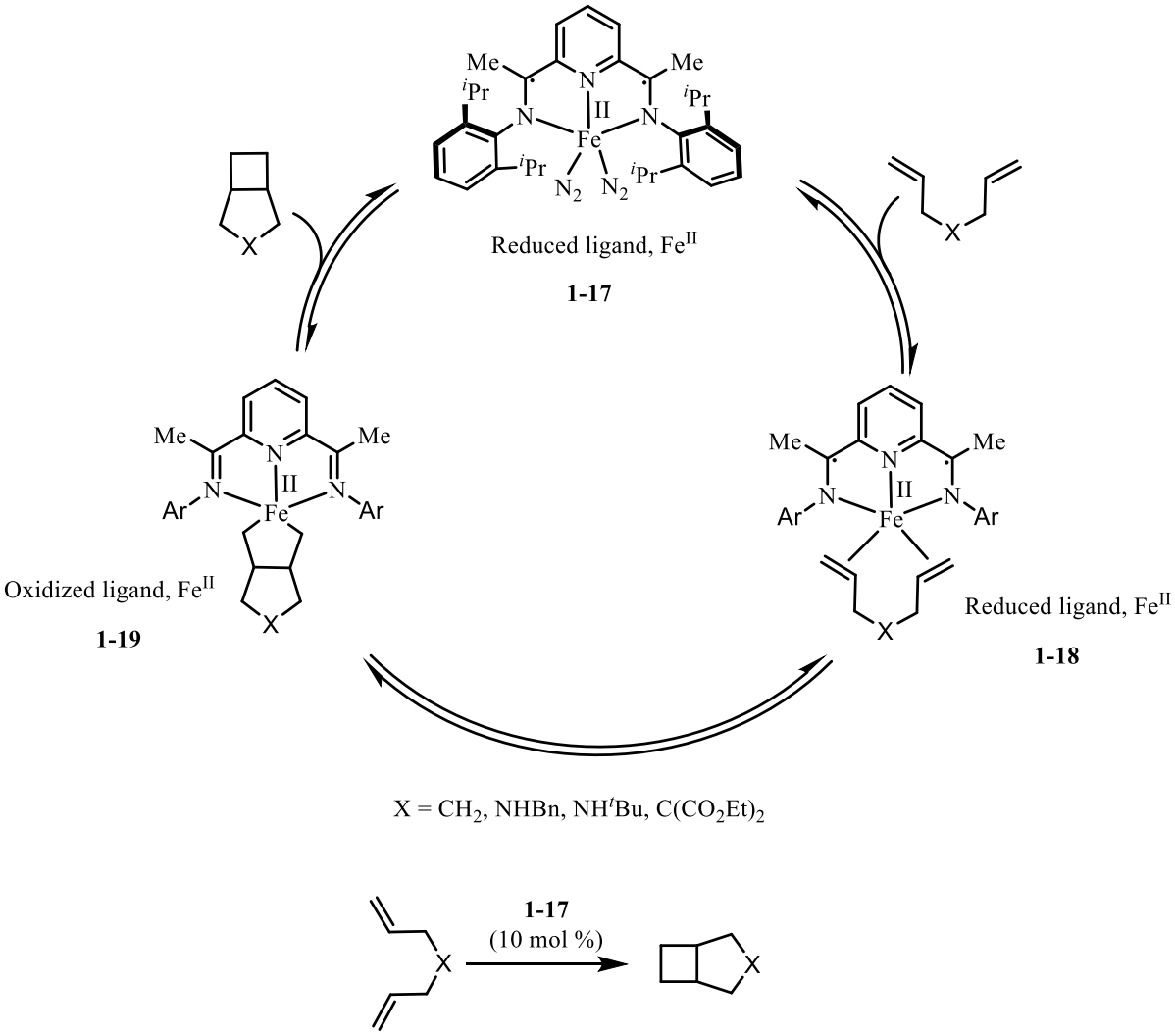

Scheme 1-9. Proposed mechanism of [2π+2π] cycloadditions by developed a bis(imino)-pyridine Fe^{II}-dinitrogen catalyst.[18,90]

In 2010, Soper and co-workers developed Co^{III} complexes with redox-active amidophenolate ligands.[91] These Co^{III} complexes reacted with alkyl halides through a pseudo oxidation process and generated five-coordinated square pyramidal alkylcobalt(III) complexes **1-21**. The intermediate **1-21** contained two one-electron-oxidized ligand radicals, while the oxidation state of the cobalt center remained unchanged. Upon adding aryl or alkyl zinc bromides into the reaction mixture, the C–C coupled products were obtained through two-electron reductive elimination (Scheme 1-10).[91]

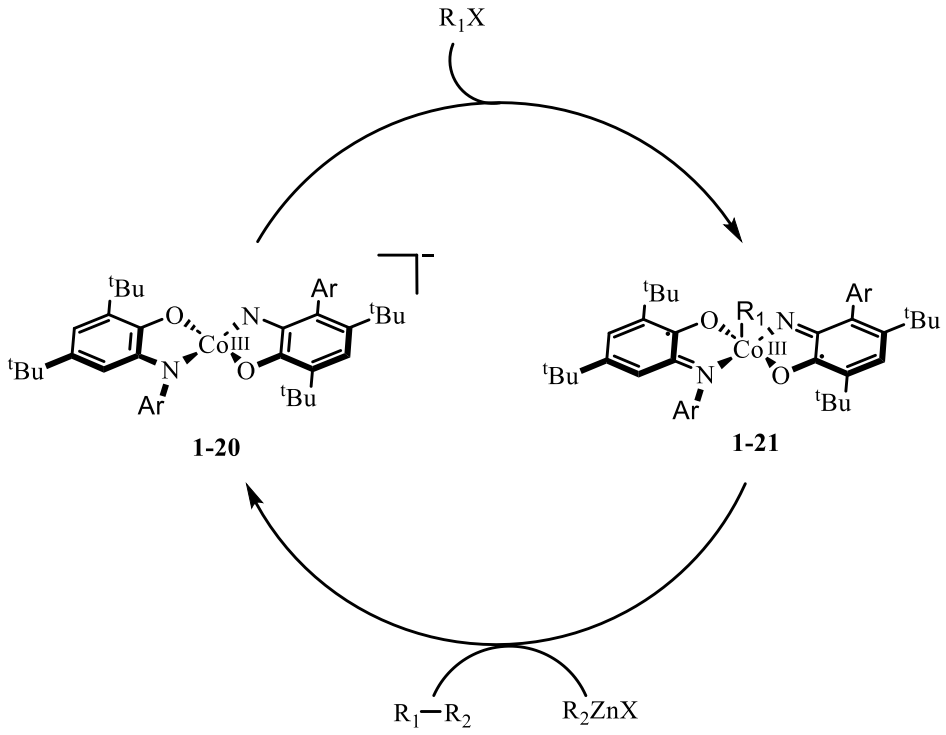

Scheme 1-10. Negishi-type C–C cross-coupling reaction by Co^{III} complexes.[91]

Carbon–Heteroatom bond formation

Like C–C bond formation, C–heteroatom bond formations such as C–N, C–S, C–O bond formations are also important in organic synthesis for the formation of value-added products from simple feedstocks.

In 2018, Desage El-Murr and co-workers reported a copper(II) catalyst with redox-active amidophenolate ligand for aziridination reaction.[92] The authors started with a tetra-coordinated quasisquare-planar **1-22** copper(II) complex which was coordinated with two one-electron-oxidized amidophenolate ligand radicals (Scheme 1-11). The two iminosemiquinone ligand radicals in the catalyst **1-22** were antiferromagnetically coupled to each other, resulting in a S=1/2 doublet ground state. Spectroscopic and computational studies suggested that the proposed mechanism began with **1-22** reacting with *N*-tosyliminobenzyliodinane, producing nitrene radical intermediates **1-23**. A subsequent

reaction with the alkene (styrene) yielded trigonal bipyramidal copper(II) complex **1-24** which contained an iminosemiquinone radical and a styrene-based radical. Finally, the radical ring closure was accomplished, generating the aziridine products and regenerating the catalyst **1-23**. This system exhibited copper(II) oxidation state throughout the catalytic cycle.

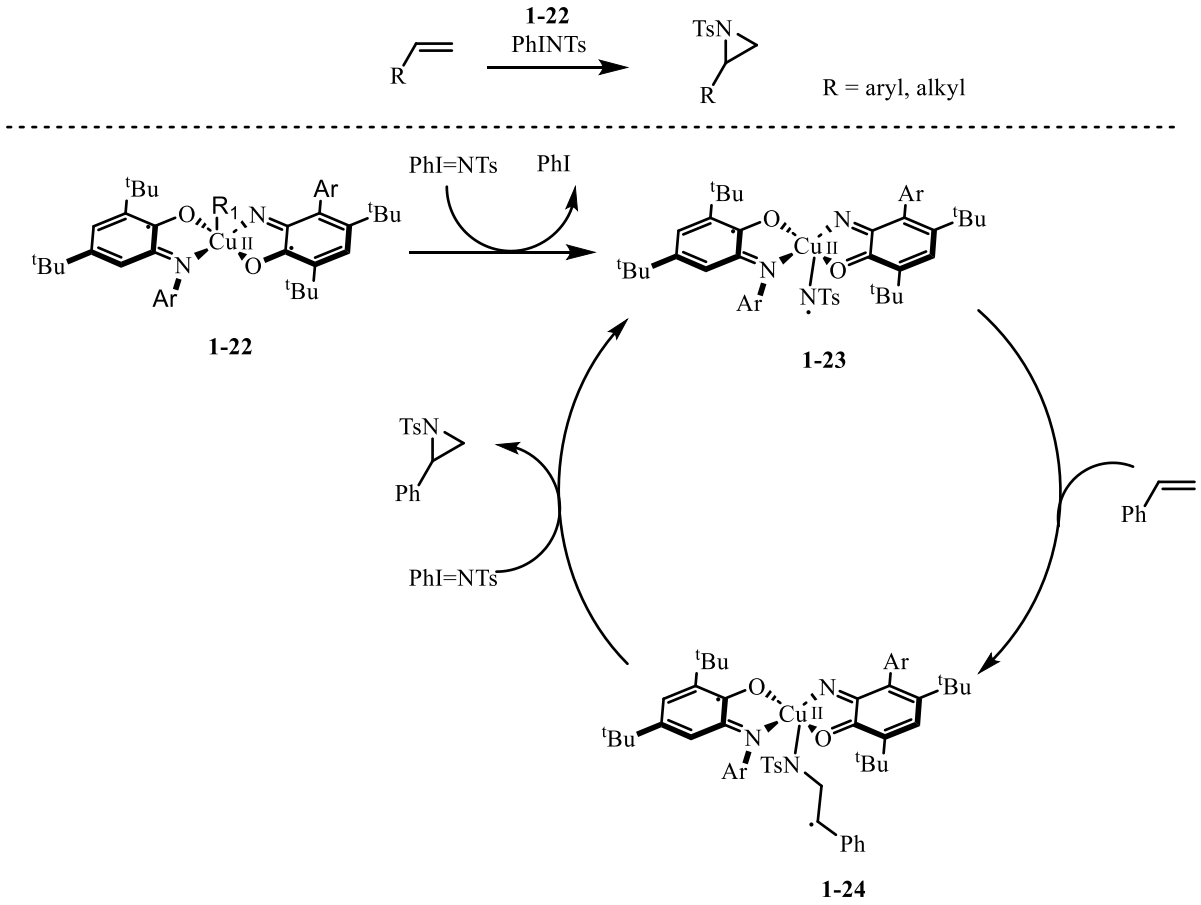

Scheme 1-11. Proposed mechanism of Cu(II) catalyzed aziridinations.

Another nickel-based C–N and C–S cross-coupling catalyst was developed by Paul in 2019.[93,94] This catalyst **1-25** contained two antiferromagnetically coupled single-electron oxidized diiminosemiquinonato type ligands. Through cooperative synergistic participation of metal and ligand-centered redox events, energetically unfavored nickel(0)/nickel(II) or nickel(I)/nickel(III) redox processes were avoided with the help of the redox-active ligands as electron reservoirs. In the proposed mechanism, the catalyst **1-25** was first deprotonated by

base ^{t}BuONa and formed the mono-anionic active species **1-26**, followed by the oxidative addition of aryl halides onto catalyst **1-26**. This oxidative addition process synergistically happened at the metal center and ligand system, resulting in one-electron oxidation of the nickel center to nickel(III) in the intermediate **1-27** and one-electron oxidation of the ligand, thus avoiding the energetically less favorable nickel(IV) center. In the next step, the nitrogen-nucleophiles replaced the halides ligand and protonated one of the ligands forming a nickel(III) intermediate **1-28**. In the end, reductive elimination of **1-28** yielded the *N*-arylated products and regenerated the catalyst **1-25**. C–S bond formation that generates aryl thioethers, commonly found in pharmaceutically relevant molecules, was also achieved by the same catalyst **1-25** through a similar mechanism.

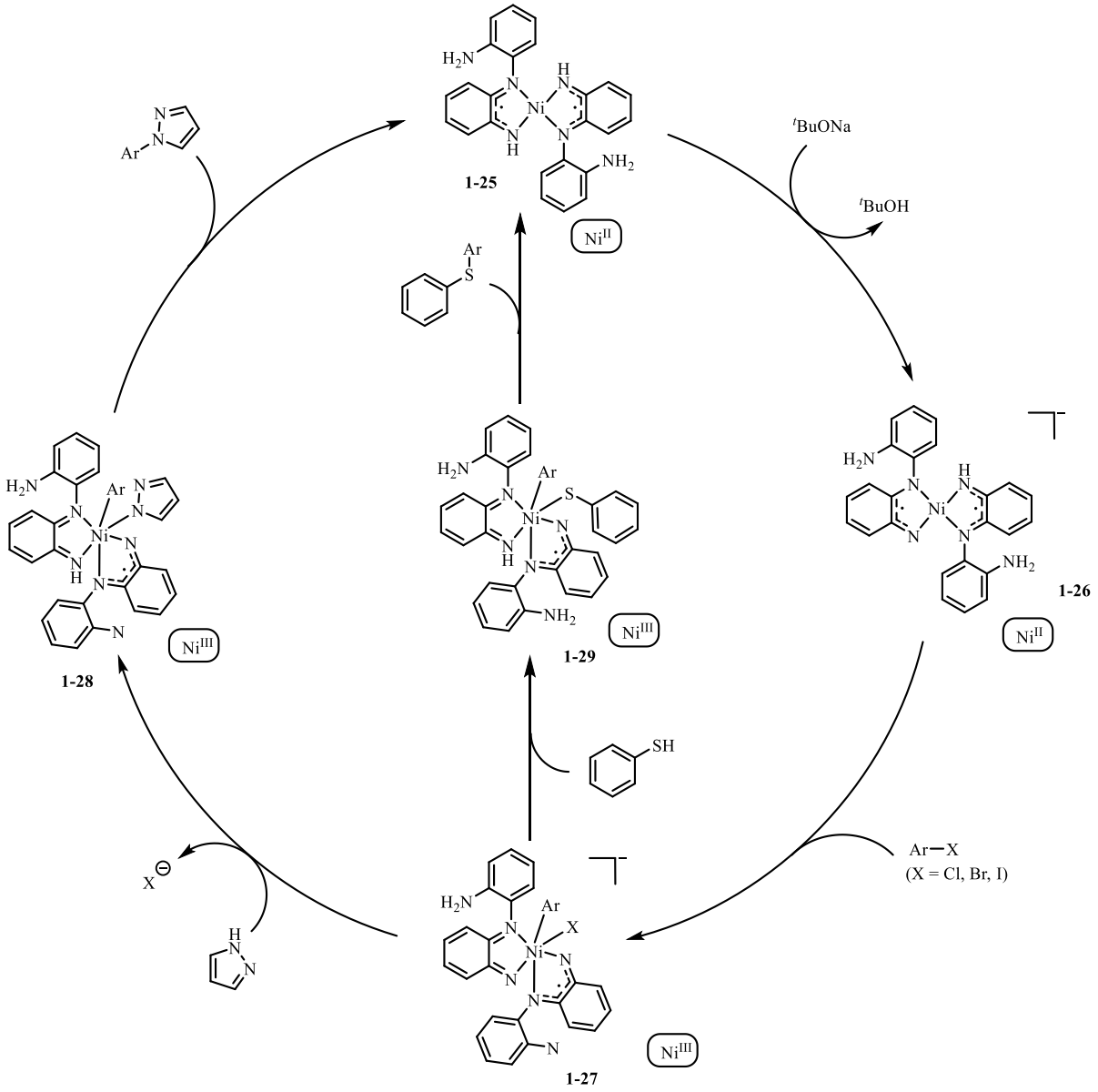

Scheme 1-12. Proposed mechanism of C–N and C–S cross-coupling using a nickel(II) catalyst.

Aerobic oxidation

Oxidation reactions are vital in many chemical transformations; thus, the development of sustainable catalysts for oxidation reactions has received rigorous attention. Much research effort has focused on first-row transition metal catalysts for aerobic oxidation reactions to achieve greener chemical processes. The alcohol oxidation to aldehydes and ketones has received particular attention because the oxidized alcohol can further be functionalized to a

wide range of valuable organic compounds.

Galactose oxidase is a naturally occurring enzyme that can achieve alcohol oxidation catalysis through the synergistic participation of copper and the coordinated phenoxyl radical in the redox events. Inspired by Galactose oxidase, the first biomimetic complex **1-30** was developed in 1996.[95,96] Although it could only catalyze the oxidation of benzylic and allylic-activated alcohols, its report raised interest in this field. In 1999, Wieghardt and co-workers reported Cu(II) and Zn(II) complexes **1-31** incorporating a tetradentate ONNO redox-active ligand as catalysts for aerobic oxidation of primary alcohols.[97] In the proposed mechanism, the alcohol substrate first coordinated with the metal center in anionic alcoholate form. This process resulted in a five-coordinate metal alkoxide with phenoxyl radical intermediate **1-32**. In **1-32**, a hydrogen bond was formed between one hydrogen atom of the α-carbon atom in the alcoholate ligand and phenoxyl radical, which helped with the intramolecular H-abstraction in the next step. A ketyl radical **1-33** formed together with the intramolecular H-abstraction. **1-33** underwent one-electron transfer and generated the aldehyde, a weak ligand that dissociated from the metal complex. The reduced catalyst **1-34** then reacted with dioxygen, yielding the activated catalyst **1-31** and H_2O_2.

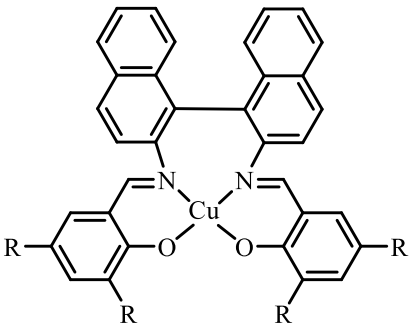

1-30

Figure 1-14. The first biomimetic complex of galactose oxidase for alcohol oxidation.

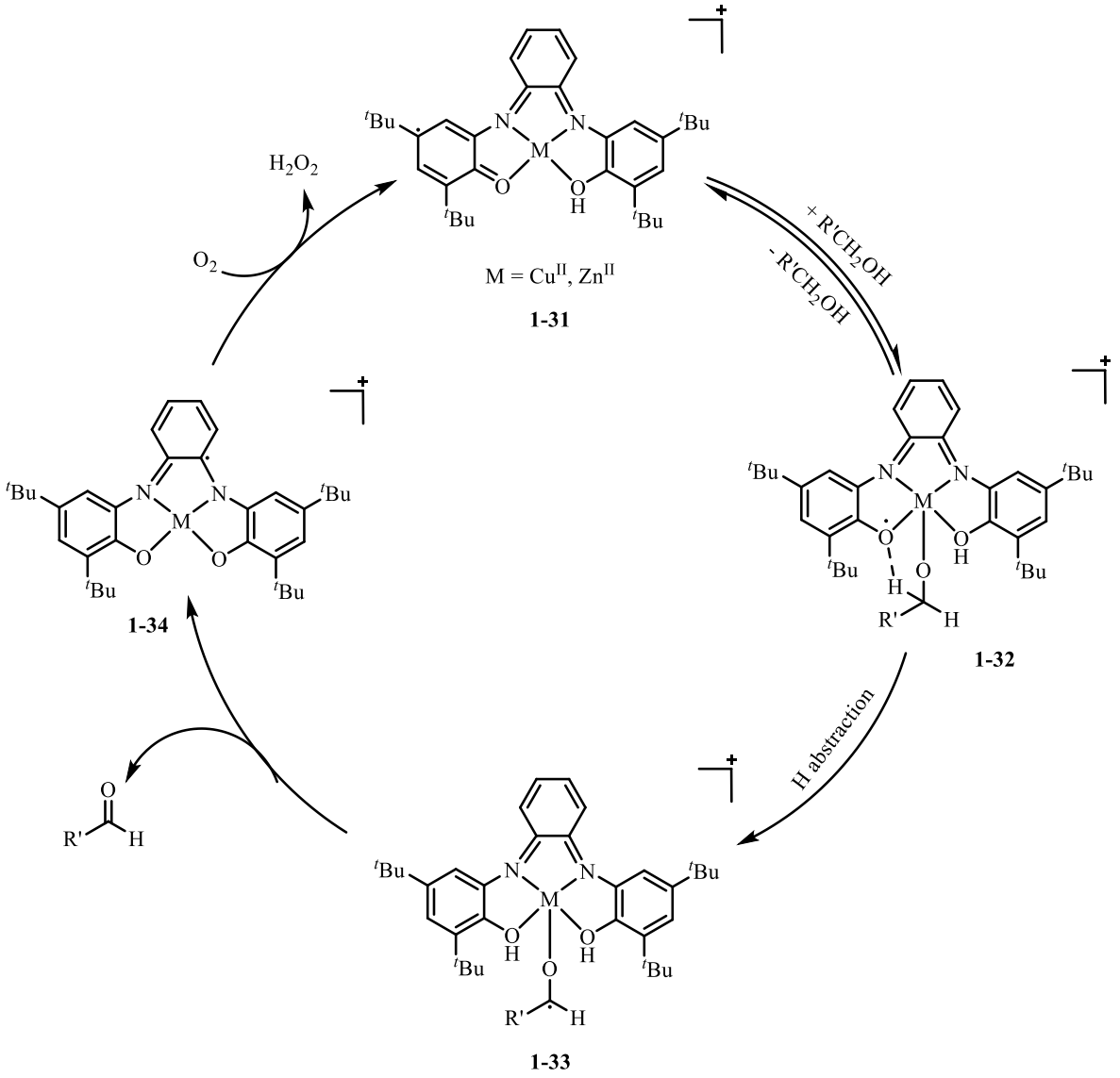

Scheme 1-13. Aerobic oxidation of primary alcohol using Cu(II) and Zn(II) catalysts featuring redox-active ONNO-pincer ligand.

The aforementioned systems are only a few examples of cooperating redox-active ligands with first-row transition metals to promote catalytic multi-electron reactions. Intensive studies have been conducted in this area with the focus of developing sustainable catalysts for useful chemical reactions.

Dissertation overview

To explore sustainable catalysis utilizing first-row transition metals and redox-active

ligands, the MacBeth lab developed a bis(amidophenyl)amine type ligand framework.[98-100] The extensive π-network in the ligand framework allows the redox-active property; the three nitrogenous groups allow up to three coordinations with the metal center and the R groups provide electronic and steric tunability. Examples of the explored R groups including isopropyl, *tert*-butyl, methyl, 2,4,6-trisopropyl phenyl (TRIP) and trifluoromethyl group.

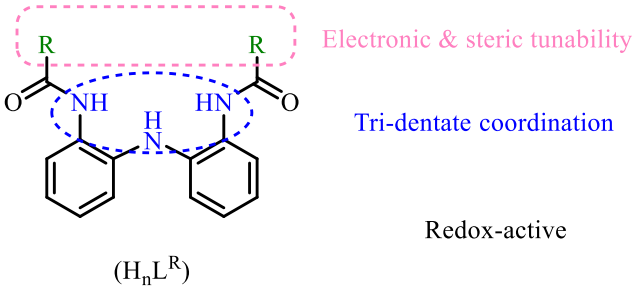

Figure 1-15. Redox-active ligand scaffold developed by the MacBeth group.

Coordinative versatility has been observed with this ligand as shown in Scheme 1-14. When two equivalents of base were applied to the ligand, it coordinated to the cobalt center in a bidentate manner, forming a mononuclear cobalt complex. While application of three equivalents of base generated a dinuclear cobalt complex with tridentate ligands. In addition, this dinuclear Co(II) complex supported by a bis(amidophenyl)amine redox-active ligand $[Co_2L^{iPr}{}_2]^{2-}$ was reported to be an efficient homogeneous catalyst for catalytic oxidations and C–H amination reactions.[98,99] Experimental and computational studies suggested that the dinuclear cobalt complex underwent rearrangement, forming a mononuclear four-coordinated cobalt complex as the active species for the catalysis (Scheme 1-15).[100] Inspired by these studies, two projects to further expand the library of redox-active ligands and their corresponding catalysis with first-row transition metals were proposed.

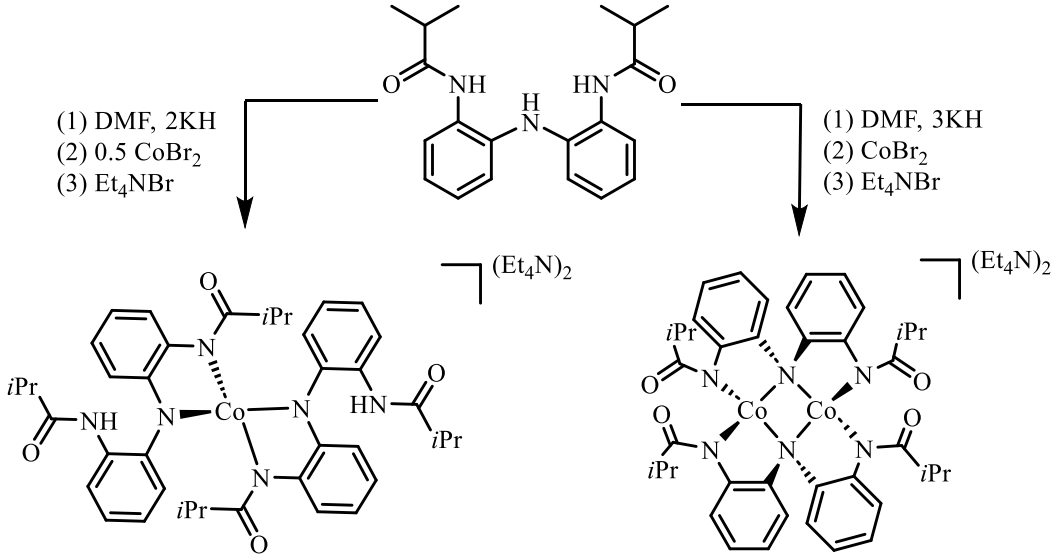

Scheme 1-14. Schematic illustration of coordinative versatility of ligand scaffold developed by the MacBeth group.

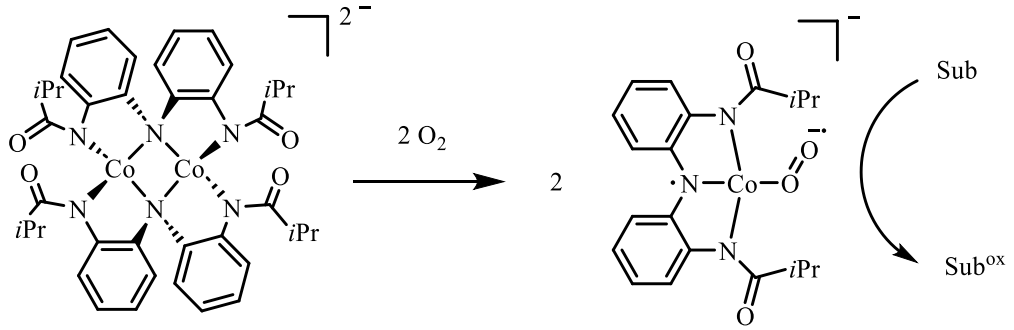

Scheme 1-15. Rearrangement of $[Co_2L^{iPr}{}_2]^{2-}$ upon oxidation.

In the first project, two novel redox-active ligands containing a multi-dentate nitrogenous moiety and catechol moieties were designed and synthesized to allow more coordinative versatility and electronic tunability of corresponding metal complexes (Figure 1-16). Metalations and recrystallizations yielded crystals of two Cu complexes, a cobalt cluster, and an iron cluster. X-ray crystallography, cyclic voltammetry and UV-vis spectroscopy were applied to study their catalytic properties.

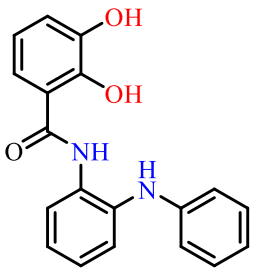

2,3-dihydroxy-*N*-(2-(phenylamino) phenyl)benzamide

H_4L^{CAT}

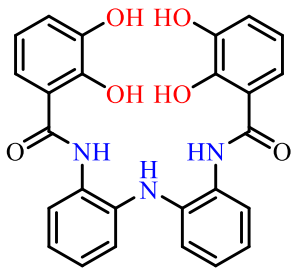

N,*N*'-(azanediylbis(2,1-phenylene)) bis(2,3-dihydroxybenzamide)

H_7L^{CAT}

Figure 1-16. Two novel redox-active ligands developed in Project 1.

In project two, inspired by the homogeneous catalyst $[Co_2L^{iPr}{}_2]^{2-}$ and the development of 'click chemistry', the terminal alkyne was proposed as the modification to the redox-active ligand framework, thus allowing the further immobilization of the homogeneous catalyst onto solid support. The terminal alkyne modified redox-active ligands were successfully synthesized through two synthetic routes. Cobalt complexes with these newly synthesized ligands were obtained and their electrochemical properties were studied by cyclic voltammetry and the electron-rich electrochemical profile showed their potential to catalyze multielectron reactions. UV-vis studies were performed to monitor the aerobic oxidation of catalysts under excess amount of oxygen. The O-atom transfer reaction of oxidizing triphenylphosphine into triphenylphosphine oxide and aerobic hydrazone oxidation of benzophenone hydrazone into diazo compound were achieved with good to moderate yield using the newly synthesized catalysts.

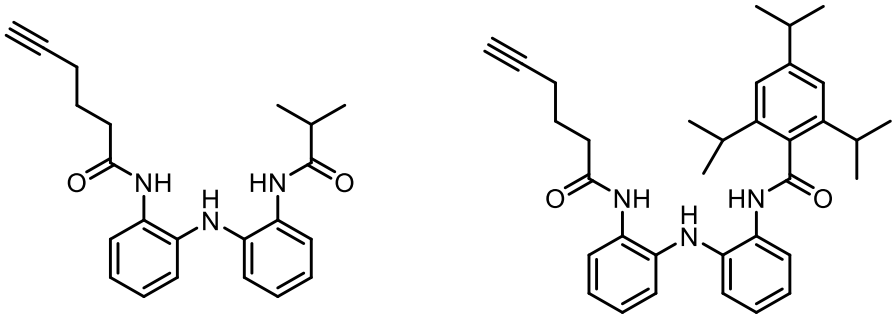

Figure 1-17. Ligand scaffolds developed in Project 2.

References

(1) Praneeth, V. K. K.; Ringenberg, M. R.; Ward, T. R. Redox-active ligands in catalysis. *Angewandte Chemie International Edition* **2012**, *51* (41), 10228-10234.

(2) Seechurn, C. C. C. J.; Kitching, M. O.; Colacot, T. J.; Snieckus, V. Palladium-catalyzed cross-coupling: A historical contextual perspective to the 2010 Nobel prize. *Angewandte Chemie International Edition* **2012**, *51* (21), 5062-5085.

(3) Verma, P.; Pratt, R. C.; Storr, T.; Wasinger, E. C.; Stack, T. D. Sulfanyl stabilization of copper-bonded phenoxyls in model complexes and galactose oxidase. *The Proceedings of the National Academy of Sciences* **2011**, *108* (46), 18600-18605.

(4) Ito, N.; Phillips, S. E.; Stevens, C.; Ogel, Z. B.; McPherson, M. J.; Keen, J. N.; Yadav, K. D.; Knowles, P. F. Novel thioether bond revealed by a 1.7 Å crystal structure of galactose oxidase. *Nature* **1991**, *350* (6313), 87-90.

(5) Himo, F.; Eriksson, L. A.; Maseras, F.; Siegbahn, P. E. Catalytic mechanism of galactose oxidase: A theoretical study. *Journal of the American Chemical Society* **2000**, *122* (33), 8031-8036.

(6) Branchaud, B. P.; Montague-Smith, M. P.; Kosman, D. J.; McLaren, F. R. Mechanism-based inactivation of galactose oxidase: evidence for a radical mechanism. *Journal of the American Chemical Society* **1993**, *115* (2), 798-800.

(7) Whittaker, M. M.; Whittaker, J. W. The active site of galactose oxidase. *Journal of Biological Chemistry* **1988**, *263* (13), 6074-6080.

(8) Whittaker, M. M.; Whittaker, J. W. Ligand interactions with galactose oxidase: mechanistic insights. *Biophysical Journal* **1993**, *64* (3), 762-772.

(9) Larsson, A.; Sjöberg, B.-M. Identification of the stable free radical tyrosine residue in ribonucleotide reductase. *The EMBO Journal* **1986**, *5* (8), 2037-2040.

(10) Eklund, H.; Uhlin, U.; Färnegårdh, M.; Logan, D. T.; Nordlund, P. Structure and function of the radical enzyme ribonucleotide reductase. *Progress in Biophysics and Molecular Biology* **2001**, *77* (3), 177-268.

(11) Capaldi, R. A. Structure and function of cytochrome *c* oxidase. *Annual Review of Biochemistry* **1990**, *59* (1), 569-596.

(12) Capaldi, R. A.; Malatesta, F.; Darley-Usmar, V. Structure of cytochrome *c* oxidase. *Biochimica et Biophysica Acta (BBA)-Reviews on Bioenergetics* **1983**, *726* (2), 135-148.

(13) Ferguson-Miller, S.; Babcock, G. T. Heme/copper terminal oxidases. *Chemical Reviews* **1996**, *96* (7), 2889-2908.

(14) Huang, X.; Groves, J. T. Oxygen activation and radical transformations in heme proteins and metalloporphyrins. *Chemical Reviews* **2017**, *118* (5), 2491-2553.

(15) Yoshikawa, S.; Shimada, A. Reaction mechanism of cytochrome *c* oxidase. *Chemical Reviews* **2015**, *115* (4), 1936-1989.

(16) Jørgensen, C. K. Differences between the four halide ligands, and discussion remarks on trigonal-bipyramidal complexes, on oxidation states, and on diagonal elements of one-electron energy. *Coordination Chemistry Reviews* **1966**, *1* (1-2), 164-178.

(17) Chirik, P. J. Preface: forum on redox-active ligands. *Inorganic Chemistry* **2011**, *50* (20), 9737-9740.

(18) Chirik, P. J.; Wieghardt, K. Radical ligands confer nobility on base-metal catalysts. *Science* **2010**, *327* (5967), 794-795.

(19) Kaim, W.; Schwederski, B. Non-innocent ligands in bioinorganic chemistry—An overview. *Coordination Chemistry Reviews* **2010**, *254* (13-14), 1580-1588.

(20) Luca, O. R.; Crabtree, R. H. Redox-active ligands in catalysis. *Chemical Society Reviews* **2013**, *42* (4), 1440-1459.

(21) Lyaskovskyy, V.; de Bruin, B. Redox non-innocent ligands: versatile new tools to control catalytic reactions. *Acs Catalysis* **2012**, *2* (2), 270-279.

(22) van der Vlugt, J. I. Redox-Active Pincer Ligands. *Metal-Ligand Co-operativity: Catalysis and the Pincer-Metal Platform* **2021**, 135-179.

(23) Schrauzer, G.; Mayweg, V. Reaction of diphenylacetylene with nickel sulfides. *Journal of the American Chemical Society* **1962**, *84* (16), 3221-3221.

(24) Eisenberg, R.; Gray, H. B. Noninnocence in metal complexes: A dithiolene dawn. *Inorganic Chemistry* **2011**, *50* (20), 9741-9751.

(25) Gray, H. B.; Williams, R.; Bernal, I.; Billig, E. A spin-free square planar cobaltous complex. *Journal of the American Chemical Society* **1962**, *84* (18), 3596-3597.

(26) Gray, H. B.; Billig, E. The electronic structures of square-planar metal complexes. III. High-spin planar cobalt(I) and iron(I). *Journal of the American Chemical Society* **1963**, *85* (13), 2019-2020.

(27) Davison, A.; Edelstein, N.; Holm, R.; Maki, A. The preparation and characterization of four-coordinate complexes related by electron-transfer reactions. *Inorganic Chemistry* **1963**, *2* (6), 1227-1232.

(28) Aragoni, M. C.; Caltagirone, C.; Lippolis, V.; Podda, E.; Slawin, A. M.; Woollins, J. D.; Pintus, A.; Arca, M. Diradical character of neutral heteroleptic bis(1,2-dithiolene) metal

complexes: Case study of [Pd(Me_2timdt)(mnt)](Me_2timdt=1,3-dimethyl-2,4,5-trithioxoimidazolidine; mnt^{2-}=1,2-dicyano-1,2-ethylenedithiolate). *Inorganic Chemistry* **2020**, *59* (23), 17385-17401.

(29) Pierpont, C. G.; Buchanan, R. M. Transition metal complexes of *o*-benzoquinone, *o*-semiquinone, and catecholate ligands. *Coordination Chemistry Reviews* **1981**, *38* (1), 45-87.

(30) Rohrscheid, F.; Balch, A. L.; Holm, R. Potential electron transfer complexes of the [M–O_4] type: Synthesis and properties of complexes derived from pyrocatechol and tetrachloropyrocatechol. *Inorganic Chemistry* **1966**, *5* (9), 1542-1551.

(31) Buchanan, R. M.; Kessel, S. L.; Downs, H. H.; Pierpont, C. G.; Hendrickson, D. N. Structural and magnetic properties of tris (*o*-semiquinone) complexes of iron(III) and chromium(III). *Journal of the American Chemical Society* **1978**, *100* (25), 7894-7900.

(32) Feigl, F.; Fürth, M. Über Verbindungen des Nickels mit *o*-Phenylendiamin und 1,3,4-Toluylendiamin. *Monatshefte für Chemie und verwandte Teile anderer Wissenschaften* **1927**, *48*, 445-450.

(33) Balch, A. L.; Holm, R. Complete electron-transfer series of the [M–N_4] type. *Journal of the American Chemical Society* **1966**, *88* (22), 5201-5209.

(34) Balch, A. L.; Röhrscheid, F.; Holm, R. New systems of complexes related by electron-transfer reactions. *Journal of the American Chemical Society* **1965**, *87* (10), 2301-2302.

(35) Chaudhuri, P.; Verani, C. N.; Bill, E.; Bothe, E.; Weyhermüller, T.; Wieghardt, K. Electronic structure of bis (*o*-iminobenzosemiquinonato) metal complexes (Cu, Ni, Pd). The art of establishing physical oxidation states in transition-metal complexes containing radical ligands. *Journal of the American Chemical Society* **2001**, *123* (10), 2213-2223.

(36) Kokatam, S.; Weyhermüller, T.; Bothe, E.; Chaudhuri, P.; Wieghardt, K. Structural characterization of four members of the electron-transfer series $[Pd^{II}(L)_2)_2]^n$ (L= *o*-iminophenolate derivative; n= 2−, 1−, 0, 1+, 2+). Ligand mixed valency in the monocation and monoanion with S= 1/2 ground states. *Inorganic chemistry* **2005**, *44* (10), 3709-3717.

(37) Blau, F. Über die trockene Destillation von pyridincarbonsauren Salzen. *Monatshefte für Chemie/Chemical Monthly* **1889**, *10* (1), 375-388.

(38) Kaes, C.; Katz, A.; Hosseini, M. W. Bipyridine: the most widely used ligand. A review of molecules comprising at least two 2,2'-bipyridine units. *Chemical Reviews* **2000**, *100* (10), 3553-3590.

(39) Biltz, W. Über Molekular-und Atomvolumina. XVII. Zur Raumchemie und Magnetochemie fester Cyanide. *Zeitschrift für anorganische und allgemeine Chemie* **1928**, *170* (1), 161-183.

(40) Constable, E. C.; Housecroft, C. E. The early years of 2, 2′-bipyridine—A ligand in its own lifetime. *Molecules* **2019**, *24* (21), 3951.

(41) Ward, M. D.; White, C. M.; Barigelletti, F.; Armaroli, N.; Calogero, G.; Flamigni, L. Assemblies of luminescent ruthenium(II)—and osmium(II)—polypyridyl complexes based on hydrogen bonding. *Coordination Chemistry Reviews* **1998**, *171*, 481-488.

(42) Pfeiffer, P.; Quehl, K. Über einen neuen Effekt in Lösungen optisch-aktiver Substanzen (I. Mitteil.). *Berichte der deutschen chemischen Gesellschaft (A and B Series)* **1931**, *64* (10), 2667-2671.

(43) Pfeiffer, P.; Quehl, K. Aktivierung von komplexsalzen in wäßriger lösung (II. Mitteil.). *Berichte der deutschen chemischen Gesellschaft (A and B Series)* **1932**, *65* (4), 560-565.

(44) Schultz, M.; Boncella, J. M.; Berg, D. J.; Tilley, T. D.; Andersen, R. A. Coordination of 2,2'-bipyridyl and 1,10-phenanthroline to substituted ytterbocenes: an experimental investigation of spin coupling in lanthanide complexes. *Organometallics* **2002**, *21* (3), 460-472.

(45) Booth, C. H.; Kazhdan, D.; Werkema, E. L.; Walter, M. D.; Lukens, W. W.; Bauer, E. D.; Hu, Y.-J.; Maron, L.; Eisenstein, O.; Head-Gordon, M. Intermediate-valence tautomerism in decamethylytterbocene complexes of methyl-substituted bipyridines. *Journal of the American Chemical Society* **2010**, *132* (49), 17537-17549.

(46) Kraft, S. J.; Fanwick, P. E.; Bart, S. C. Synthesis and characterization of a uranium(III) complex containing a redox-active 2,2′-bipyridine ligand. *Inorganic Chemistry* **2010**, *49* (3), 1103-1110.

(47) Scarborough, C. C.; Wieghardt, K. Electronic structure of 2,2′-bipyridine organotransition-metal complexes. Establishing the ligand oxidation level by density functional theoretical calculations. *Inorganic Chemistry* **2011**, *50* (20), 9773-9793.

(48) Scarborough, C. C.; Sproules, S.; Weyhermüller, T.; DeBeer, S.; Wieghardt, K. Electronic and molecular structures of the members of the electron transfer series $[Cr(^{t}bpy)_3]^n$ (n= 3+, 2+, 1+, 0): an X-ray absorption spectroscopic and density functional theoretical study. *Inorganic Chemistry* **2011**, *50* (24), 12446-12462.

(49) Bowman, A. C.; Sproules, S.; Wieghardt, K. Electronic structures of the $[V(^{t}bpy)_3]^z$ (z= 3+, 2+, 0, 1−) electron transfer series. *Inorganic Chemistry* **2012**, *51* (6), 3707-3717.

(50) England, J.; Scarborough, C. C.; Weyhermüller, T.; Sproules, S.; Wieghardt, K. Electronic structures of the electron transfer series $[M(bpy)_3]^n$, $[M(tpy)_2]^n$, and $[Fe(^{t}bpy)_3]^n$

(M= Fe, Ru; n= 3+, 2+, 1+, 0, 1–): A Mössbauer spectroscopic and DFT study. *European Journal of Inorganic Chemistry* **2012**, *2012* (29), 4605-4621.

(51) Bowman, A. C.; England, J.; Sproules, S.; Weyhermüller, T.; Wieghardt, K. Electronic structures of homoleptic [tris(2,2′-bipyridine)M]^{n} complexes of the early transition metals (M= Sc, Y, Ti, Zr, Hf, V, Nb, Ta; n= 1+, 0, 1–, 2–, 3−): An experimental and density functional theoretical study. *Inorganic Chemistry* **2013**, *52* (4), 2242-2256.

(52) Wang, M.; Weyhermüller, T.; England, J.; Wieghardt, K. Molecular and electronic structures of six-coordinate "low-valent" [M(^{Me}bpy)$_3$]^0 (M= Ti, V, Cr, Mo) and [M(tpy)$_2$]^0 (M= Ti, V, Cr), and seven-coordinate [MoF(^{Me}bpy)$_3$](PF$_6$) and [MX(tpy)$_2$](PF$_6$)(M= Mo, X= Cl and M= W, X= F). *Inorganic Chemistry* **2013**, *52* (21), 12763-12776.

(53) Wang, M.; England, J.; Weyhermüller, T.; Wieghardt, K. Molecular and electronic structures of the members of the electron transfer series [Mn(bpy)$_3$]^n (n= 2+, 1+, 0, 1−) and [Mn(tpy)$_2$]^m (m= 4+, 3+, 2+, 1+, 0). An experimental and density functional theory study. *Inorganic Chemistry* **2014**, *53* (4), 2276-2287.

(54) Lu, C. C.; Bill, E.; Weyhermüller, T.; Bothe, E.; Wieghardt, K. Neutral bis(α-iminopyridine) metal complexes of the first-row transition ions (Cr, Mn, Fe, Co, Ni, Zn) and their monocationic analogs: mixed valency involving a redox noninnocent ligand system. *Journal of the American Chemical Society* **2008**, *130* (10), 3181-3197.

(55) Budzelaar, P. H.; de Bruin, B.; Gal, A. W.; Wieghardt, K.; van Lenthe, J. H. Metal-to-ligand electron transfer in diiminopyridine complexes of Mn−Zn. A theoretical study. *Inorganic Chemistry* **2001**, *40* (18), 4649-4655.

(56) Bart, S. C.; Chłopek, K.; Bill, E.; Bouwkamp, M. W.; Lobkovsky, E.; Neese, F.;

Wieghardt, K.; Chirik, P. J. Electronic structure of bis(imino)pyridine iron dichloride, monochloride, and neutral ligand complexes: a combined structural, spectroscopic, and computational study. *Journal of the American Chemical Society* **2006**, *128* (42), 13901-13912.

(57) Moss, G. Nomenclature of tetrapyrroles . *Pure and Applied Chemistry* **1987**, *59* (6), 779-832.

(58) Cohen, S. M.; Halper, S. R. Dipyrromethene complexes of iron. *Inorganica Chimica Acta* **2002**, *341*, 12-16.

(59) Halper, S. R.; Cohen, S. M. Heterometallic metal−organic frameworks based on tris (dipyrrinato) coordination complexes. *Inorganic Chemistry* **2005**, *44* (3), 486-488.

(60) King, E. R.; Betley, T. A. Unusual electronic structure of first row transition metal complexes featuring redox-active dipyrromethane ligands. *Journal of the American Chemical Society* **2009**, *131* (40), 14374-14380.

(61) King, E. R.; Betley, T. A. C−H bond amination from a ferrous dipyrromethene complex. *Inorganic Chemistry* **2009**, *48* (6), 2361-2363.

(62) Taube, R. New aspects of the chemistry of transition metal phthalocyanines. *Pure and Applied Chemistry* **1974**, *38* (3), 427-438.

(63) Geiger, D.; Ferraudi, G.; Madden, K.; Granifo, J.; Rillema, D. Redox reactivity of transition-metal phthalocyanines: ligand radical formation vs. metal center oxidation. *The Journal of Physical Chemistry* **1985**, *89* (18), 3890-3894.

(64) Kobayashi, N.; Nakajima, S. i.; Ogata, H.; Fukuda, T. Synthesis, spectroscopy, and electrochemistry of tetra-*tert*-butylated tetraazaporphyrins, phthalocyanines, naphthalocyanines, and anthracocyanines, together with molecular orbital calculations.

Chemistry–A European Journal **2004**, *10* (24), 6294-6312.

(65) Agboola, B.; Ozoemena, K. I.; Nyokong, T. Synthesis and electrochemical characterisation of benzylmercapto and dodecylmercapto tetra substituted cobalt, iron, and zinc phthalocyanines complexes. *Electrochimica Acta* **2006**, *51* (21), 4379-4387.

(66) Shaffer, D. W.; Ryken, S. A.; Zarkesh, R. A.; Heyduk, A. F. Redox behavior of rhodium 9,10-phenanthrenediimine complexes. *Inorganic Chemistry* **2011**, *50* (1), 13-21.

(67) Li, X.-J.; Sun, S.-L.; Ma, N.-N.; Sun, X.-X.; Yang, G.-C.; Qiu, Y.-Q. Theoretical investigations on electronic spectra and the redox-switchable second-order nonlinear optical responses of rhodium(I)-9,10-phenanthrenediimine complexes. *Journal of Molecular Graphics and Modelling* **2012**, *33*, 19-25.

(68) Kazakov, G.; Druzhkov, N.; Cherkasov, V. Iminoquinones and diimines, *N*-hetero analogs of 9,10-phenanthrenequinone, in coordination chemistry. *Russian Journal of Coordination Chemistry* **2020**, *46*, 178-192.

(69) Abakumov, G.; Druzhkov, N.; Kocherova, T.; Kozhanov, K.; Murugova, A.; Egorova, E. Coordination ability of *N*,*N*'-disubstituted 9,10-phenanthrenediimines. In *Doklady Chemistry*, **2016**; Springer: Vol. 467, pp 109-112.

(70) Csok, Z.; Vechorkin, O.; Harkins, S. B.; Scopelliti, R.; Hu, X. Nickel complexes of a pincer NN_2 ligand: multiple carbon−chloride activation of CH_2Cl_2 and $CHCl_3$ leads to selective carbon−carbon bond formation. *Journal of the American Chemical Society* **2008**, *130* (26), 8156-8157.

(71) Vechorkin, O.; Csok, Z.; Scopelliti, R.; Hu, X. Nickel complexes of a pincer amidobis (amine) ligand: synthesis, structure, and activity in stoichiometric and catalytic C−C

bond-forming reactions of alkyl halides. *Chemistry–A European Journal* **2009**, *15* (15), 3889-3899.

(72) Ren, P.; Vechorkin, O.; Allmen, K. v.; Scopelliti, R.; Hu, X. A structure–activity study of Ni-catalyzed alkyl–alkyl Kumada coupling. Improved catalysts for coupling of secondary alkyl halides. *Journal of the American Chemical Society* **2011**, *133* (18), 7084-7095.

(73) Milaeva, E.; Androsova, A.; Polyakova, O.; Prokof'ev, A.; Petrosyan, V. Influence of the redox state of the ligand on the dealkylation of substituted methylcobaloximes in the presence of heavy metal ions. *Russian Chemical Bulletin* **1996**, *45*, 1734-1739.

(74) Milaeva, E.; Kolnin, S.; Petrosyan, V. Synthesis of tetrasubstituted acylaminophthalocyanines of cobalt. *Russian Chemical Bulletin* **1996**, *45*, 2027-2028.

(75) Kleij, A. W.; Kuil, M.; Tooke, D. M.; Lutz, M.; Spek, A. L.; Reek, J. N. Zn^{II}–salphen complexes as versatile building blocks for the construction of supramolecular box assemblies. *Chemistry–A European Journal* **2005**, *11* (16), 4743-4750.

(76) Hui, J. K. H.; Yu, Z.; Mirfakhrai, T.; MacLachlan, M. J. Supramolecular assembly of carbohydrate-functionalized salphen–metal complexes. *Chemistry–A European Journal* **2009**, *15* (48), 13456-13465.

(77) Vagin, S. I.; Reichardt, R.; Klaus, S.; Rieger, B. Conformationally flexible dimeric salphen complexes for bifunctional catalysis. *Journal of the American Chemical Society* **2010**, *132* (41), 14367-14369.

(78) Shingai, H.; Houjou, H.; Yoshikawa, I.; Araki, K. A Redox-active, amphoteric pyrogallolaldehyde derivative: electrochemical characterization and schiff base formation for constructing multifunctional salphen complexes. *Bulletin of the Chemical Society of Japan*

2013, *86* (6), 698-706.

(79) Doistau, B.; Benda, L.; Cantin, J.-L.; Chamoreau, L.-M.; Ruiz, E.; Marvaud, V.; Hasenknopf, B.; Vives, G. Six states switching of redox-active molecular tweezers by three orthogonal stimuli. *Journal of the American Chemical Society* **2017**, *139* (27), 9213-9220.

(80) Safaei, E.; Wojtczak, A.; Bill, E.; Hamidi, H. Synthesis, crystal structure, magnetic and redox properties of Cu(II)–Cu(II) binuclear complexes of bis(phenol)amine ligands. *Polyhedron* **2010**, *29* (14), 2769-2775.

(81) Safaei, E.; Sheykhi, H.; Wojtczak, A.; Jagličić, Z.; Kozakiewicz, A. Synthesis and characterization of an iron(III) complex of glycine derivative of bis(phenol)amine ligand in relevance to catechol dioxygenase active site. *Polyhedron* **2011**, *30* (7), 1219-1224.

(82) Rajput, A.; Kumar, A.; Sengupta, A.; Tyagi, P.; Arora, H. Copper(II) dimers stabilized by bis(phenol)amine ligands: theoretical and experimental insights. *New Journal of Chemistry* **2018**, *42* (15), 12621-12631.

(83) Karimpour, T.; Safaei, E.; Karimi, B. A supported manganese complex with amine-bis(phenol) ligand for catalytic benzylic C(sp^3)–H bond oxidation. *RSC Advances* **2019**, *9* (25), 14343-14351.

(84) Paine, T. K.; Rentschler, E.; Weyhermüller, T.; Chaudhuri, P. Polynuclear nickel(II) complexes: preparation and magnetic properties of Ni^{II}_4, Ni^{II}_5, and Ni^{II}_6 species with ligands containing $O^{\cap}X^{\cap}O$ (X= S, Se or N) donor atoms. *European Journal of Inorganic Chemistry* **2003**, (17), 3167-3178.

(85) Paine, T. K.; Weyhermüller, T.; Bill, E.; Bothe, E.; Chaudhuri, P. Non-oxo vanadium(IV) complexes of aminebis (phenolate)[O,N,O] donor ligands and solution studies of isostructural

V^{IV} and Mn^{IV} complexes. *European Journal of Inorganic Chemistry* **2003**, (24), 4299-4307.

(86) Balch, A. L. Electron-transfer series of the [M–O_2S_2] type. Complexes derived from *o*-mercaptophenol, 1-mercapto-2-naphthol, and 1-hydroxy-2-pyridinethione. *Journal of the American Chemical Society* **1969**, *91* (8), 1948-1953.

(87) Martin, J. L.; Takats, J. Complexes of the early transition metals with *o*-mercaptophenol and 1,2-dihydroxybenzene. *Canadian Journal of Chemistry* **1975**, *53* (4), 572-577.

(88) Kang, B.-S.; Xu, Y.-J.; Xie, X.-L.; Chen, C.-N.; Liu, Q.-T.; Liu, H.-Q.; Lu, J.-X. Phosphine-participated cluster formation: syntheses, structures, and magnetic properties of tri-and tetracobalt phosphine complexes of *o*-mercaptophenol (H_2mp), $Co_3(mp)_2(Hmp)_2(PEt_3)_3$ and $Co_4(mp)_4(PBu^n_3)_3Cl(MeOH)$. *Inorganic Chemistry* **1994**, *33* (17), 3770-3776.

(89) Shi, J.-C.; Wen, T.-B.; Zheng, Y.; Zhong, S.-J.; Wu, D.-X.; Liu, Q.-T.; Kang, B.-S.; Wu, B.-M.; Mak, T. C. Palladium complexes with simultaneous O:S coordination, syntheses, structures and characterization of complexes with 2-mercaptophenol or 2-mercaptopyridine N-oxide. *Polyhedron* **1997**, *16* (3), 369-375.

(90) Bouwkamp, M. W.; Bowman, A. C.; Lobkovsky, E.; Chirik, P. J. Iron-catalyzed [2π+ 2π] cycloaddition of α,ω-dienes: the importance of redox-active supporting ligands. *Journal of the American Chemical Society* **2006**, *128* (41), 13340-13341.

(91) Smith, A. L.; Hardcastle, K. I.; Soper, J. D. Redox-active ligand-mediated oxidative addition and reductive elimination at square planar cobalt(III): Multielectron reactions for cross-coupling. *Journal of the American Chemical Society* **2010**, *132* (41), 14358-14360.

(92) Ren, Y.; Cheaib, K.; Jacquet, J.; Vezin, H.; Fensterbank, L.; Orio, M.; Blanchard, S.; Desage-El Murr, M. Copper-catalyzed aziridination with redox-active ligands: Molecular

spin catalysis. *Chemistry–A European Journal* **2018**, *24* (20), 5086-5090.

(93) Sikari, R.; Sinha, S.; Chakraborty, G.; Das, S.; van Leest, N. P.; Paul, N. D. C−N cross-coupling reactions under mild conditions using singlet di-radical nickel(II)-complexes as catalyst: *N*-arylation and quinazoline synthesis. *Advanced Synthesis & Catalysis* **2019**, *361* (18), 4342-4353.

(94) Sikari, R.; Sinha, S.; Das, S.; Saha, A.; Chakraborty, G.; Mondal, R.; Paul, N. D. Achieving nickel catalyzed C–S cross-coupling under mild conditions using metal–ligand cooperativity. *The Journal of Organic Chemistry* **2019**, *84* (7), 4072-4085.

(95) Wang, Y.; Stack, T. Galactose oxidase model complexes: Catalytic reactivities. *Journal of the American Chemical Society* **1996**, *118* (51), 13097-13098.

(96) Chaudhuri, P.; Hess, M.; Flörke, U.; Wieghardt, K. From structural models of galactose oxidase to homogeneous catalysis: efficient aerobic oxidation of alcohols. *Angewandte Chemie International Edition* **1998**, *37* (16), 2217-2220.

(97) Chaudhuri, P.; Hess, M.; Müller, J.; Hildenbrand, K.; Bill, E.; Weyhermüller, T.; Wieghardt, K. Aerobic oxidation of primary alcohols (including methanol) by Copper(II)− and Zinc(II)−phenoxyl radical catalysts. *Journal of the American Chemical Society* **1999**, *121* (41), 9599-9610.

(98) Sharma, S. K.; May, P. S.; Jones, M. B.; Lense, S.; Hardcastle, K. I.; MacBeth, C. E. Catalytic dioxygen activation by Co(II) complexes employing a coordinatively versatile ligand scaffold. *Chemical Communications* **2011**, *47* (6), 1827-1829.

(99) Villanueva, O.; Weldy, N. M.; Blakey, S. B.; MacBeth, C. E. Cobalt catalyzed sp^3 C–H amination utilizing aryl azides. *Chemical Science* **2015**, *6* (11), 6672-6675.

(100) Corcos, A. R.; Villanueva, O.; Walroth, R. C.; Sharma, S. K.; Bacsa, J.; Lancaster, K. M.; MacBeth, C. E.; Berry, J. F. Oxygen activation by Co(II) and a redox non-innocent ligand: spectroscopic characterization of a radical–Co(II)–superoxide complex with divergent catalytic reactivity. *Journal of the American Chemical Society* **2016**, *138* (6), 1796-1799.

2. Chapter 2: Design and Syntheses of Novel Catecholamine Redox-Active Ligands and the Subsequent Metalations

Abstract

The design and application of redox-active ligands for facilitating first-row transition metal catalysis has grown in importance over the past decades. Traditionally, noble metals are used in catalysis due to their efficacy in promoting multi-electron reactions. On the other hand, first-row transition metals, although less expensive and more earth-abundant, are prone to undergo single-electron transformations, which pose limitations to their use in catalysis for common chemical reactions. One efficient strategy to promote multi-electron catalysis at first-row transition metal centers is by coordinating the first-row transition metals with redox-active ligands.[1] In this context, the development of novel redox-active ligands and their first-row transition metal complexes for catalysis is valuable for improving the sustainability of chemical transformations. In this work, two novel redox-active ligands containing both a multi-dentate nitrogenous moiety and catechol moieties were designed and synthesized to increase the coordinative versatility and electronic tunability of the corresponding metal complexes. Two synthetic routes will be presented for the preparation of the redox-active catecholamine ligands, 2,3-dihydroxy-*N*-(2-(phenylamino)phenyl)benzamide (H_4L^{CAT}) and *N*,*N'*-(azanediylbis(2,1-phenylene))bis(2,3-dihydroxybenzamide) (H_7L^{CAT}). With the newly synthesized ligands in hand, a large amount of effort was devoted to the investigation of different varieties of metalations. Crystals of $K_2[Cu(H_2L^{CAT})_2]$, $(PPh_4)_2[Cu(H_2L^{CAT})_2]$, $K_2CuH_3L^{CAT}$, a cobalt cluster complex, and an iron cluster complex were obtained and analyzed by X-ray crystallography. Cyclic voltammetry studies were carried out on

$K_2[Cu(H_2L^{CAT})_2]$ and the cobalt cluster. In addition, the oxidation of $K_2[Cu(H_2L^{CAT})_2]$ by dioxygen was monitored by UV-vis spectroscopy.

Introduction

Catalysts are widely used in modern chemical synthesis for the transformations of simple feedstocks into valuable products. Most catalytic reactions are mediated by transition metal complexes. Thus, developing efficient transition metal catalysts for the preparation of organic compounds is of crucial importance. One approach for catalyst design involves expensive noble metals, such as second-row and third-row transition metals, for multi-electron transformations. This approach has been widely studied over the past 200 years.[2] However, noble transition metal catalysts have been facing sustainability-related challenges since the limited natural abundance of such metals may not meet the increasing demand for chemical products. Furthermore, the utilization of those noble metals involves high cost and concerns about toxicity.

Being less expensive, earth-abundant, and environmentally benign, first-row transition metal catalysts have attracted increasing attention in sustainable catalyst design. One limitation to this approach is that the first-row transition metal complexes tend to undergo one-electron redox events rather than two-electron processes which are necessary for a variety of catalytic conversions, including oxidative addition, reductive elimination, and atom transfer reactions. Nature, on the other hand, has offered ample examples of incorporating redox-active moieties to the first-row transition metal active sites of different enzymes to solve the issue. The redox-active ligands in the complexes can store and mediate electron-transfer as well as promote multi-electron catalytic reactions.[2] Inspired by nature, significant effort has been devoted to developing complexes that incorporate redox-active ligands to facilitate stoichiometric and catalytic multi-electron reactions. This approach

imparts noble-metal character to more abundant, less toxic first-row transition metals, such as Fe, Co, Ni, Cu and Zn in the multi-electron reactions.[2]

Because of redox-active ligands' potential in catalytic systems, their design and application in metal complexes have attracted extensive attention during the past decades. By incorporating redox-active ligands, the reactivity of the metal centers could be modified, offering more possibilities in elementary bond activation steps in a catalytic cycle.[3,4] In these complexes, the metal centers and redox active ligands can work synergistically to facilitate chemical processes[1] and enhance activity in catalytic reactions.[5]

A variety of redox-active moieties have been explored over the past 90 years. Examples of developed redox-active ligands include dithiolene, diimine, and catechol functionalities.[6] A common feature for most redox-active ligands is the presence of extensive π-networks that can help stabilize ligand-based radicals. Catechol groups are frequently incorporated in redox-active ligands with their ability to access three different oxidation states as shown in Scheme 2-1. Iron and manganese complexes coordinated to catechol groups have been studied to be catechol oxidation catalysts (Figure 2-1).[7,8]

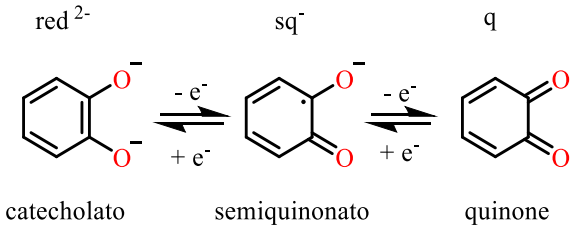

Scheme 2-1. The three possible oxidation states of the catechol ligands.

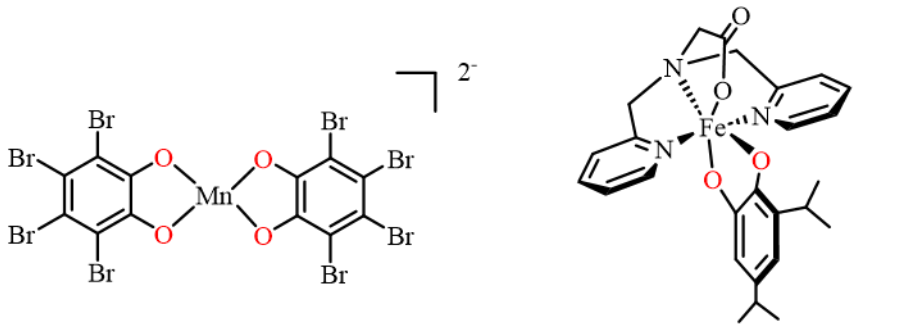

Tyson, C. A. and Martell A. E.,
J. Am. Chem. Soc., **1972**, *94*, 939 .

Cox, D. D. and L. Que, Jr.
J. Am. Chem. Soc., **1988**, *110*, 8085.

Figure 2-1. Reported examples of catalysts involving catechol groups in the redox-active ligand frameworks.

Ligand systems with nitrogenous groups have also received attention with transition metals for a variety of catalytic transformations.[9,10] Attaching another donor-moiety to a diamine backbone produces modular ligand with bidentate and tridentate possibilities as shown in Figure 2-2.[11] Like catechols, these tridentate, pincer-type ligands can act as reservoirs for multi-electron transformations in the catalytic reactions (Scheme 2-2). The first-row transition metal complexes coordinated to these ligands have been shown to be efficient catalysts for alcohol oxidation (Ni(II) center),[11] dioxygen activation, and C–H activation (Co(II) center) (Figure 2-3).[12]

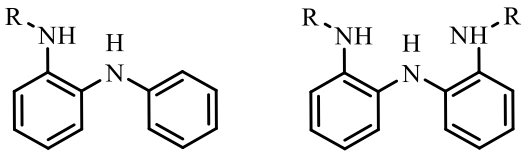

Figure 2-2. Bidentate (L^A) and tridentate (L^B) ligands from diamine backbone.

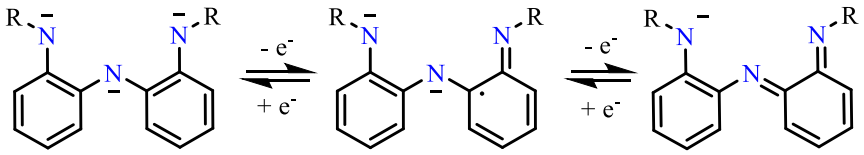

Scheme 2-2. The three possible oxidation states of triamine tridentate pincer-type ligands.

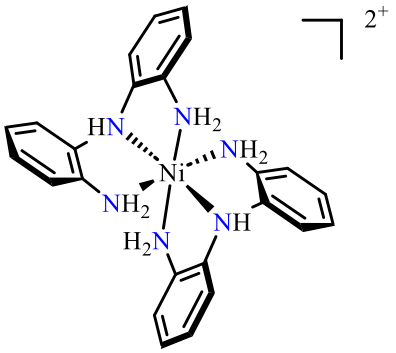

Sikari, R. et al. Inorg. Chem. **2016**, *55* (12), 6114-6123.

Alcohol oxidation catalyst

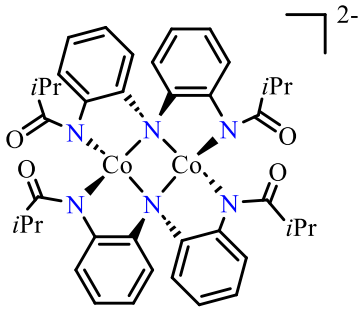

Corcos, A. R. et al. J. Am. Chem. Soc. **2016**, *138* (6), 1796-1799.

Dioxygen activation and C-H activation catalyst

Figure 2-3. Reported catalysts involving nitrogenous groups in the redox-active ligand frameworks.

Inspired by the reactivity of the catechol and nitrogenous systems, we proposed that the incorporation of both the nitrogenous system and the catechol system in the same ligand scaffolds would provide the ligands with coordinative versatility and increased electronic tunability. When coordinated to first-row transition metal centers as electron reservoirs, these ligands would give rise to a variety of multi-electron transformations, thus affording more potential catalytic reactivity. To this end, we designed both the mono- and di-substituted amine ligand scaffolds as shown in Figure 2-4.

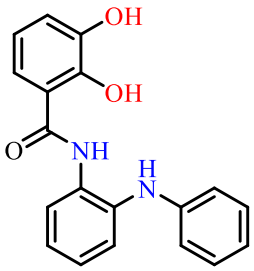

2,3-dihydroxy-*N*-(2-(phenylamino) phenyl)benzamide

H_4L^{CAT}

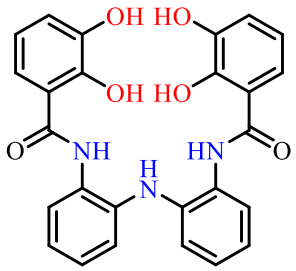

N,*N*'-(azanediylbis(2,1-phenylene)) bis(2,3-dihydroxybenzamide)

H_7L^{CAT}

Figure 2-4. Target redox-active ligands, H_4L^{CAT} and H_7L^{CAT}.

In addition, the designed redox-active ligands have two potential sites for metalation: the amine sites on the diamine/ triamine moiety and alcohol sites on the catechol moiety. We believe that these metalation sites would allow the synthesis of hetero- and homo-bimetallic complexes (Figure 2-5) which can mimic metalloenzymes involving multi-metallic systems, such as copper-based oxidases and oxygenases,[13,14] non-heme iron-based active sites,[15] dinuclear nickel-containing systems[16] as well as many mixed-metal biocatalysts.[17]

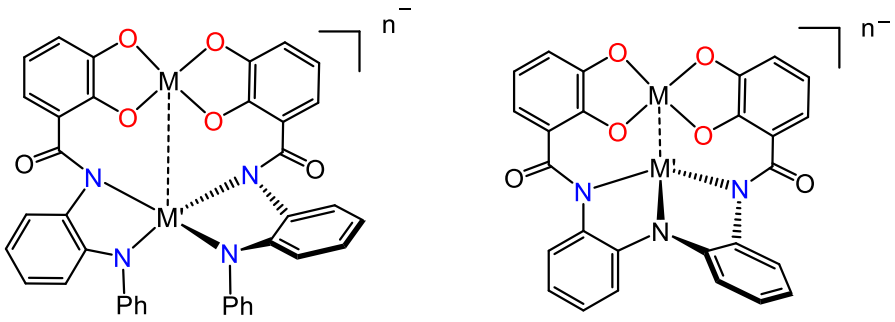

Complex **1** Complex **2**

Figure 2-5. Target complexes.

Results and discussions

To obtain the desired redox-active ligands, two synthetic pathways were proposed: (1) a condensation/demethylation pathway and (2) a protection/condensation/deprotection pathway.

Syntheses of the designed redox-active ligands through pathway I

The condensation reaction of bis(2-aminophenyl)amine and 2,3-dimethoxybenzoic acid forms *N*,*N*′-(azanediylbis(2,1-phenylene))bis(2,3-dimethoxybenzamide) (**2-1**) in 82% yield (Scheme 2-3). Compound **2-1** was characterized by ^{1}H NMR (Figure 2-6), ^{13}C NMR (Figure 2-7), electrospray ionization mass spectrometry, and X-ray crystallography (Figure 2-8).

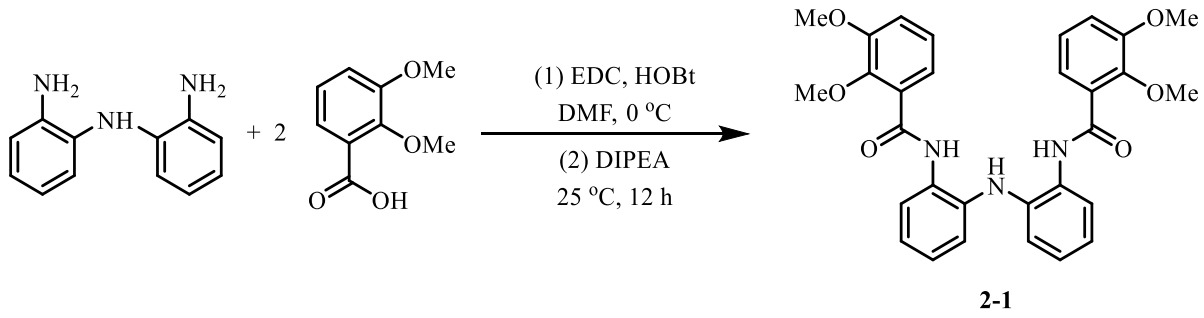

2-1

Scheme 2-3. Synthesis of compound **2-1**.

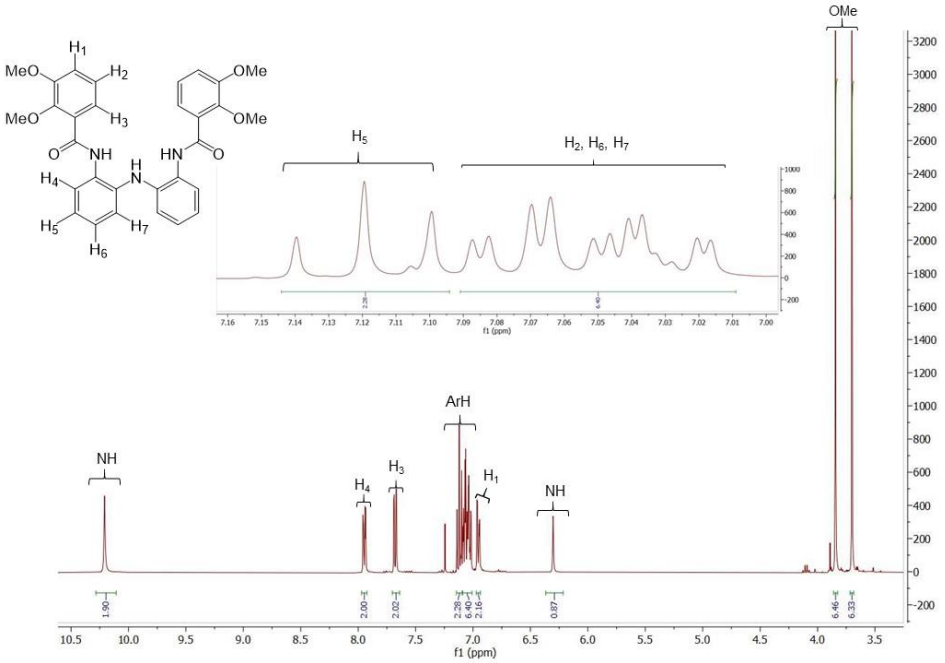

Figure 2-6. ^{1}H NMR of compound **2-1**.

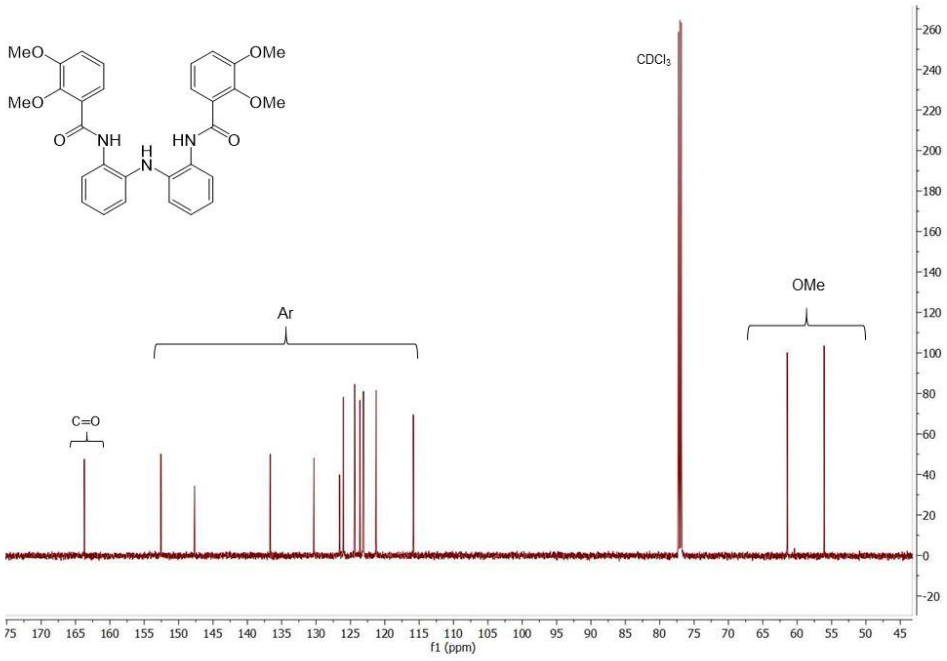

Figure 2-7. ^{13}C NMR of compound **2-1**.

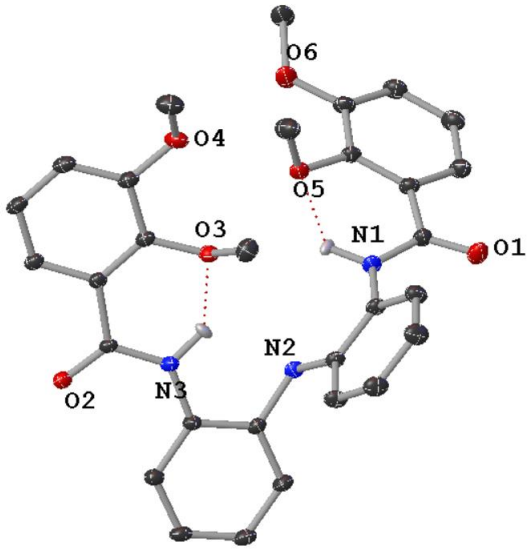

Figure 2-8. Solid-state structure of compound **2-1** as determined by single X-ray crystallography. Most hydrogen atoms are omitted for clarity.

A crystal of compound **2-1** was obtained by vapor diffusion of hexane into a dichloromethane (DCM) solution of compound **2-1** (Figure 2-8). The solid-state structure determined by X-ray crystallography reveals the presence of hydrogen bonding interactions between each pair of amides and methoxy moieties in compound **2-1**.

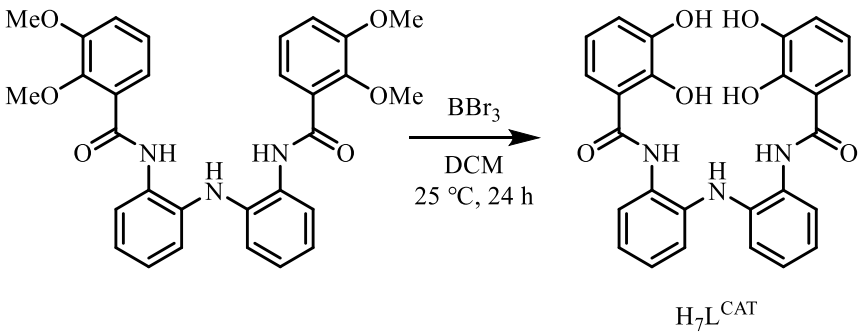

Scheme 2-4. Synthesis of H_7L^{CAT}.

The demethylation was performed with boron tribromide in dichloromethane for 24 hours (Scheme 2-4).[18] It is worth mentioning that the initial demethylations were carried out using an old bottle of 1.0 M BBr_3 in dichloromethane solution that appeared brown, likely

due to Br_2 contamination. H_7L^{CAT} was characterized by ^1H NMR, ^{13}C NMR, electrospray ionization mass spectrometry. Crystallization attempts were not successful.

Initial metalation attempts were made by deprotonating the ligand with four equivalents of KH, followed by the addition of one equivalent of $NiBr_2$ and two equivalents of PPh_4Br (Scheme 2-5). The product isolated from this reaction turned out to be a boron complex instead of the proposed Ni complex. The solid-state structure of the unexpected boron complex as determined by single X-ray crystallography is shown in Figure 2-9.

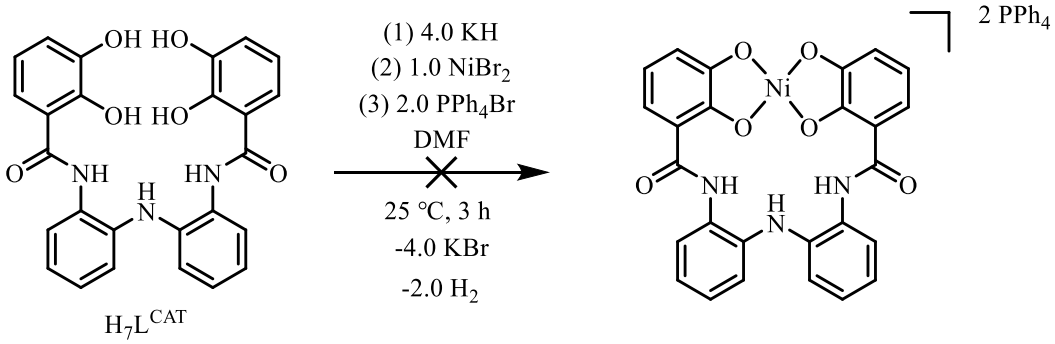

H_7L^{CAT}

Scheme 2-5. Attempted metalation of H_7L^{CAT}.

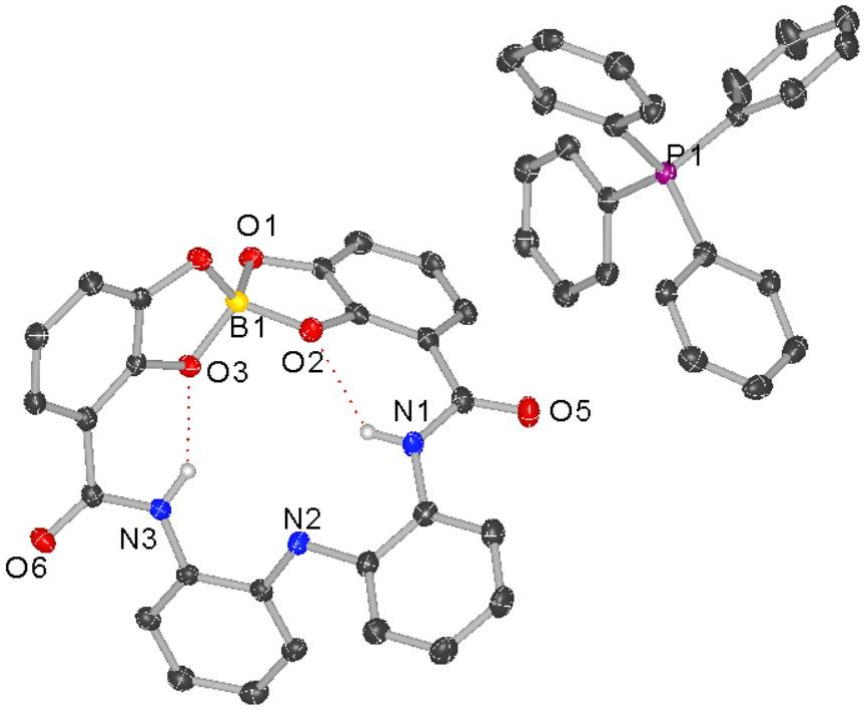

Figure 2-9. Solid-state structure of boron complex as determined by single X-ray

crystallography. Most hydrogen atoms are omitted for clarity.

We postulated that the boron atom is introduced from the demethylation step where BBr_3 is used. A ^{11}B NMR was taken to prove the presence of boron in the demethylated product. The ^{11}B NMR result (Figure 2-10) showed boron peaks at around 14 ppm, which is typical of tetra-alkoxy borate species, suggesting that boron is present in the product after demethylation. The other two peaks might correspond to disassociated boron species in the deuterated methanol solvent, and the broad peak is the result of boron species from the NMR tube. The formation of the boron compound is possibly due to the proximity of two catechol moieties that provide favorable environment for the coordination of electron deficient boron atom.

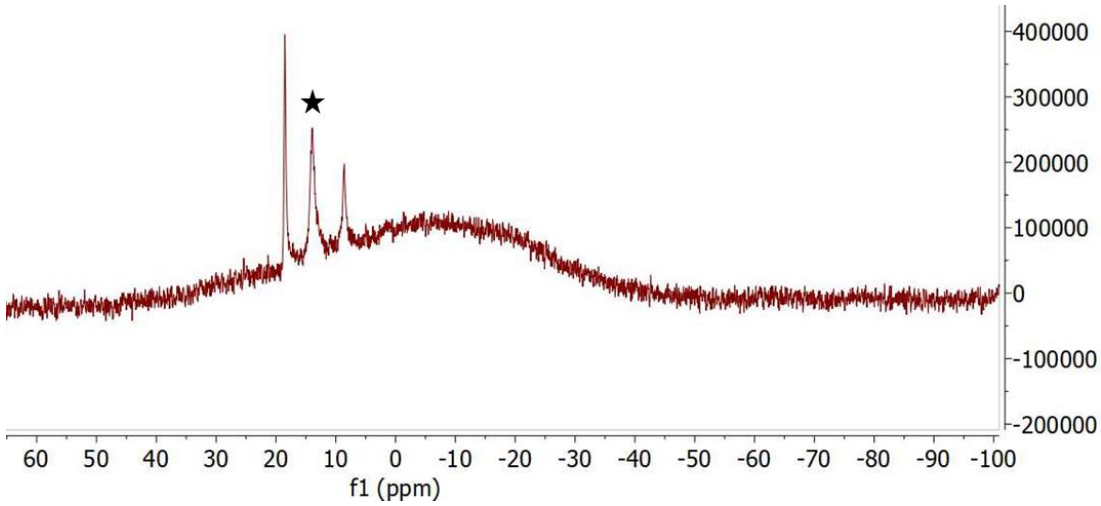

Figure 2-10. ^{11}B NMR of the product after demethylation.

Demethylation was attempted through several other approaches such as by using iodocyclohexane[19] or aluminium powder with iodine[20]; however, these methods were not able to achieve the simultaneous demethylation of four methoxy groups (Scheme 2-6).

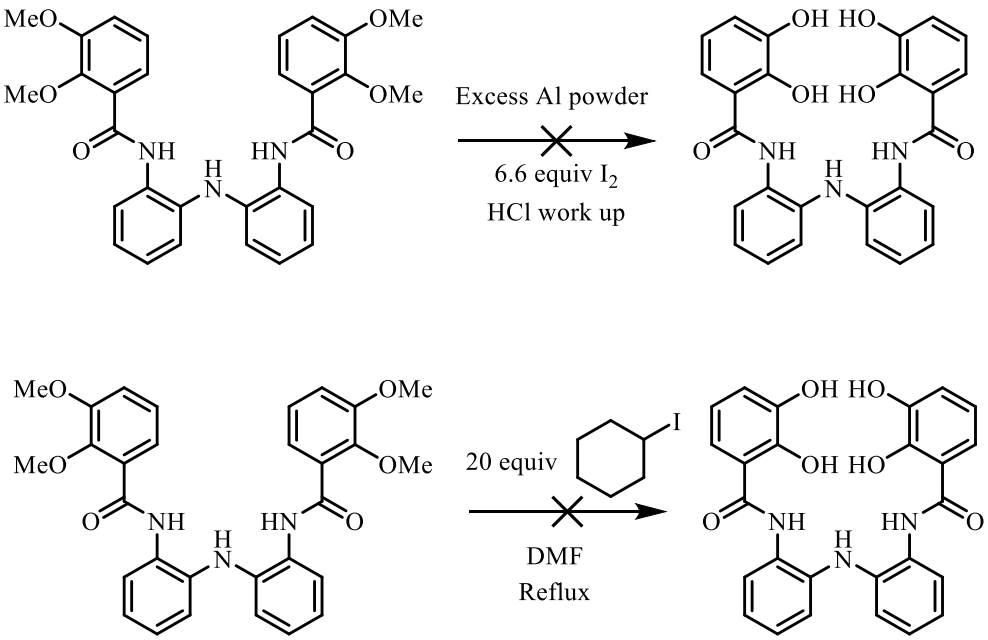

Scheme 2-6. Other attempted demethylation reactions.

While we were investigating the formation of the boron complex, the odd brown color of the old BBr_3 solution caught our attention. This brown color was likely due to the Br_2 contamination which indicates the decomposition of BBr_3 in the reagent used. To exclude this possibility, a new bottle of 1 mol/L BBr_3 solution in dichloromethane was purchased and used in the following demethylation reaction. The quenching process by DI water was prolonged until clear separation of the aqueous and organic layer was observed to ensure full removal of water-soluble boron species in the product. After these adjustments, the demethylation of **2-1** by BBr_3 was able to be achieved with full conversion in 26 hours by using three equivalents of BBr_3. A single colorless block crystal of the product H_7L^{CAT} was obtained from dichloromethane by slow evaporation. The X-ray crystal structure of H_7L^{CAT} is shown in Figure 2-11.

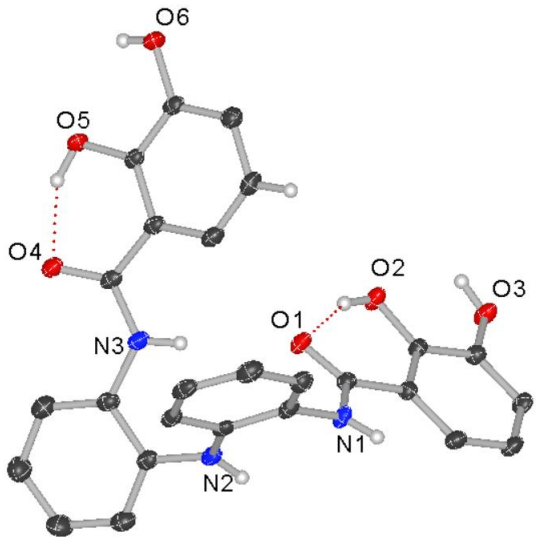

Figure 2-11. Solid-state structure of H_7L^{CAT} as determined by single X-ray crystallography. Most hydrogen atoms are omitted for clarity.

Syntheses of the designed redox-active ligands through pathway II

Inspired by the recently reported synthesis of β-dicarbonyl(bis-catecholamine) ligands,[21] the protection of hydroxy groups by benzyl groups and deprotection by hydrogenation reaction was applied in pathway II. Pathway II allowed the successful syntheses of desired redox-active ligands H_4L^{CAT} and H_7L^{CAT} (Scheme 2-7). Various techniques such as ^{1}H NMR (Figure 2-12), ^{13}C NMR (Figure 2-13), MS-ESI and X-ray crystallography were used to characterize the ligands.

Step 1: Protection of -OH groups

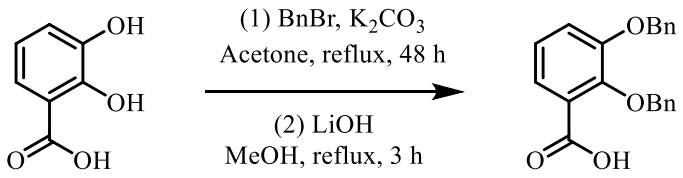

Step 2: Condensation reaction

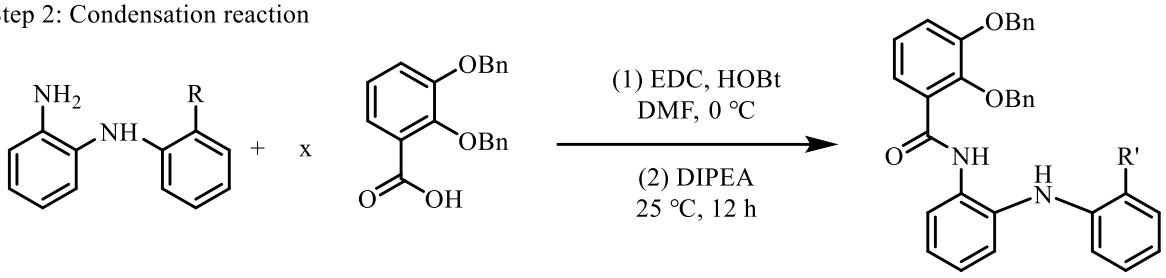

H_4L^{CAT}: R= H, X=1,R'=H

H_7L^{CAT}: R=NH_2, X=2, R'=

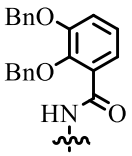

Step 3: Hydrogenation

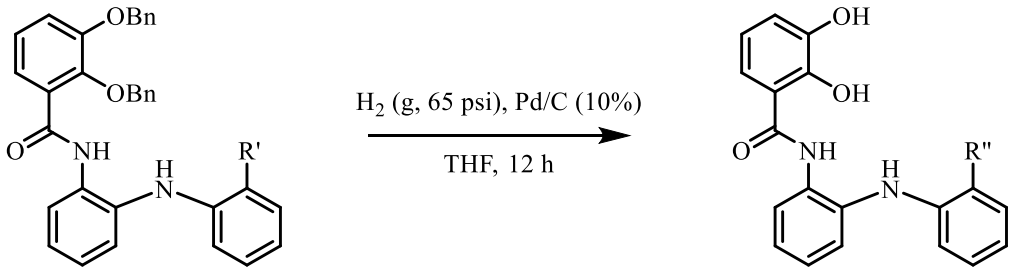

H_4L^{CAT}: R'=H, R''=H

H_7L^{CAT}: R'=

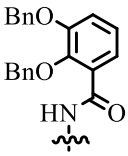

R''=

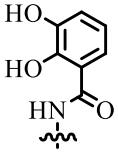

Scheme 2-7. Syntheses of H_4L^{CAT} and H_7L^{CAT} ligand through pathway II.

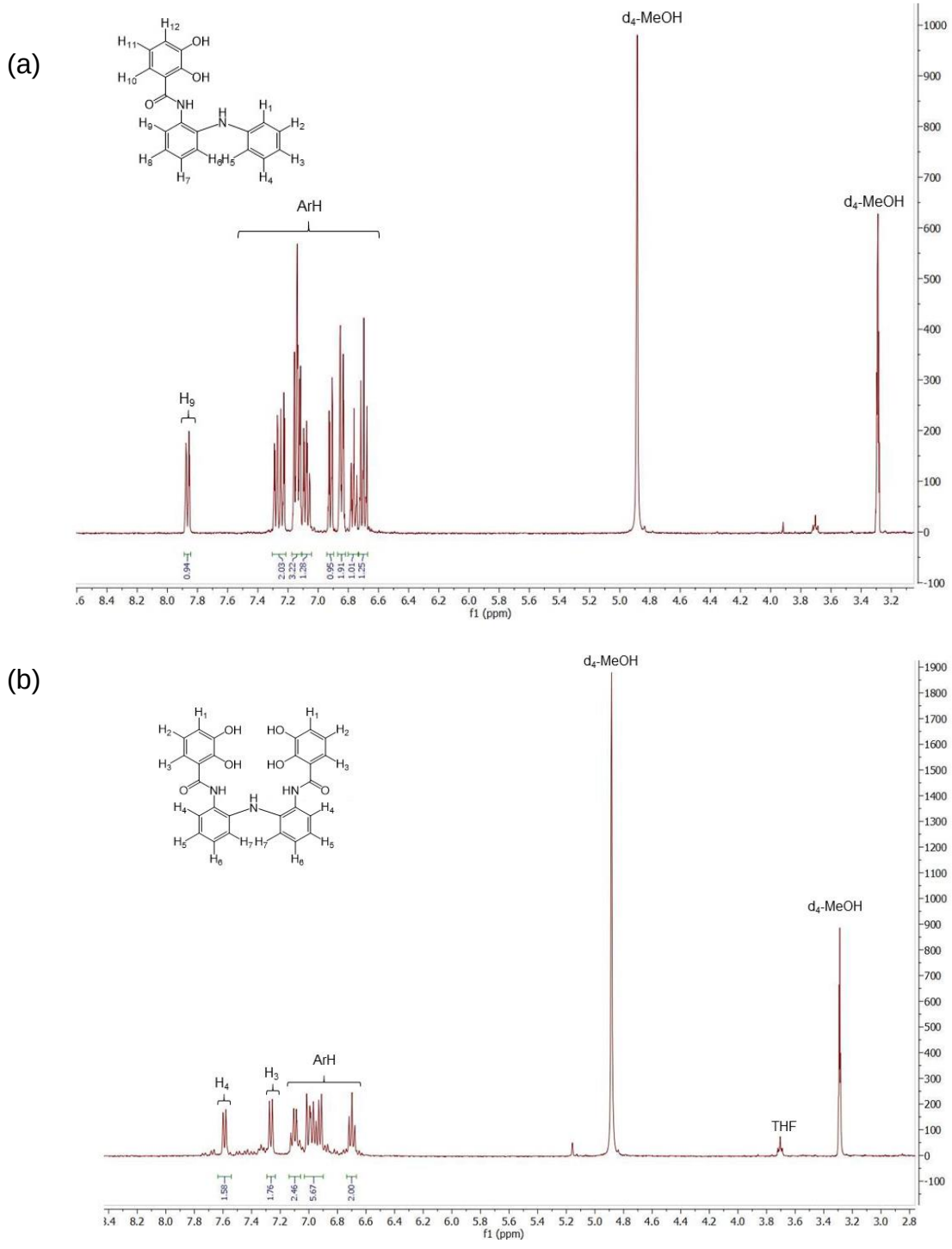

Figure 2-12. ^{1}H NMR of (a) ligand H_4L^{CAT} and (b) ligand H_7L^{CAT} in deuterated methanol.

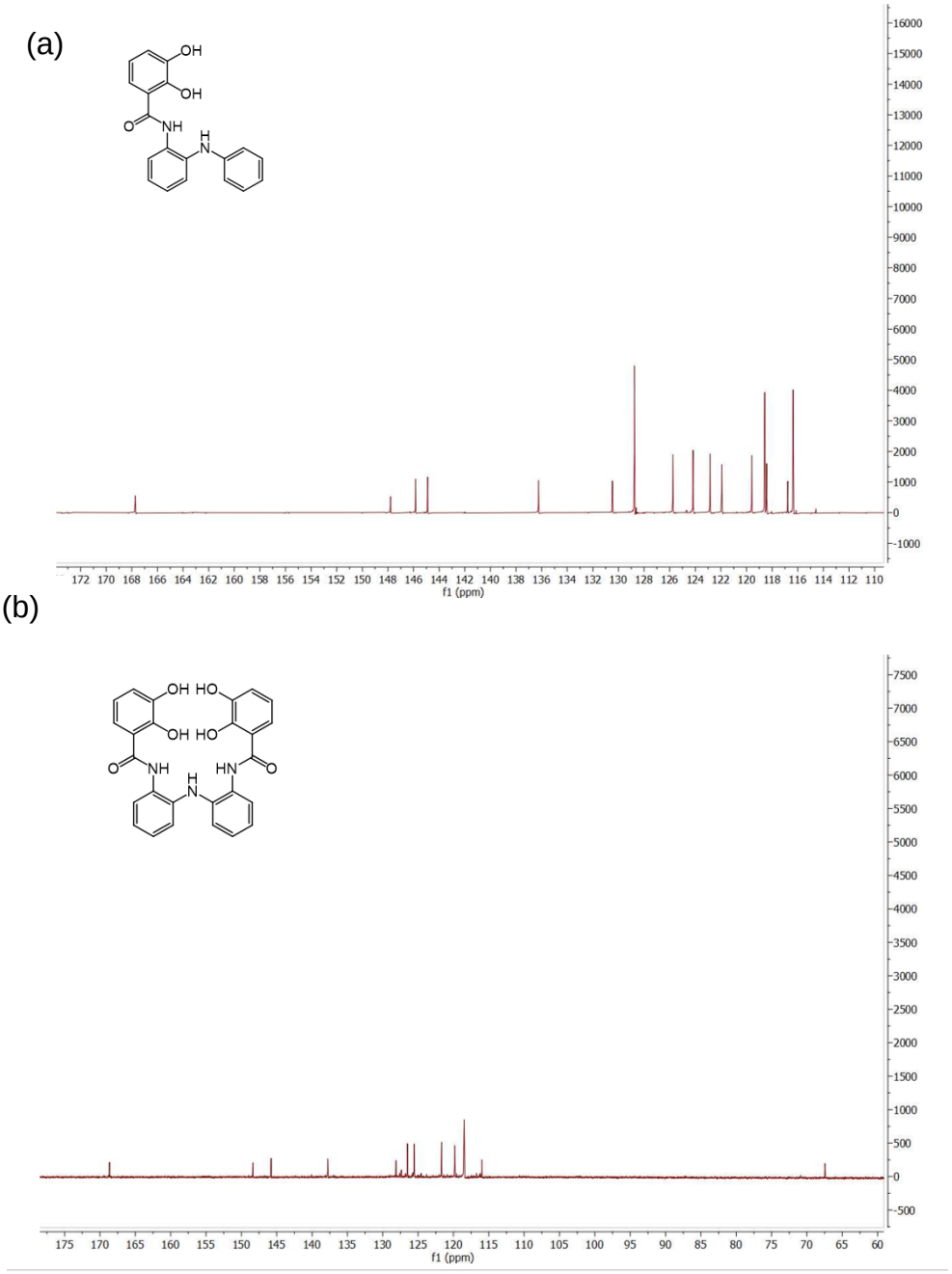

Figure 2-13. ^{13}C NMR of (a) ligand H_4L^{CAT} and ligand (b) H_7L^{CAT}.

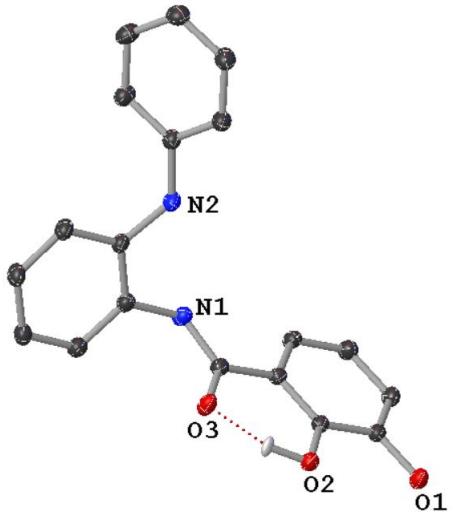

Figure 2-14. Solid-state structure of ligand H_4L^{CAT} as determined by single X-ray crystallography. Most hydrogen atoms are omitted for clarity.

Orange prism-shaped single crystals of ligand H_4L^{CAT} suitable for X-ray diffraction studies were obtained by vapor diffusion of pentane into a toluene solution of H_4L^{CAT} (Figure 2-14).

Syntheses of metal complexes

With the designed H_4L^{CAT} and H_7L^{CAT} ligands synthesized and fully characterized, they were then utilized for metalations. In the deprotonation step, catechol moieties in the ligands tend to be deprotonated first due to their smaller pKa value compared to protons on nitrogenous group. Metalations were attempted with a) a deprotonation of catechol moieties followed by an addition of one metal salt; (b) a deprotonation of catechol moieties followed by an addition of one metal salt, and then another deprotonation of nitrogenous moieties followed by an addition of another metal salt; (c) a full deprotonation of the ligand followed by an addition of two different metal salts (Scheme 2-8). The attempted metalations are summarized in Table 2-1. Countercation exchange using PPh_4Br was attempted to facilitate recrystallization of the metal complexes.

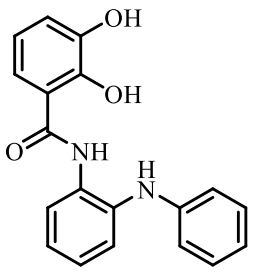

H_4L^{CAT}

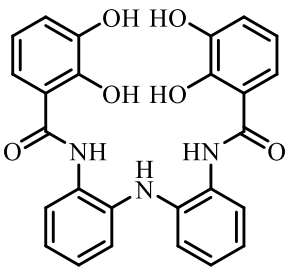

H_7L^{CAT}

(a) H_4L^{CAT} + 2 KH + 0.5 Metal salt

H_7L^{CAT} + 4 KH + 1.0 Metal salt

(b) H_4L^{CAT} + 2 KH + 0.5 Metal salt A + 2 KH + 0.5 Metal salt B

H_7L^{CAT} + 4 KH + 1.0 Metal salt A + 3 KH + 1.0 Metal salt B

(c) H_4L^{CAT} + 4 KH + 0.5 Metal salt A + 0.5 Metal salt B

H_7L^{CAT} + 7 KH + 1.0 Metal salt A + 1.0 Metal salt B

Scheme 2-8. Three metalation approaches.

Table 2-1. Attempted metalations.

(a) H_4L^{CAT} + 2 KH + 0.5 Metal salt

H_7L^{CAT} + 4 KH + 1.0 Metal salt

Metalations (a)		
Ligand	Metal A	Countercation
H_4L^{CAT}	$CuBr_2$	K^+
H_4L^{CAT}	$FeCl_2$	K^+
H_4L^{CAT}	$NiBr_2$	K^+
H_4L^{CAT}	$CoBr_2$	K^+
H_4L^{CAT}	CuBr	K^+
H_4L^{CAT}	$ZnBr_2$	K^+
H_7L^{CAT}	$CuBr_2$	PPh_4^+
H_7L^{CAT}	$FeCl_2$	PPh_4^+
H_7L^{CAT}	$NiBr_2$	PPh_4^+
H_7L^{CAT}	$CoBr_2$	PPh_4^+
H_7L^{CAT}	$CuBr_2$	K^+
H_7L^{CAT}	$FeBr_3$	PPh_4^+

(b) H_4L^{CAT} + 2 KH + 0.5 Metal salt A + 2 KH + 0.5 Metal salt B

H_7L^{CAT} + 4 KH + 1.0 Metal salt A + 3 KH + 1.0 Metal salt B

Metalations (b)			
Ligand	Metal A	Metal B	Countercation
H_4L^{CAT}	$ZnCl_2$	$CuBr_2$	K^+
H_4L^{CAT}	$ZnCl_2$	$CuBr_2$	PPh_4^+
H_4L^{CAT}	$NiBr_2$	$CuBr_2$	K^+
H_4L^{CAT}	$NiBr_2$	$CuBr_2$	PPh_4^+
H_4L^{CAT}	$ZnCl_2$	$CoBr_2$	K^+
H_4L^{CAT}	$FeCl_2$	$CoBr_2$	K^+
H_4L^{CAT}	$FeCl_2$	$ZnBr_2$	K^+
H_4L^{CAT}	$CoBr_2$	$ZnBr_2$	K^+
H_4L^{CAT}	CuBr	$CoBr_2$	K^+
H_4L^{CAT}	CuBr	$FeBr_3$	K^+
H_4L^{CAT}	$ZnBr_2$	$CuBr_2$	PPh_4^+
H_7L^{CAT}	$ZnCl_2$	$CoBr_2$	K^+
H_7L^{CAT}	$ZnCl_2$	$FeCl_2$	K^+
H_7L^{CAT}	$FeBr_3$	$NiBr_2$	K^+
H_7L^{CAT}	$FeCl_2$	$CoBr_2$	K^+
H_7L^{CAT}	$FeCl_2$	$ZnBr_2$	K^+
H_7L^{CAT}	$CoBr_2$	$ZnBr_2$	K^+
H_7L^{CAT}	CuBr	$CoBr_2$	K^+
H_7L^{CAT}	CuBr	$FeBr_3$	K^+

(c) H_4L^{CAT} + 4 KH + 0.5 Metal salt A + 0.5 Metal salt B

H_7L^{CAT} + 7 KH + 1.0 Metal salt A + 1.0 Metal salt B

Metalations (c)			
Ligand	Metal A	Metal B	Countercation
H_4L^{CAT}	$CuBr_2$	$CuBr_2$	K^+
H_4L^{CAT}	$CuBr_2$	$NiBr_2$	K^+
H_4L^{CAT}	$CuBr_2$	$CoBr_2$	K^+
H_4L^{CAT}	$CuBr_2$	$FeCl_2$	K^+
H_4L^{CAT}	$CuBr_2$	$FeCl_2$	PPh_4^+
H_4L^{CAT}	$CuBr_2$	$ZnCl_2$	K^+
H_7L^{CAT}	$CuBr_2$	$NiBr_2$	PPh_4^+
H_7L^{CAT}	$CuBr_2$	$CoBr_2$	PPh_4^+
H_7L^{CAT}	$ZnCl_2$	$CoBr_2$	PPh_4^+
H_7L^{CAT}	$CuBr_2$	$CoBr_2$	K^+
H_7L^{CAT}	$CuBr_2$	$FeCl_2$	K^+
H_7L^{CAT}	$CuBr_2$	$FeBr_3$	K^+
H_7L^{CAT}	$CuBr_2$	$ZnBr_2$	K^+

Although many metalations and a significant number of recrystallizations were attempted, only a few successfully yielded the crystals that were suitable for single X-ray crystallography. Shown in Scheme 2-9 are the syntheses of two monometallic Cu(II) complexes with ligand H_4L^{CAT} in two different countercations. Ligand H_4L^{CAT} was first treated with two equivalents of KH, followed by addition of half equivalent of $CuBr_2$ to form the metal complexes.

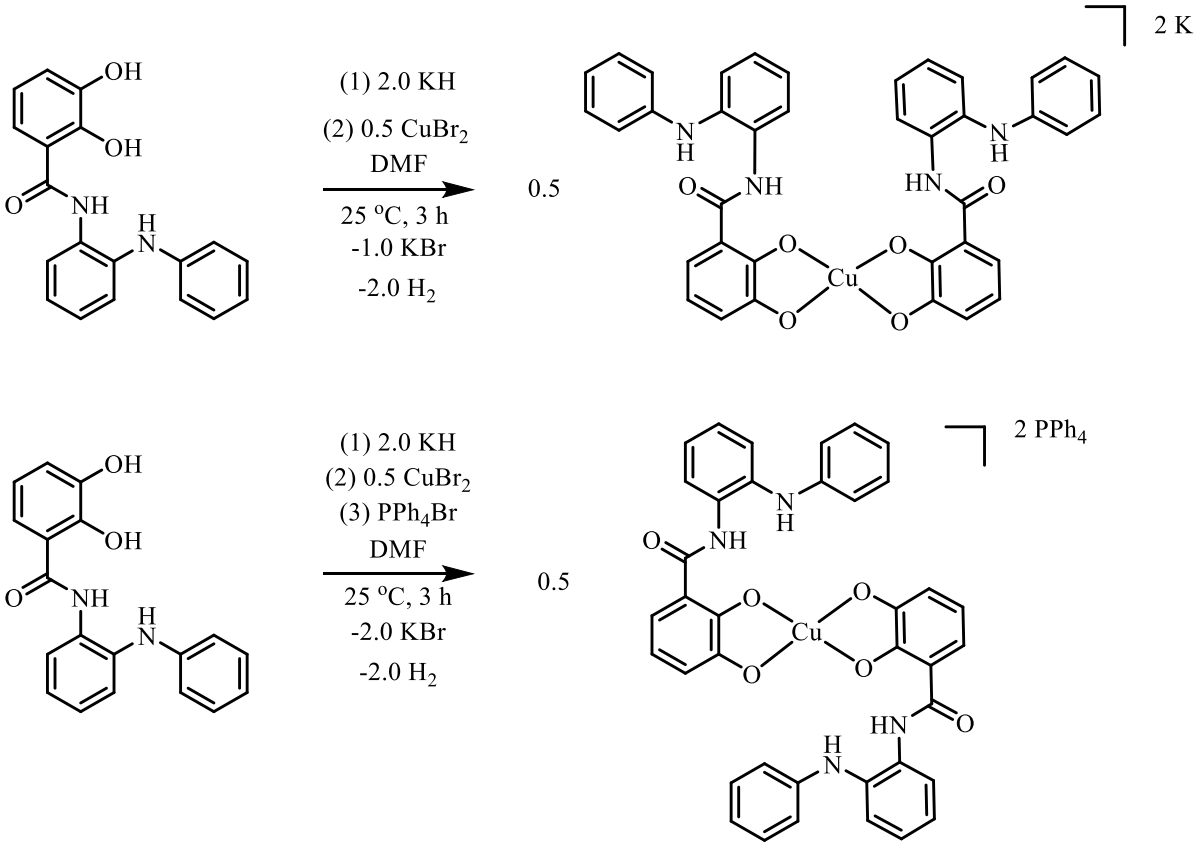

Scheme 2-9. Syntheses of monometallic Cu(II) complexes with ligand H_4L^{CAT}.

The solid-state structures of $K_2[Cu(H_2L^{CAT})_2]$ and $(PPh_4)_2[Cu(H_2L^{CAT})_2]$ as determined by single X-ray crystallography are shown in Figure 2-15. Different coordination environments were observed in their structures. In $K_2[Cu(H_2L^{CAT})_2]$, two potassium countercations are coordinated to the oxygen atoms of ligand backbone and the solvent

dimethylformamide. This is not observed in the corresponding $(PPh_4)_2[Cu(H_2L^{CAT})_2]$ complex because the PPh_4^+ countercations are non-coordinating. In addition, the structure of $K_2[Cu(H_2L^{CAT})_2]$ is less linear likely due to the interaction between potassium and oxygen atom that pulls the ligand together. The Cu–O distances are compared and summarized in Table 2-2.

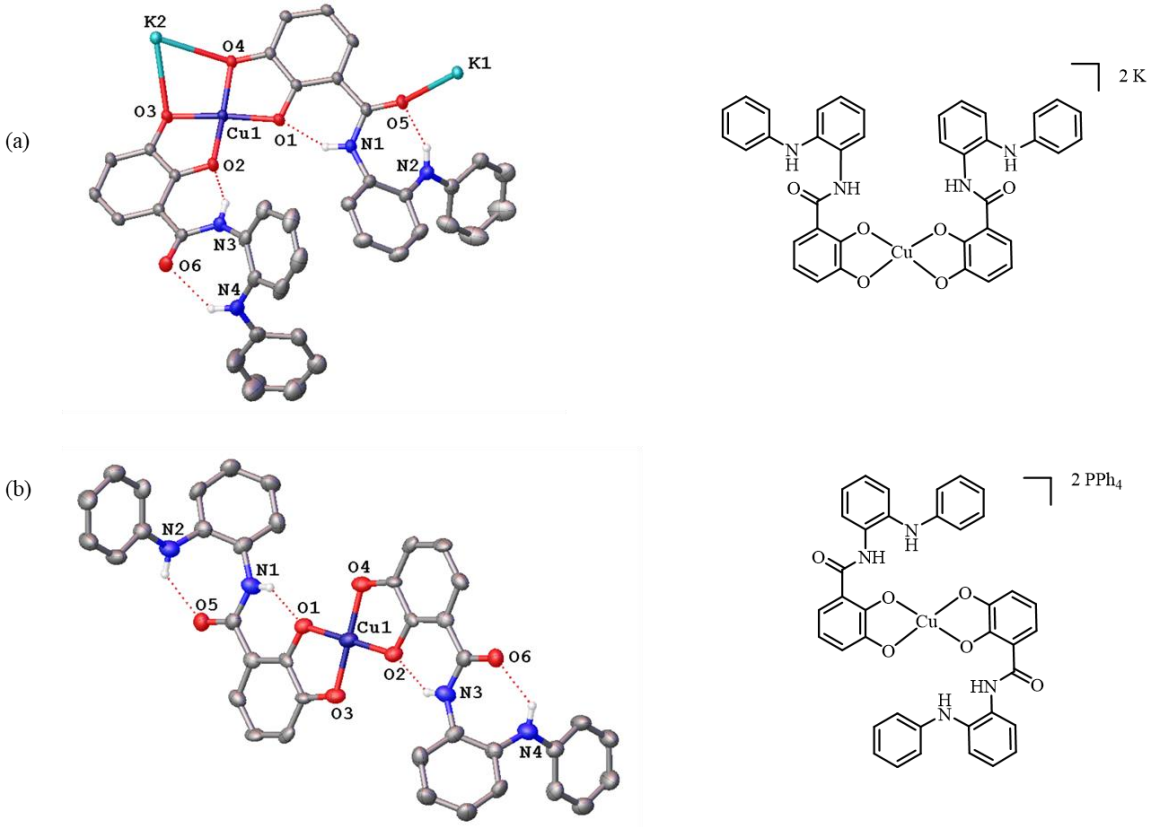

Figure 2-15. Solid-state structures of monometallic Cu(II) complexes with ligand H_4L^{CAT} as determined by single X-ray crystallography, (a) K^+ as the countercation, (b) PPh_4^+ as the countercation. Hydrogen atoms except those involved in H-bonds are omitted for clarity.

Table 2-2. Comparison of distances between Cu and O atoms in $K_2[Cu(H_2L^{CAT})_2]$ and $(PPh_4)_2[Cu(H_2L^{CAT})_2]$.

	$K_2[Cu(H_2L^{CAT})_2]$	$(PPh_4)_2[Cu(H_2L^{CAT})_2]$
Cu–O1	1.914 Å	1.916 Å
Cu–O2	1.920 Å	1.916 Å
Cu–O3	1.916 Å	1.886 Å
Cu–O4	1.919 Å	1.886 Å

A crystal of monometallic Cu(II) complex with ligand H_7L^{CAT} (Scheme 2-10) was also obtained by vapor diffusion of pentane into a tetrahydrofuran and dimethylformamide solution of the complex. Its solid-state structure as determined by single X-ray crystallography is shown in Figure 2-16.

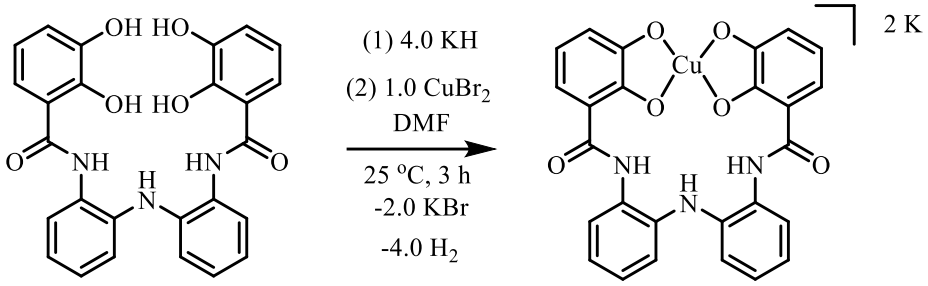

Scheme 2-10. Synthesis of $K_2CuH_3L^{CAT}$.

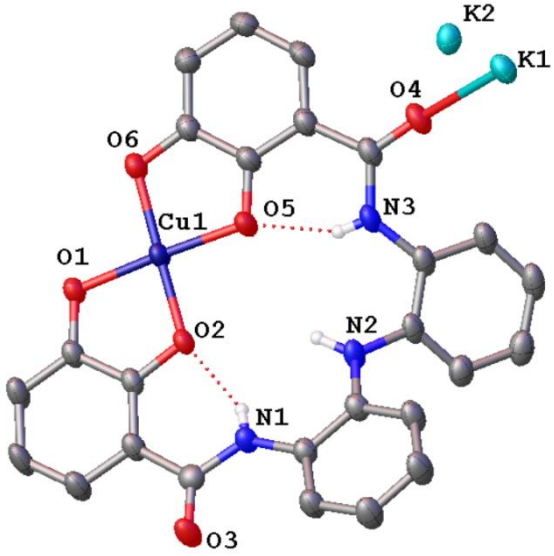

Figure 2-16. Solid-state structure of $K_2CuH_3L^{CAT}$ as determined by single X-ray crystallography. Most hydrogen atoms are omitted for clarity.

τ_4 is a geometry parameter for 4-coordinate compound. $\tau_4 = \frac{360°-(\alpha+\beta)}{360°-2\theta} \approx -0.00709\,(\alpha+\beta) + 2.55$, where α and β are the two greatest valence angles of coordination center; θ ≈ 109.5° which is a tetrahedral angle. When τ_4 is close to 0, the geometry is similar to square planar; while if τ_4 is close to 1, then the geometry is similar to tetrahedral. A

comparison of the τ_4 values of coordination centers in Cu(II) complexes $K_2[Cu(H_2L^{CAT})_2]$, $(PPh_4)_2[Cu(H_2L^{CAT})_2]$, and $K_2CuH_3L^{CAT}$ is shown in Figure 2-17. All three Cu(II) complexes show square planar or pseudo-square planar geometry around the coordination center.

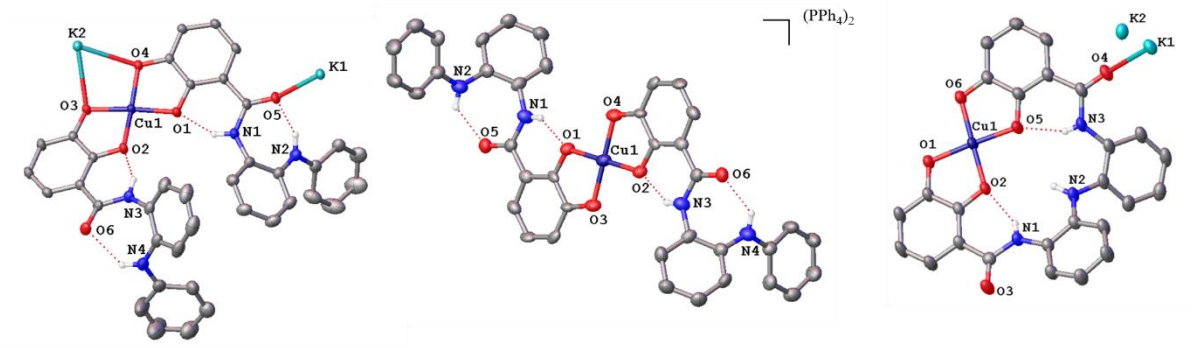

$K_2[Cu(H_2L^{CAT})_2]$ τ_4= 0.15

$(PPh_4)_2[Cu(H_2L^{CAT})_2]$ τ_4= 0, Square planar

$K_2CuH_3L^{CAT}$ τ_4= 0.06

Figure 2-17. A comparison of the τ_4 values of coordination centers in Cu(II) complexes $K_2[Cu(H_2L^{CAT})_2]$, $(PPh_4)_2[Cu(H_2L^{CAT})_2]$, and $K_2CuH_3L^{CAT}$.

In addition, two interesting cluster complexes were obtained. One is ligand H_7L^{CAT} coordinated with cobalt centers as shown in Scheme 2-11. Its solid-state structure was identified to contain three ligand units, four cobalt ions and two tetraphenyl phosphonium countercations in a unit cell (Figure 2-18). The zoomed-in coordination environment around the cobalt centers is shown in Figure 2-19. This cobalt cluster complex was also studied by cyclic voltammetry and the result is shown in Figure 2-20.

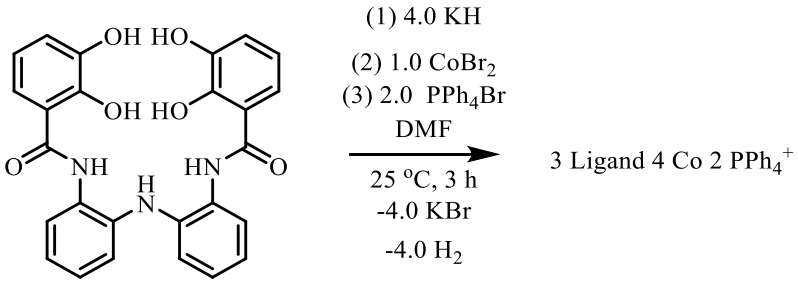

Scheme 2-11. Synthesis of cobalt cluster.

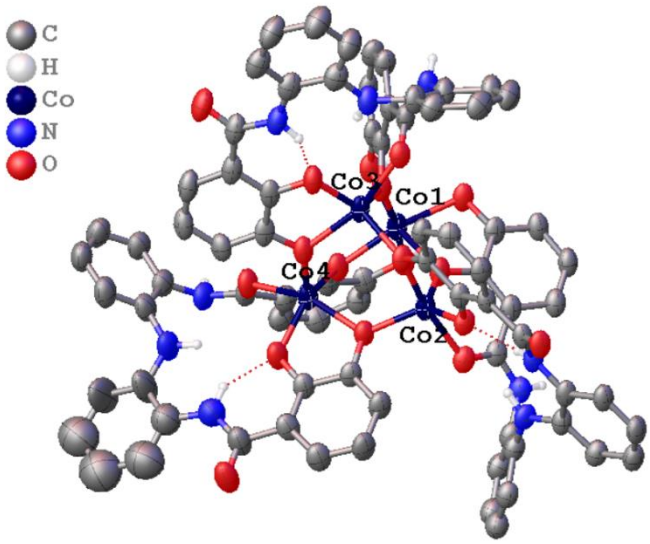

Figure 2-18. Solid-state structure of cobalt cluster as determined by single X-ray crystallography.

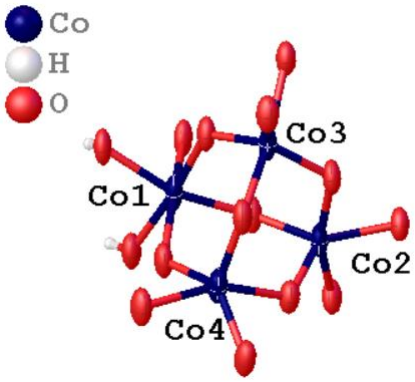

Figure 2-19. The zoomed-in coordination environment around the metal centers in the cobalt cluster complex with ligand H_7L^{CAT}.

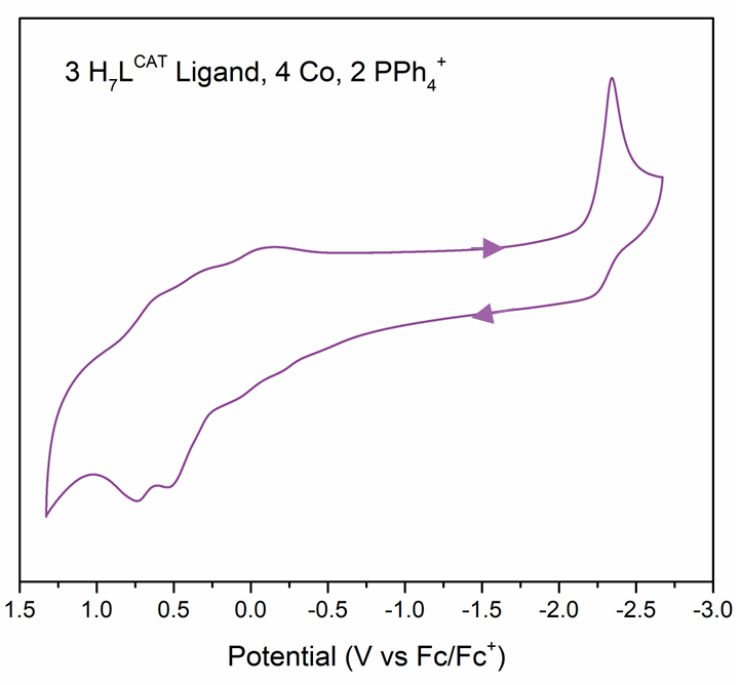

Figure 2-20. Cyclic voltammetry of the cobalt cluster complex in acetonitrile.

Another cluster complex that was able to be isolated in a crystal form was a Fe complex with H_4L^{CAT} ligand (Scheme 2-12). Its solid-state structure was identified to contain six ligand units, four iron ions and four potassium counteractions in a unit cell (Figure 2-21). The zoomed-in coordination environment around the iron centers is shown in Figure 2-22.

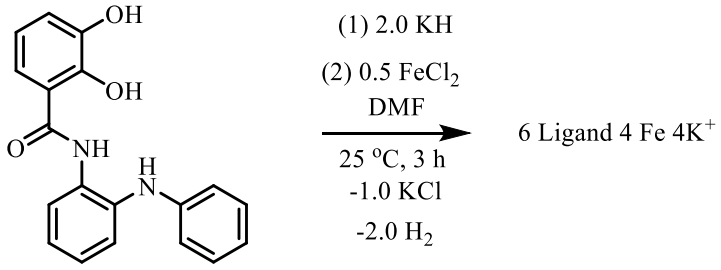

Scheme 2-12. Synthesis of iron cluster.

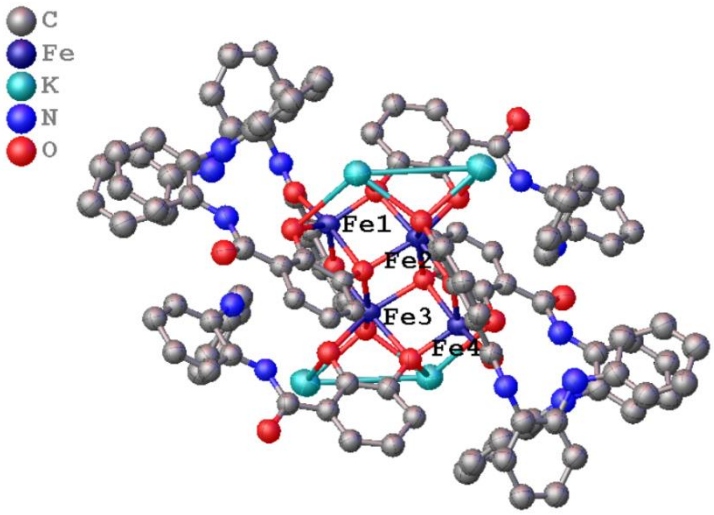

Figure 2-21. Solid-state structure of iron cluster as determined by single X-ray crystallography.

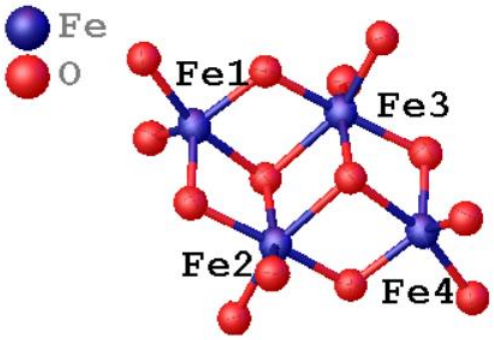

Figure 2-22. The zoomed-in coordination environment around the metal centers in the iron cluster complex with ligand H_4L^{CAT}.

Oxidation of $K_2[Cu(H_2L^{CAT})_2]$ by dioxygen

Aerobic oxidation of $K_2[Cu(H_2L^{CAT})_2]$ was investigated. A solution of $K_2[Cu(H_2L^{CAT})_2]$ was treated with an excess amount of O_2, and the reaction was monitored by UV-visible spectroscopy. As shown in Figure 2-23, the orange trace represents Cu(II) metal complex before oxidation, and the green trace represents the complex after being exposed to oxygen for 24 hours.

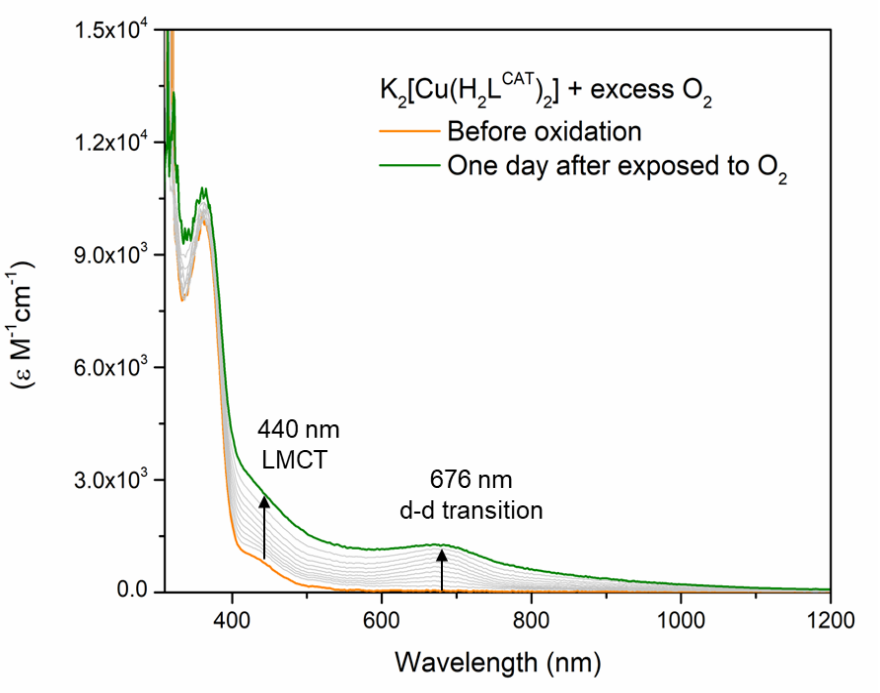

Figure 2-23. UV-visible spectra of $K_2[Cu(H_2L^{CAT})_2]$ before and after oxidation by O_2 in acetonitrile.

The absorption at 676 nm is likely due to the d-d transition. Since $K_2[Cu(H_2L^{CAT})_2]$ has a square planar geometry which is centrosymmetric around Cu center, the d-d transition of $K_2[Cu(H_2L^{CAT})_2]$ is Laporte forbidden, showing nearly no absorption in the spectra before oxidation. However, when $K_2[Cu(H_2L^{CAT})_2]$ was exposed to an excess amount of dioxygen, the geometry around the Cu center might become distorted during the oxidation process, thus the d-d transition is allowed to happen, giving rise to the absorption at around 676 nm. The other absorption at around 440 nm is likely due to the ligand-to-metal charge transfer. One possible interpretation of this observation is the formation of a Cu-semiquinone species as oxidation product (Figure 2-24).

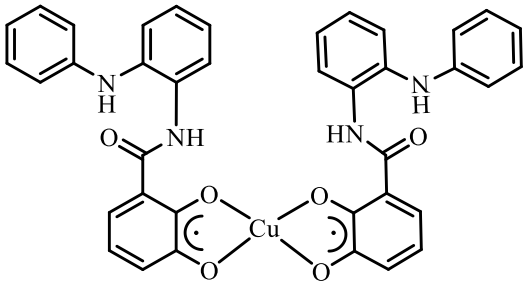

Figure 2-24. The proposed Cu-semiquinone species as oxidized product.

$K_2[Cu(H_2L^{CAT})_2]$ was also studied by cyclic voltammetry, and the result is shown in Figure 2-25.

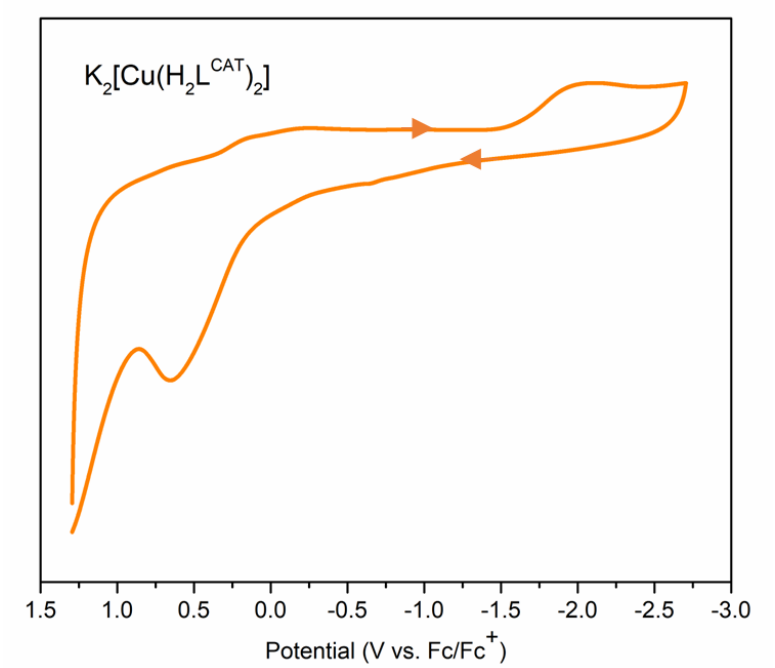

Figure 2-25. Cyclic voltammetry of $K_2[Cu(H_2L^{CAT})_2]$ in acetonitrile.

Conclusions and future directions

In summary, two new redox-active ligands, H_4L^{CAT} and H_7L^{CAT}, that incorporate catechol and nitrogenous groups have been synthesized. A variety of metalations have been attempted. Crystals of $K_2[Cu(H_2L^{CAT})_2]$, $(PPh_4)_2[Cu(H_2L^{CAT})_2]$, $K_2CuH_3L^{CAT}$, a cobalt cluster complex, and an iron cluster complex were obtained and analyzed by single X-ray crystallography. Cyclic voltammetry studies were carried out on $K_2[Cu(H_2L^{CAT})_2]$ and the cobalt cluster. The oxidation of $K_2[Cu(H_2L^{CAT})_2]$ by dioxygen was monitored by UV-visible spectroscopy, and a Cu-semiquinone species as the oxidation product was proposed. Electromagnetic studies such as EPR, EXAFS, XES, and magnetic susceptibility can be performed to further confirm the structure of the oxidized product.

Since the newly synthesized H_4L^{CAT} ligand potentially has four ligand based redox-events and the H_7L^{CAT} ligand has seven oxidation states, they can be further used to study the multi-electron processes beyond two-electron processes. For example, atom transfer reactions, oxygen evolution reaction, CO_2 and N_2 fixation reactions are possible multi-electron processes that can be achieved.

Experimental section

General considerations

Manipulations under inert atmosphere were carried out using standard Schlenk techniques or conducted in an MBRAUN LabMaster 130 drybox under a nitrogen atmosphere. All reagents used were purchased from commercial vendors and used as received unless otherwise noted. Anhydrous solvents were purchased from Sigma-Aldrich with a Sure/Seal^{TM} bottle or were further purified by sparging with Argon gas followed by passaging through activated alumina columns. NMR experiments were performed on INOVA 400, 500, 600 and Bruker 400, 600 MHz instruments at ambient temperature. Chemical shifts are referenced to the residual solvent. Mass spectra were recorded in the mass spectroscopy center at Emory university on a Thermo LTQ-FTMS mass spectrometer. Infrared spectra were recorded as KBr pellets on a Nicolet iS10 Series FT-IR spectrophotometer. UV-visible absorption spectra were recorded on a Shimadzu UV-3600 (UV-vis/NIR) spectrophotometer using 1.0 cm quartz cuvettes at room temperature. X-ray diffraction studies were carried out in the X-ray crystallography laboratory at Emory university on a XtaLAB Synergy, Dualflex, HyPix diffractometer. Cyclic voltammetry experiments were carried out using a CH instrument (Austin, TX) Model 660C potentiostat. All experiments were conducted in acetonitrile (MeCN) with 0.10 M tetrabutylammonium hexafluorophosphate as the supporting electrolyte. Electrochemical experiments were conducted in a three-component cell consisting of a Pt-wire auxiliary electrode, a non-aqueous reference electrode ($Ag/AgNO_3$), and a glassy-carbon working electrode. All electrochemical measurements are referenced and reported versus the ferrocene/ferrocenium couple.

Ligand syntheses

Bis(2-nitrophenyl)amine [HN(*o*-PhNO$_2$)$_2$]. *Prepared using a modified literature procedure*.[22]

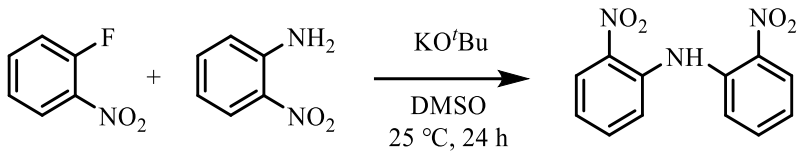

A mixture of 2-nitroaniline (13.814 g, 0.1 mol) and 1-fluoro-2-nitrobenzene (10.55 mL, 0.1 mol) was stirred in dimethyl sulfoxide (DMSO, 150 mL) at 25 °C. KO^{t}Bu (22.442 g, 0.2 mol) was added slowly, and the reaction was stirred at 25 °C for 24 hours. The reaction mixture was then quenched with DI water (600 mL) and filtered to give a bright orange solid. This bright orange solid was washed with DI water (4 × 50 mL), followed by diethyl ether (3 × 30 mL), and then dried under vacuum to give a bright orange powder. (19.69 g, 76%) ^{1}H NMR (400 MHz, $CDCl_3$) δ 11.04 (s, 1H), 8.23 (dd, *J* = 8.4, 1.5 Hz, 2H), 7.61 (dd, *J* = 8.5, 1.4 Hz, 2H), 7.55 (dddd, *J* = 8.5, 7.0, 1.6, 0.5 Hz, 2H), 7.12 (ddd, *J* = 8.5, 7.0, 1.5 Hz, 2H). ^{13}C NMR (151 MHz, $CDCl_3$,) δ 137.40, 134.30, 127.01, 121.32, 119.20. MS-ESI: $C_{12}H_9N_3O_4$ *m/z* Calcd: 259.06, Found: 260.06 $[M+1]^+$.

Bis(2-aminophenyl)amine [HN(*o*-PhNH$_2$)$_2$]. *Prepared using a modified literature procedure*.[23,24]

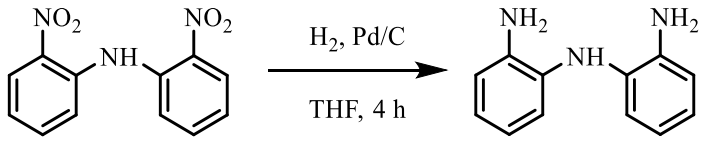

To a THF (50.0 mL) solution of HN(*o*-PhNO$_2$)$_2$ (4.0 g, 15.4 mmol) was added 10 wt.% Pd/C (1.0 g, 0.9 mmol, 6 mol%). The reaction mixture was placed in a pressure-safe reaction vessel and shaken under H_2 at 50 psi for 4 hours. The reaction mixture was filtered through a pad of celite, and then the resulting filtrate was concentrated under vacuum to give a thick,

colorless oil. Washing the oil with hexanes afforded the product as a solid. This solid was filtered and dried under vacuum to yield the final product as pink powder (2.9 g, 95%). ^{1}H NMR (400 MHz, $CDCl_3$) δ 6.93 (ddd, *J* = 7.8, 5.2, 3.5 Hz, 2H), 6.85–6.80 (m, 2H), 6.79–6.73 (m, 4H), 5.02 (s, 1H). ^{13}C NMR (151 MHz, $CDCl_3$,) δ 138.56, 131.21, 124.12, 122.61, 120.84, 118.78. MS-ESI: $C_{12}H_{13}N_3$ *m/z* Calcd: 199.11, Found: 200.11 $[M+1]^+$.

***N,N'*-(azanediylbis(2,1-phenylene))bis(2,3-dimethoxybenzamide)**

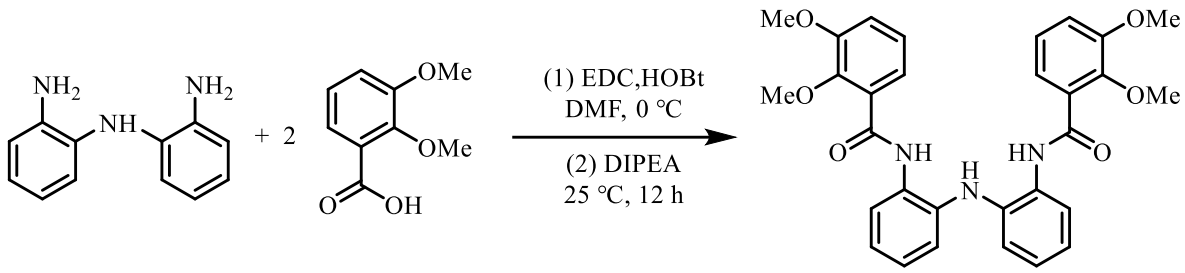

A mixture of bis(2-aminophenyl)amine (398.5 mg, 2 mmol) and 2,3-dimethoxybenzoic acid (728.7 mg, 4 mmol) was dissolved in 15 mL dimethylformamide and cooled to 0 ℃. 3-(ethyliminomethylideneamino)-*N*,*N*-dimethylpropan-1-amine hydrochloride (805.2 mg, 4.2 mmol) and 1-hydrozybenzotriazole monohydrate (643.1 mg, 4.2 mmol) were dissolved in 6 mL dimethylformamide, and this solution was added dropwise to the stirred mixture from the first step. Then the reaction was allowed to return to 25 ℃ and *N*,*N*-diisopropylethylamine (646.2 g, 5 mmol) was added dropwise. The mixture was stirred at 25 ℃ for 12 hours. The resulting light-orange solution was diluted with 150 mL ethyl acetate and extracted with saturated NaCl solution (4 × 30 mL), dried over $MgSO_4$, and concentrated under vacuum to afford pink powder (1.055 g, 86%). ^{1}H NMR (400 MHz, $CDCl_3$) δ 10.21 (s, 2H), 7.95 (dd, *J* = 7.5, 2.1 Hz, 2H), 7.68 (dd, *J* = 8.0, 1.6 Hz, 2H), 7.17–6.99 (m, 8H), 6.95 (dd, *J* = 7.4, 2.1 Hz, 2H), 6.30 (s, 1H), 3.84 (s, 6H), 3.70 (s, 6H). ^{13}C NMR (151 MHz, $CDCl_3$) δ 164.36, 152.58, 147.68, 136.65, 130.30, 126.58, 126.02, 124.38, 123.61, 123.13, 123.07,

121.25, 115.85, 61.44, 56.08. MS-ESI: $C_{30}H_{29}N_3O_6$ *m/z* Calcd: 527.21, Found: 528.21 $[M+1]^+$.

***N,N′*-(azanediylbis(2,1-phenylene))bis(2,3-dihydroxybenzamide)**

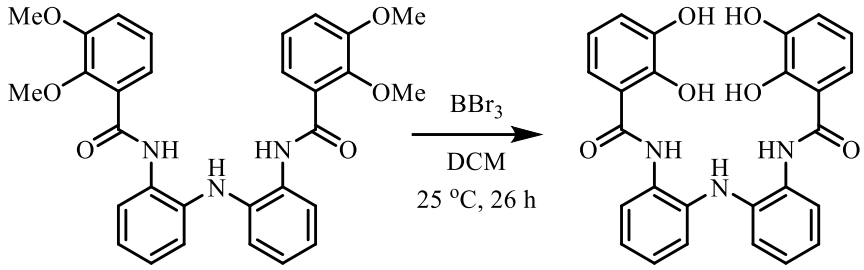

To a 20 mL dichloromethane (DCM) solution of *N,N′*-(azanediylbis(2,1-phenylene))bis(2,3-dimethoxybenzamide) (268.3 mg, 0.5 mmol) was added excess amount of fresh 1.0 M boron tribromide solution in dichloromethane (1.5 mL, 1.5 mmol). The reaction mixture was stirred at room temperature for 26 hours. Then the reaction was quenched with 200 mL ice-cold DI water and left stirred overnight until the clear separation of organic layer and aqueous layer was observed. Afterwards, the reaction mixture was extracted with dichloromethane (DCM) (5 × 50 mL), and the organic layers were combined. The combined organic layer was then extracted with saturated NaCl solution (3 × 100 mL), dried over $MgSO_4$, and concentrated under vacuum to afford pale-white powder. (235.7 mg, 98 %) ^{1}H NMR (400 MHz, CD_3OD) δ 7.59 (dd, *J* = 7.9, 1.5 Hz, 2H), 7.26 (dd, *J* = 8.2, 1.5 Hz, 2H), 7.15–7.06 (m, 2H), 7.02–6.94 (m, 4H), 6.92 (dd, *J* = 7.8, 1.5 Hz, 2H), 6.70 (t, *J* = 8.0 Hz, 2H). ^{13}C NMR (151 MHz, CD_3OD) δ 168.64, 148.33, 145.77, 137.77, 128.10, 126.52, 125.57, 121.67, 119.82, 118.53, 118.48, 115.97. MS-ESI: $C_{26}H_{21}N_3O_6$ *m/z* Calcd: 471.14, Found: 472.15 $[M+1]^+$.

2,3-bis(benzyloxy)benzoic acid

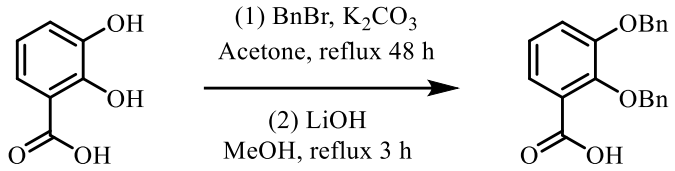

A solution of 2,3-dihydroxybenzoic acid (1.5412 g, 10 mmol), benzyl bromide (3.7627 g, 22 mmol), and K_2CO_3 (3.0406 g, 22 mmol) in acetone (35 mL) was refluxed for 48 hours. After filtration, the solution was concentrated under vacuum to obtain the crude product as clear oil. The crude product was dissolved in methanol (30 mL), and LiOH•H_2O (2.31 g, 55 mmol) was slowly added. The mixture was refluxed and stirred for 3 hours. Then, the solution was acidified with 3.0 M HCl to pH=2.0 and filtered to obtain the product as white solid (2.07 g, 62%). ^{1}H NMR (400 MHz, $CDCl_3$) δ 7.73 (ddd, *J* = 7.9, 1.7, 0.8 Hz, 1H), 7.50–7.29 (m, 9H), 7.27–7.23 (m, 2H), 7.18 (td, *J* = 8.0, 0.8 Hz, 1H), 5.25 (s, 2H), 5.18 (s, 2H). ^{13}C NMR (151MHz, $CDCl_3$): δ 165.61, 151.45, 147.25, 135.94, 134.84, 129.30, 129.25, 128.85, 128.83, 128.55, 127.81, 125.02, 124.42, 123.19, 119.06, 71.57. MS-ESI: $C_{21}H_{18}O_4$ *m/z* Calcd: 334.12, Found: 333.11 $[M-1]^-$.

2,3-bis(benzyloxy)-*N*-(2-(phenylamino)phenyl)benzamide

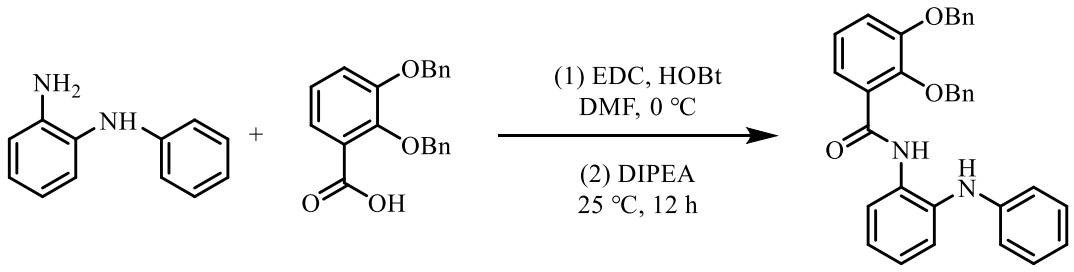

A mixture of N^1-phenylbenzene-1,2-diamine (737.0 mg, 4.0 mmol) and 2,3-bis(benzyloxy)benzoic acid (1.3376 g, 4.0 mmol) was dissolved in 20 mL dimethylformamide (DMF) and cooled to 0 ℃. 3-(ethyliminomethylideneamino)-*N*,*N*-

dimethylpropan-1-amine hydrochloride (843.6 mg, 4.4 mmol) and 1-hydrozybenzotriazole monohydrate (673.4 g, 4.4 mmol) were dissolved in 15 mL dimethyl formamide (DMF), and then this solution was added dropwise to the stirred mixture from the first step. Then the reaction was allowed to return to 25 ℃, and *N*,*N*-diisopropylethylamine (1.0858 g, 8.4 mmol) was added dropwise. The mixture was stirred at 25 ℃ for 12 hours. The resulting solution was diluted with 200 mL ethyl acetate and extracted with saturated NaCl solution (4 × 75 mL), dried over $MgSO_4$, and concentrated under vacuum to afford powder product (1.8589 g, 93%). ^{1}H NMR (400 MHz, $CDCl_3$) δ 10.08 (s, 1H), 7.77 (dd, *J* = 6.0, 3.6 Hz, 1H), 7.64 (dd, *J* = 7.9, 1.6 Hz, 1H), 7.48–7.42 (m, 2H), 7.42–7.33 (m, 3H), 7.32–7.18 (m, 6H), 7.19–7.06 (m, 5H), 7.02 (td, *J* = 7.6, 1.6 Hz, 1H), 6.83–6.72 (m, 1H), 6.68–6.61 (m, 2H), 5.49 (s, 1H), 5.15 (s, 2H), 5.09 (s, 2H). ^{13}C NMR (151MHz, $CDCl_{3,}$): δ 163.74, 151.84, 146.65, 144.73, 136.34, 136.19, 135.26, 131.35, 129.14, 129.04, 128.71, 128.66, 128.31, 127.71, 125.61, 124.60, 123.74, 123.54, 123.29, 122.81, 119.88, 117.59, 116.69, 76.50, 71.42. MS-ESI: $C_{33}H_{28}N_2O_3$ *m/z* Calcd: 500.21, Found: 501.22 $[M+1]^+$.

***N,N*'-(azanediylbis(2,1-phenylene))bis(2,3-bis(benzyloxy)benzamide)**

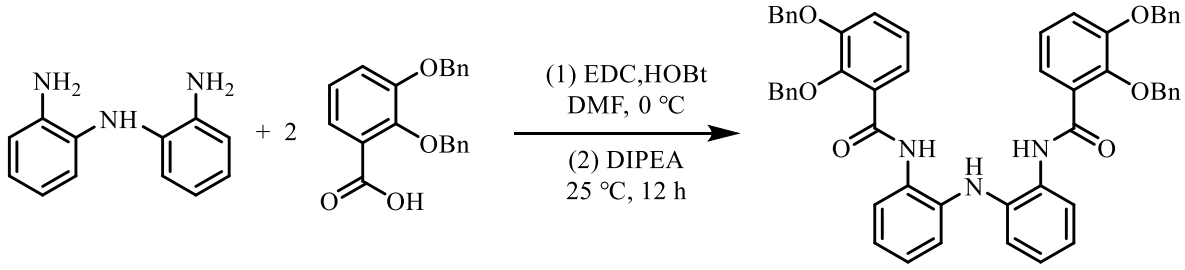

A mixture of N^1-(2-aminophenyl)benzene-1,2-diamine (398.5 mg, 2.0 mmol) and 2,3-bis(benzyloxy)benzoic acid (1.3376 g, 4.0 mmol) was dissolved in 15 mL dimethylformamide (DMF) and cooled to 0 ℃. 3-(ethyliminomethylideneamino)-*N*,*N*-dimethylpropan-1-amine hydrochloride (805.2 mg, 4.2 mmol) and 1-hydrozybenzotriazole

monohydrate (642.8 mg, 4.2 mmol) were dissolved in 10 mL dimethylformamide (DMF), and this solution was added dropwise to the stirred mixture from the first step. Then the reaction was allowed to return to 25 ℃ and *N*,*N*-diisopropylethylamine (1.0858 g, 8.4 mmol) was added dropwise. The mixture was stirred at 25 ℃ for 12 hours. The resulting solution was diluted with 150 mL ethyl acetate and extracted with saturated NaCl solution (4 × 30 mL), dried over $MgSO_4$, and concentrated under vacuum to afford powder product (1.5012 g, 90%). ^{1}H NMR (400 MHz, $CDCl_3$) δ 9.73 (s, 2H), 7.54 (dd, *J* = 7.7, 1.9 Hz, 2H), 7.41–7.21 (m, 14H), 7.20–6.95 (m, 16H), 6.86 (td, *J* = 7.5, 1.7 Hz, 2H), 6.44 (s, 1H), 5.17 (s, 1H), 5.05 (d, *J* = 7.1 Hz, 8H).

2,3-dihydroxy-N-(2-(phenylamino)phenyl)benzamide (H_4L^{CAT})

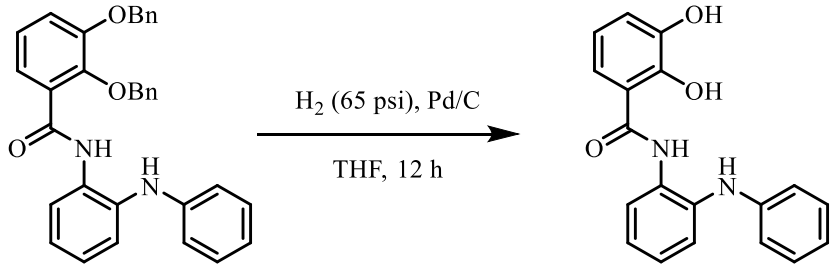

To a THF (100 mL) solution of 3-bis(benzyloxy)-*N*-(2-(phenylamino)phenyl)benzamide (1.8020 g, 3.6 mmol) was added 10 wt.% Pd/C (0.6 g, 0.56 mmol, 15 mol%). The reaction mixture was placed in a pressure-safe reaction vessel and shaken under H_2 at 65 psi for 12 hours. The reaction mixture was filtered through a pad of celite, and the resulting filtrate was concentrated under vacuum to obtain a thick, colorless oil. Washing the oil with hexanes afforded the product as a solid. This solid was filtered and dried under vacuum to yield the product as pink powder (0.9126 g, 79%). ^{1}H NMR (400 MHz, CD_3OD) δ 7.87 (dt, *J* = 8.0, 1.4 Hz, 1H), 7.26 (ddt, *J* = 17.3, 8.1, 1.4 Hz, 2H), 7.19–7.11 (m, 3H), 7.10–7.04 (m, 1H), 6.92 (ddd, *J* = 7.9, 2.9, 1.5 Hz, 1H), 6.85 (ddt, *J* = 7.8, 2.0, 1.0 Hz,

2H), 6.77 (dddd, *J* = 7.3, 6.3, 1.8, 1.0 Hz, 1H), 6.73–6.67 (m, 1H). ^{13}C NMR (151 MHz, CD_3OD) δ 167.73, 147.80, 145.85, 144.90, 136.24, 130.47, 128.75, 125.75, 124.17, 122.84, 121.93, 119.59, 118.58, 118.43, 116.78, 116.36. MS-ESI: $C_{19}H_{16}N_2O_3$ *m/z* Calcd: 320.12, Found: 319.11 $[M-1]^-$.

***N,N'*-(azanediylbis(2,1-phenylene))bis(2,3-dihydroxybenzamide) (H_7L^{CAT})**

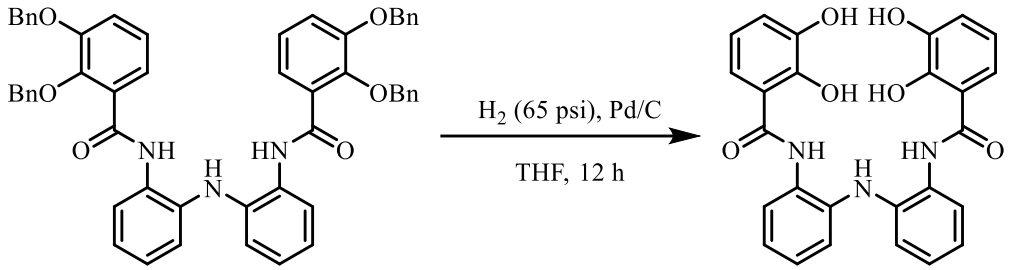

To a THF (50 mL) solution of *N,N'*-(azanediylbis(2,1-phenylene))bis(2,3-bis(benzyloxy)benzamide) (1.5 g, 1.8 mmol) was added 10 wt.% Pd/C (0.6 g, 0.56 mmol, 31 mol%). The reaction mixture was placed in a pressure-safe reaction vessel and shaken under H_2 at 65 psi for 12 hours. The reaction mixture was filtered through a pad of celite, and the filtrate was concentrated in vacuo to obtain a thick, colorless oil. Washing the oil with hexanes afforded the product as a solid. This solid was filtered and dried under vacuo to yield the product as pink powder (0.1874 g, 82%). ^{1}H NMR (400 MHz, CD_3OD) δ 7.59 (dd, *J* = 7.8, 1.5 Hz, 2H), 7.26 (dd, *J* = 8.1, 1.4 Hz, 2H), 7.15–7.06 (m, 2H), 7.03–6.90 (m, 6H), 6.70 (t, *J* = 8.1 Hz, 2H). ^{13}C NMR (151 MHz, CD_3OD) δ 168.64, 148.36, 145.78, 137.77, 128.13, 126.51, 125.57, 121.67, 119.82, 118.52, 118.48, 115.98, 67.46. MS-ESI: $C_{26}H_{21}N_3O_6$ *m/z* Calcd: 471.14, Found: 470.14 $[M-1]^-$.

References

(1) Hindson, K.; de Bruin, B. Cooperative & redox non-innocent ligands in directing organometallic reactivity. *European Journal of Inorganic Chemistry* **2012**, *2012* (3), 340-342.

(2) Praneeth, V. K. K.; Ringenberg, M. R.; Ward, T. R. Redox-active ligands in catalysis. *Angewandte Chemie International Edition* **2012**, *51* (41), 10228-10234.

(3) Grützmacher, H. Cooperating ligands in catalysis. *Angewandte Chemie International Edition* **2008**, *47* (10), 1814-1818.

(4) van der Vlugt, J. I.; Reek, J. N. Neutral tridentate PNP ligands and their hybrid analogues: Versatile non-innocent scaffolds for homogeneous Catalysis. *Angewandte Chemie International Edition* **2009**, *48* (47), 8832-8846.

(5) Lyaskovskyy, V.; de Bruin, B. Redox non-innocent ligands: versatile new tools to control catalytic reactions. *ACS Catalysis* **2012**, *2* (2), 270-279.

(6) Chirik, P. J.; Wieghardt, K. Radical ligands confer nobility on base-metal catalysts. *Science* **2010**, *327* (5967), 794-795.

(7) Cox, D. D.; Que, L. Functional models for catechol 1,2-dioxygenase. The role of the iron (III) center. *Journal of the American Chemical Society* **1988**, *110* (24), 8085-8092.

(8) Tyson, C. A.; Martell, A. E. Kinetics and mechanism of the metal chelate catalyzed oxidation of pyrocatechols. *Journal of the American Chemical Society* **1972**, *94* (3), 939-945.

(9) Herebian, D.; Bothe, E.; Neese, F.; Weyhermüller, T.; Wieghardt, K. Molecular and electronic structures of bis-(*o*-diiminobenzosemiquinonato) metal(II) complexes (Ni, Pd, Pt), their monocations and anions, and of dimeric dications containing weak metal−metal bonds. *Journal of the American Chemical Society* **2003**, *125* (30), 9116-9128.

(10) Herebian, D.; Wieghardt, K. E.; Neese, F. Analysis and interpretation of metal-radical coupling in a series of square planar nickel complexes: Correlated ab initio and density functional investigation of [Ni(LISQ)$_2$] (LISQ=3,5-di-*tert*-butyl-*o*-diiminobenzosemiquinonate (1-)). *Journal of the American Chemical Society* **2003**, *125* (36), 10997-11005.

(11) Sikari, R.; Sinha, S.; Jash, U.; Das, S.; Brandao, P.; de Bruin, B.; Paul, N. D. Deprotonation induced ligand oxidation in a Ni^{II} complex of a redox noninnocent N^1-(2-aminophenyl)benzene-1,2-diamine and its use in catalytic alcohol oxidation. *Inorganic Chemistry* **2016**, *55* (12), 6114-6123.

(12) Corcos, A. R.; Villanueva, O.; Walroth, R. C.; Sharma, S. K.; Bacsa, J.; Lancaster, K. M.; MacBeth, C. E.; Berry, J. F. Oxygen activation by Co(II) and a redox non-innocent ligand: spectroscopic characterization of a radical–Co(II)–superoxide complex with divergent catalytic reactivity. *Journal of the American Chemical Society* **2016**, *138* (6), 1796-1799.

(13) Koval, I. A.; Gamez, P.; Belle, C.; Selmeczi, K.; Reedijk, J. Synthetic models of the active site of catechol oxidase: mechanistic studies. *Chemical Society Reviews* **2006**, *35* (9), 814-840.

(14) Rolff, M.; Hamann, J. N.; Tuczek, F. Benzylic ligand hydroxylation starting from a dicopper μ-η^2:η^2 peroxo intermediate: dramatic acceleration of the reaction by hydrogen-atom donors. *Angewandte Chemie International Edition* **2011**, *50* (30), 6924-6927.

(15) Yao, S.; Herwig, C.; Xiong, Y.; Company, A.; Bill, E.; Limberg, C.; Driess, M. Monooxygenase-like reactivity of an unprecedented heterobimetallic {FeO_2Ni} moiety. *Angewandte Chemie International Edition* **2010**, *49* (39), 7054-7058.

(16) van der Vlugt, J. I.; Meyer, F. Synthetic models for the active sites of nickel-containing enzymes. *Metal Ions in Life Sciences* **2007**, *2*, 181-240.

(17) Bertini, I.; Sigel, A. *Handbook on metalloproteins*; CRC Press, 2001.

(18) McOmie, J.; Watts, M.; West, D. Demethylation of aryl methyl ethers by boron tribromide. *Tetrahedron* **1968**, *24* (5), 2289-2292.

(19) Zuo, L.; Yao, S.; Wang, W.; Duan, W. An efficient method for demethylation of aryl methyl ethers. *Tetrahedron Letter* **2008**, *49* (25), 4054-4056.

(20) Tian, J.; Yue, H.; Yang, P.; Sang, D. One-pot cleavage of aryl alkyl ethers by aluminum and iodine in acetonitrile. *ChemistrySelect* **2019**, *4* (1), 38-41.

(21) Zhang, Q.; Jin, B.; Zheng, T.; Tang, X.; Guo, Z.; Peng, R. Hexadentate β-dicarbonyl (bis-catecholamine) ligands for efficient uranyl cation decorporation: Thermodynamic and antioxidant activity studies. *Inorganic Chemistry* **2019**, *58* (21), 14626-14634.

(22) Gorvin, J. H. The synthesis of di-and tri-arylamines through halogen displacement by base-activated arylamines: comparison with the Ullmann condensation. *Journal of the Chemical Society, Perkin Transactions 1* **1988**, (6), 1331-1335.

(23) Black, D. S. C.; Rothnie, N. Metal template reactions. XVI. Design and synthesis of primary diamine ligands with additional nitrogen donor atoms. *Australian Journal of Chemistry* **1983**, *36* (6), 1141-1147.

(24) Black, D. S. C.; Rothnie, N. Metal template reactions. XVII. The attempted dimerization of amino carbonyl compounds containing a supporting donor atom. *Australian Journal of Chemistry* **1983**, *36* (6), 1149-1157.

3. Chapter 3: The Design, Syntheses and Metalation of Alkyne Modified Redox-Active Ligands for Applications in Flow Chemistry

Abstract

Diazo compounds have versatile utilities in organic syntheses and are specifically used as carbene precursors. However, their unstable nature and safety concerns limit their long-term storage and use in large-scale syntheses. One way to overcome the safety issue is through flow chemistry where the diazo compounds can be synthesized in situ and consumed immediately in downstream reactions with other transition metal catalysts. Having previously developed a bis(amidophenyl)amine redox-active ligand, whose cobalt complex was capable of catalyzing the transformation of hydrazones to diazo compounds in homogeneous systems, we are motivated to modify the ligand for its use in heterogeneous diazo syntheses. To achieve the heterogeneous catalysis, the ligand in the homogeneous catalyst needs to be modified for immobilization on solid support. Terminal alkyne was chosen as the modification for our ligand system because azide-alkyne cycloaddition (click chemistry)[1] can straightforwardly react azide with alkyne compound to selectively give 1,2,3-triazoles with high yields, simple purification, and good functional group tolerance.[2] Ideally, with an alkyne-modified ligand system involved in the catalyst, it would be able to be immobilized on azide modified support such as silica, polymer or MOF material for heterogeneous catalysis.

The terminal alkyne moiety was explored to be installed onto the bis(amidophenyl)amine redox-active ligand at aromatic or amide site. Two asymmetric alkyne-functionalized bis(amidophenyl)amine redox-active ligands

N-(2-((2-isopropylamidophenyl)amino)phenyl)hex-5-ynamide ($H_3L^{ipr}L^{hexyne}$) and *N*-(2-((2-(hex-5-ynamido)phenyl)amino)phenyl)-2,4,6-triisopropylbenzamide ($H_3L^{TRIP}L^{hexyne}$) were designed, synthesized, and optimized through two synthetic routes. The Co^{II} catalyst $[Co_2(L^{ipr}L^{hexyne})_2]^{2-}$ **[1]**$^{2-}$, $[Co_2(L^{TRIP}L^{hexyne})_2]^{2-}$ **[2]**$^{2-}$ were synthesized. Another unexpected Co^{II} catalyst $[Co_2(L^{ipr}L^{internal\text{-}hexyne})_2]^{2-}$ **[3]**$^{2-}$ with an internal alkyne chain was obtained when slightly excess amount of base was used in the metalation step. Crystals of $(PPh_4)_2$**[1]**, K_2**[3]**, $(Et_4N)_2$**[3]** and $(PPh_4)_2$**[3]** were analyzed by X-ray crystallography. Their electrochemical properties were studied by cyclic voltammetry, and the electron-rich electrochemical profile showed their potential to catalyze multielectron reactions. UV-vis studies were performed to monitor the aerobic oxidation of catalysts under excess amount of oxygen. The O-atom transfer reaction of oxidizing triphenylphosphine into triphenylphosphine oxide and aerobic hydrazone oxidation of benzophenone hydrazone into a diazo compound were achieved with good to moderate yield using the newly synthesized catalysts. With the confirmation of the reactivity of these new cobalt catalysts with asymmetric alkyne functionalized redox-active ligands, we believe their efficacy can be further explored by immobilizing the catalyst onto different solid supports for heterogeneous catalysis in flow systems.

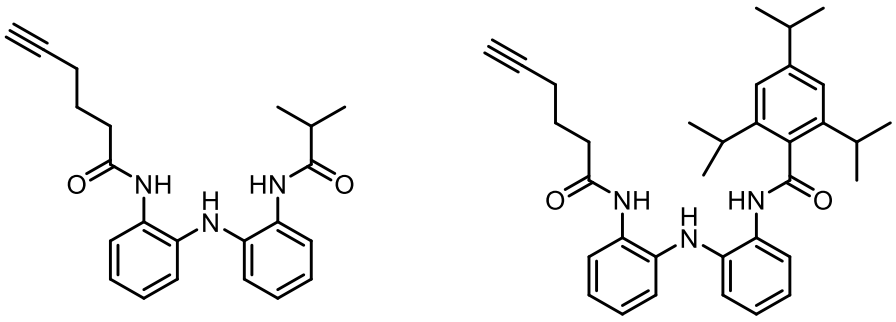

Figure 3-1. Structure of ligands $H_3L^{ipr}L^{alkyne}$ and $H_3L^{Trip}L^{alkyne}$ in this study.

Introduction

C–H functionalization is a powerful transformation in the construction of complex molecules from simple feedstock chemicals.[3,4] Diazo compounds, with far-reaching applications in C–H functionalization including cyclopropanation,[5] C–H and C–X bond activation,[6-9] and ylide formation,[10] have received rigorous attention.[11] In addition, diazo compounds have shown potential in the field of chemical biology for protein modification.[12] However, diazo compounds' tendency to undergo exothermic decomposition, which may be explosive[13], draw concerns regarding their long-term storage and use in large-scale syntheses. One way to overcome the safety issue is through flow chemistry which allows the diazo compounds to be synthesized in situ and consumed immediately in downstream reactions (Figure 3-2).[14,15] Given the safety concerns, it is of crucial importance to develop heterogeneous catalysts that can be used in the flow reactors to synthesize diazo compounds.

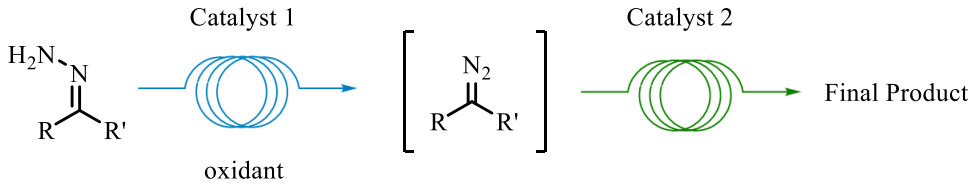

Figure 3-2. Oxidation of hydrazones to diazo compounds in flow chemistry.

In 1883, Curtius developed a method to synthesize ethyl diazoacetate[16] which leaded to interest in using diazo compounds as building blocks for C–C bond formation. Since then, several other synthetic approaches for accessing diazo compounds have been developed. One common approach is through diazo transfer, where a diazo group from a donor, such as sulfonyl azide, is transferred to a suitable acceptor. Examples of diazo transfer agents used in the syntheses are tosyl azide;[17] *p*-acetamidobenzenesulfonyl azide[18] and imidazolesulfonyl azide.[19] Although diazo transfer is a relatively efficient approach to synthesize diazo

compounds, some diazo transfer agents and/or by-products from the synthesis of diazo transfer agent are highly explosive[20] and the side-products can be challenging to remove.

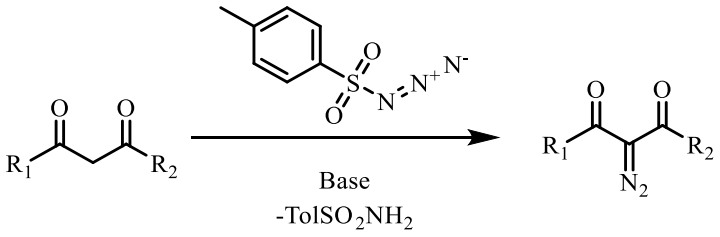

Scheme 3-1. Synthesis of diazo compounds through diazo transfer approach using tosyl azide.[17]

Another widely used synthetic approach for the synthesis of diazo compounds is dehydrogenation of hydrazones; however, most of the previously reported methods involve heavy and toxic metals as oxidants. For example, $Pb(OAc)_4$,[21] HgO,[22,23] Ag_2O,[24] MnO_2,[25] $KMnO_4$[26] have been used in the syntheses of diazo compounds through hydrazone dehydrogenation. Compared to the aforementioned methods that involve the generation of stoichiometric amount of toxic waste, synthesis of diazo compounds through catalytic aerobic oxidation of hydrazone is more favorable because this process uses dioxygen as the green oxidant, can be carried out under mild conditions, and water is the only by-product.

The MacBeth group has developed a series of symmetric bis(2-R-amidophenyl)amine ($(HN(o\text{-}PhNHC(O)R)_2)$) redox-active ligands for catalyzing aerobic oxidation reactions (Figure 3-3).[27-29] The *N*-amidate groups in this ligand system are strong σ-donors that can help stabilize metal compound in high oxidation states.[30]

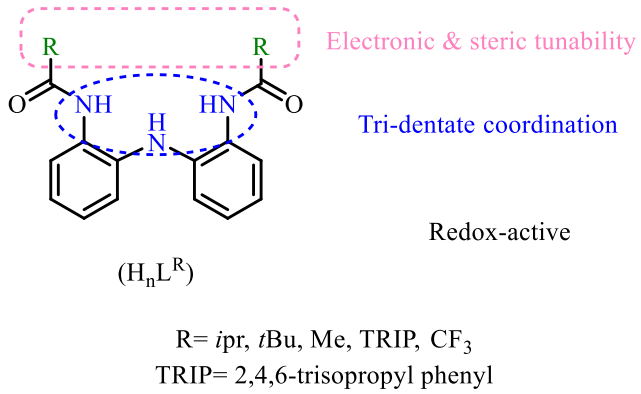

Figure 3-3. Bis(2-R-amidophenyl)amine redox-active ligands developed by the MacBeth group.

Previous studies have shown that a Co(II) complex supported by a bis(amidophenyl)amine redox-active ligand $(PPh_4)_2[Co_2L^{iPr}_2]$ is an efficient homogeneous catalyst for the aerobic oxidation of hydrazone to diazo compounds (Scheme 3-2).

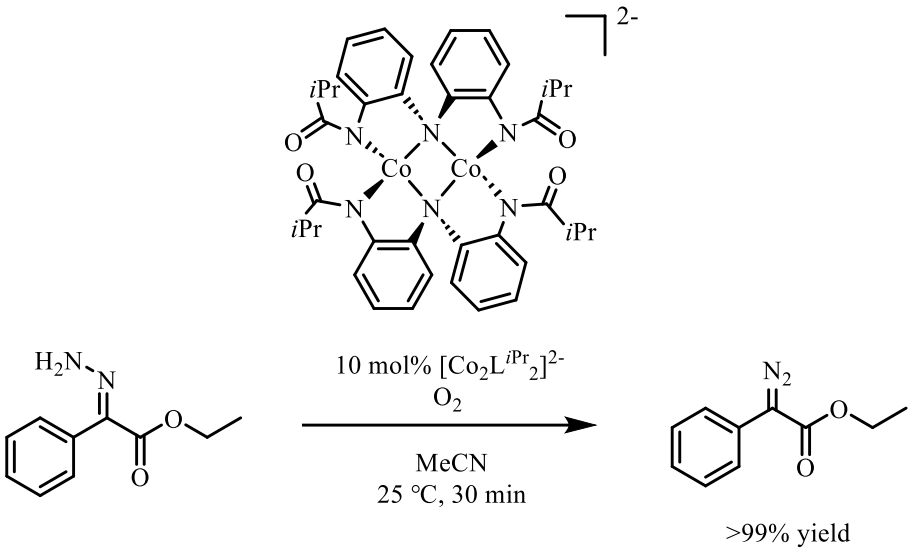

Scheme 3-2. $[Co_2L^{iPr}_2]^{2-}$ as homogeneous catalyst for hydrazone oxidation reaction.

The discovery of this homogeneous hydrazone oxidation catalyst and the idea of involving flow reactor to solve the safety issue during the production of diazo compounds inspired us to design heterogeneous catalysts for safer diazo synthesis. We are motivated to synthesize modified redox-active ligands that can be easily incorporated into heterogeneous

catalytic systems and/or attached to solid supports so that we can apply the catalytic aerobic oxidation of hydrazones for diazo production in flow reactors. Literature examples of solid supports for heterogeneous catalysis including silica,[31] polymer resin[32] and MOF materials.[33]

Our goal is to develop catalysts that incorporate less-expensive and abundant first row transition metals with terminal alkyne modified asymmetric redox-active ligand, as well as using dioxygen as green oxidant for catalytic hydrazone oxidation. The asymmetric ligands are more challenging to synthesize chemically due to more complicated substitutions in the ligand scaffold.[34] In this work, we will report the design, syntheses and characterizations of terminal alkyne functionalized asymmetric redox-active ligands and their subsequent metalations with a cobalt center. The reactivity of these Co complexes towards aerobic oxidation, O-atom transfer reaction, and hydrazone oxidation reaction will also be discussed.

Ligand syntheses

Design of redox-active ligands functionalized with a terminal alkyne

Functionalizing the redox-active ligand with a terminal alkyne was proposed to achieve the goal of anchoring the homogeneous catalyst onto a solid support as heterogeneous catalyst for flow chemistry. Terminal alkyne modification was selected because azide-alkyne cycloaddition (click chemistry)[1] can straightforwardly react azide with alkyne compound to selectively give 1,2,3-triazoles with high yields, simple purification, and good functional group tolerance.[2]. To functionalize the redox-active ligand framework, one proposed approach is to install the terminal alkyne onto the aromatic ring, and the other is to install the terminal alkyne as one of the amide substituents (Scheme 3-3).

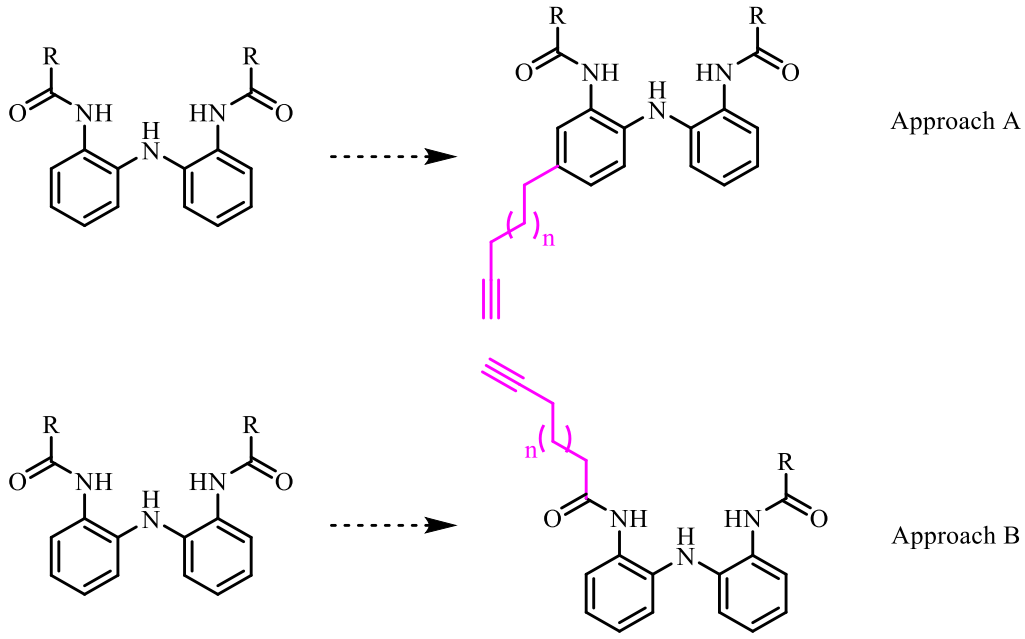

Scheme 3-3. The proposed syntheses of terminal alkyne functionalized ligands through two approaches.

Ligand syntheses in approach A: Terminal alkyne on the aromatic ring

In approach A, a terminal alkyne was proposed to be installed on the aromatic ring. An alkyne chain longer than four members was proposed to introduce flexibility to the

anchored ligand system. Previous studies suggested that the dimeric cobalt complexes would undergo rearrangement to form monometallic active species under oxidizing conditions, this flexibility is essential for the rearrangement that might form active species (Scheme 3-4).[28]

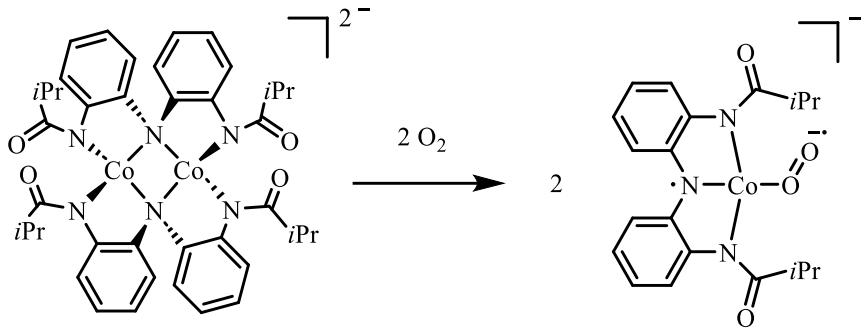

Scheme 3-4. Rearrangement of $[Co_2L^{iPr}{}_2]^{2-}$ upon oxidation.

Two synthetic routes were proposed and tested to install the terminal alkyne chain onto the aromatic ring. In route one, ligand with a benzyl bromide moiety was proposed to react with an alkyne tethered organolithium reagent via lithium-halogen exchange. In route two, cross coupling was proposed to synthesize the final alkyne functionalized product (Scheme 3-5).

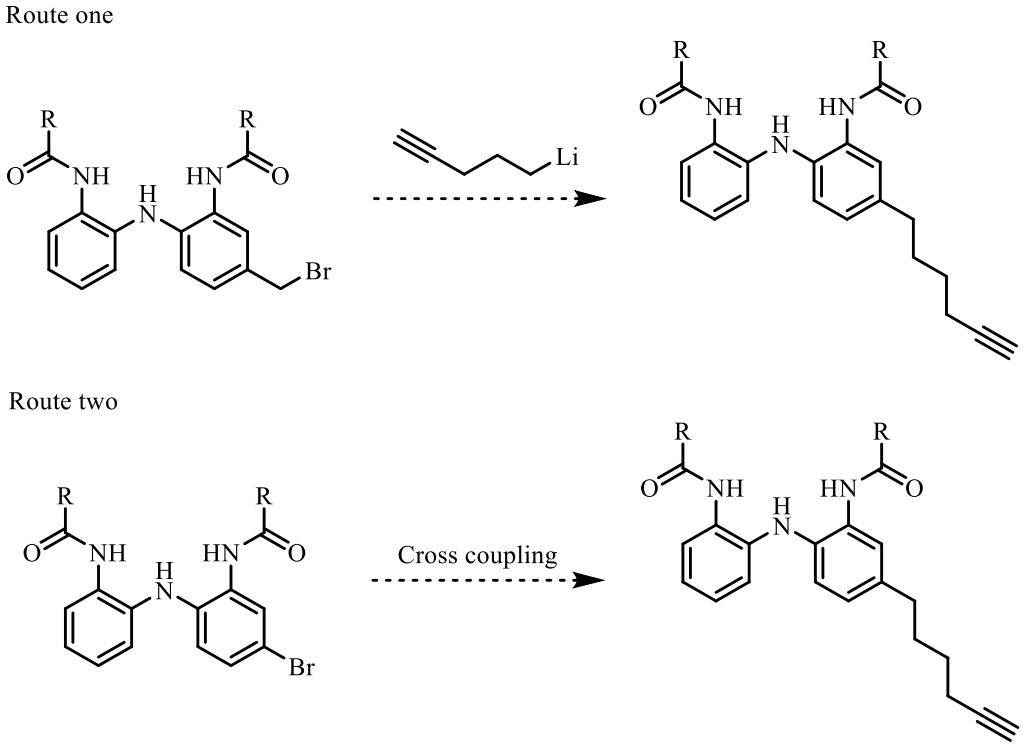

Scheme 3-5. Proposed synthetic routes in approach A.

Ligand syntheses–Approach A: Route 1

In route one, 4-methyl-2-nitro-*N*-(2-nitrophenyl)aniline **3-1** was obtained in 88% yield through a nucleophilic aromatic substitution using 1-fluoro-2-nitrobenzene and 4-methyl-2-nitroaniline as starting materials (Scheme 3-6). Then N^1-(2-aminophenyl)-4-methylbenzene-1,2-diamine **3-2** was synthesized in 81% through catalytic hydrogenation using palladium-on-carbon (Pd/C, 10 wt.%) as the catalyst (Scheme 3-6).

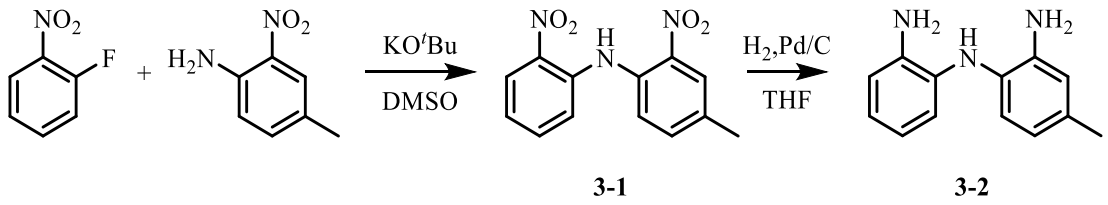

Scheme 3-6. Two step synthesis of N^1-(2-aminophenyl)-4-methylbenzene-1,2-diamine **3-2**.

After the N^1-(2-aminophenyl)-4-methylbenzene-1,2-diamine **3-2** ligand precursor was

successfully synthesized, it was then utilized in the acylation reaction using isobutyryl chloride to form the desired ligand **3-3** in 91% yield (Scheme 3-7).

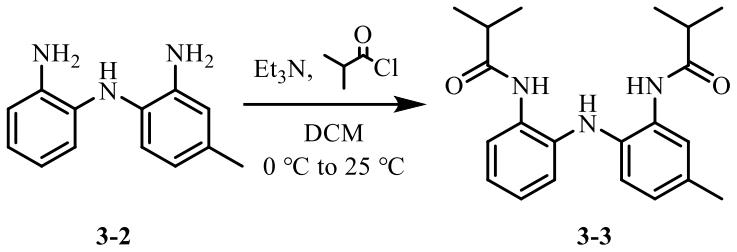

3-2 **3-3**

Scheme 3-7. Synthesis of **3-3**.

Then *N*-bromosuccinimide was used in the bromination reaction with **3-3** to form the alkyl bromide. However, the product isolated from the bromination reaction was not the desired ligand with the benzyl bromide moiety, instead, bromine atom directly attached to the aromatic ring forming an aryl bromide (Scheme 3-8). Different solvents including DMF, MeCN, $CHCl_3$ and CCl_4, various reaction temperatures, reaction times, and radical initiator adduct benzoyl peroxide were attempted for reaction optimizations to generate the desired ligand with benzyl bromide moiety but were not successful.

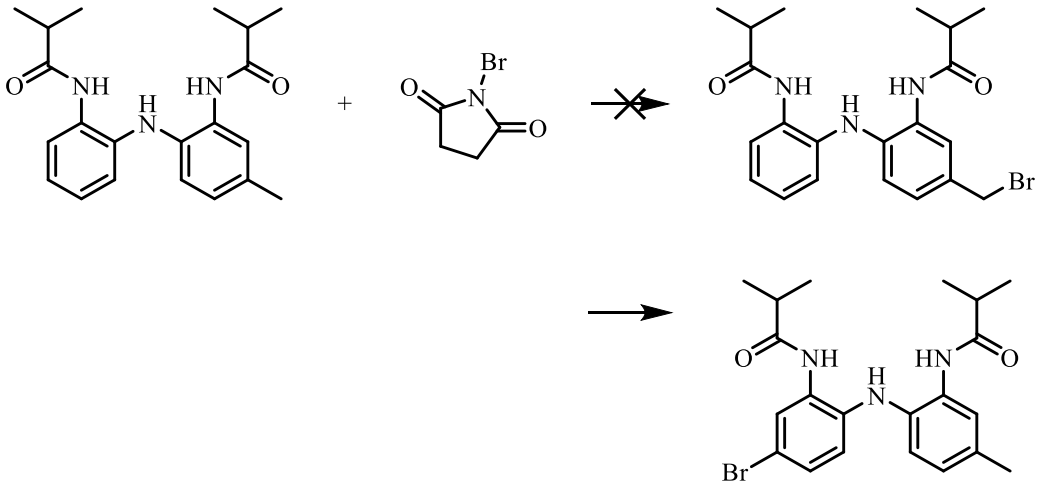

3-4

Scheme 3-8. Aryl bromide product formed in the bromination reaction.

Ligand syntheses–Approach A: Route 2

With the aryl bromide product in hand, route two was proposed to form alkyne functionalized ligand through coupling reactions. This time, with the intention of brominating the aromatic ring, *N*-bromosuccinimide (NBS) was added to **3-3** in $CHCl_3$ under reflux condition for 24 hours, and **3-4** was yielded in 83% yield (Scheme 3-9).

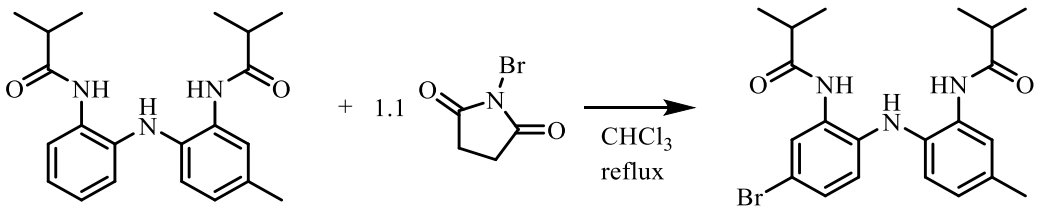

3-3 **3-4**

Scheme 3-9. Synthesis of the aryl bromide **3-4**.

A crystal of **3-4** that was suitable for X-ray diffraction was obtained by slow evaporation of hexane into a concentrated dichloromethane (DCM) solution of **3-4** (Figure 3-4).

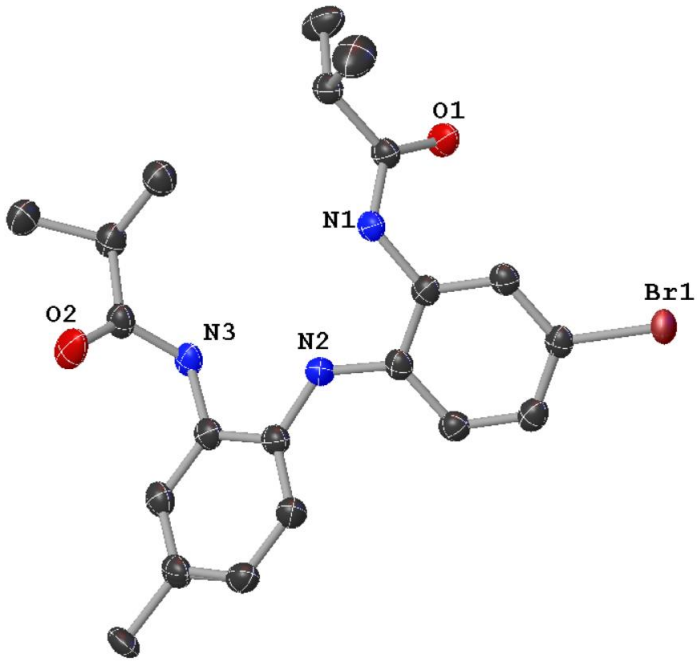

Figure 3-4. Solid-state structure of **3-4** as determined by single X-ray crystallography. Hydrogen atoms are omitted for clarity.

With compound **3-4**, the starting material of route two synthesized and isolated, it was used in cross coupling reactions for the installation of the terminal alkyne chain. Sonogashira coupling reaction was first tested by mixing ligand **3-4**, $Pd(PPh_3)_2Cl_2$ (3 mol%), *N*,*N*-diisopropylethylamine and CuI (10 mol%) in *N*,*N*-dimethylformamide (DMF), and purged with nitrogen. Then hex-1-yn-1-yltrimethylsilane was added to the mixture, which was stirred for 24 to 48 hours (Scheme 3-10). The reaction mixture was then poured into saturated $NaHCO_3$ solution and extracted with ethyl acetate (EtOAc). Then the organic layer was combined and washed with saturated NaCl aqueous solution, dried over $MgSO_4$, and filtered. Optimizations of reaction time, temperature or catalyst loading were attempted; however, they did not help yield the desired product. Thin layer chromatography studies after the reactions showed that starting material was recovered (Table 3-1).

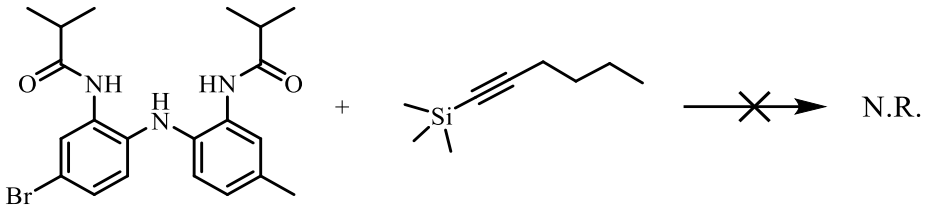

Scheme 3-10. Attempts of Sonogashira coupling reactions.

Table 3-1. Conditions used in Sonogashira cross coupling attempts.

	Solvent	Time	Temperature	Pd catalyst loading	
1	DMF	24 h	25 ℃	3 mol%	SM recovered
2	DMF	24 h	Reflux	3 mol%	
3	DMF	48 h	Reflux	3 mol%	
4	DMF	24 h	Reflux	5 mol%	

Besides Sonogashira coupling, Negishi coupling reaction was also attempted by first synthesizing the organozinc bromide compound in situ, followed by addition of aryl bromide

and 5 mol% of $Pd(PPh_3)_4$ as catalyst (Scheme 3-11). A large amount of effort was devoted to separating the product by manual column chromatography; however, due to low yield and undesired side-reactions, the separation attempts were not successful.

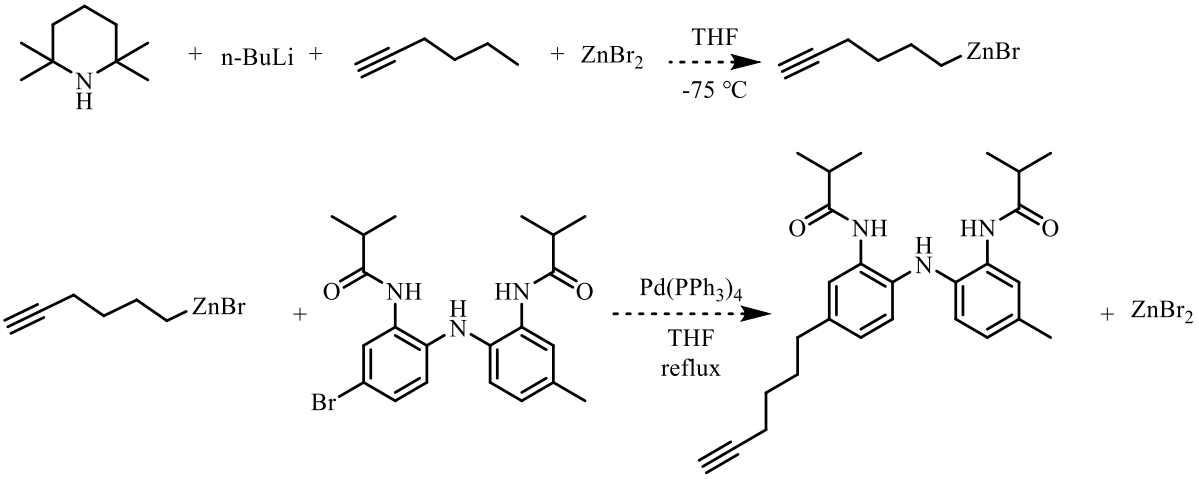

Scheme 3-11. Attempts of Negishi coupling reactions.

Ligand syntheses in approach B: Terminal alkyne as the amide substituent

Ligand syntheses–Approach B: Route 3

In efforts to successfully synthesize the alkyne functionalized ligands, focus was shifted to installing the terminal alkyne chain as the amide substituent as illustrated in Approach B. Bis(2-aminophenyl)amine [$HN(o\text{-}PhNH_2)_2$] was first prepared using a modified literature procedure[35] (Scheme 3-12).

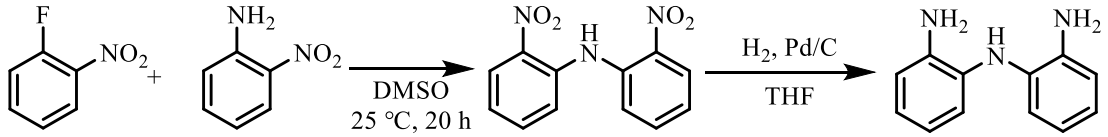

Scheme 3-12. Two step synthesis of bis(2-aminophenyl)amine [$HN(o\text{-}PhNH_2)_2$].

Monoacylation was then attempted to prepare **3-5** using isobutyryl chloride (Scheme 3-13). Due to the electronic and steric effect, monosubstituted ligand should be the major product. It is confirmed by the NMR result where the molar ratio of mono **3-5** and di **3-6**

substituted ligand product is calculated to be 1:0.39.

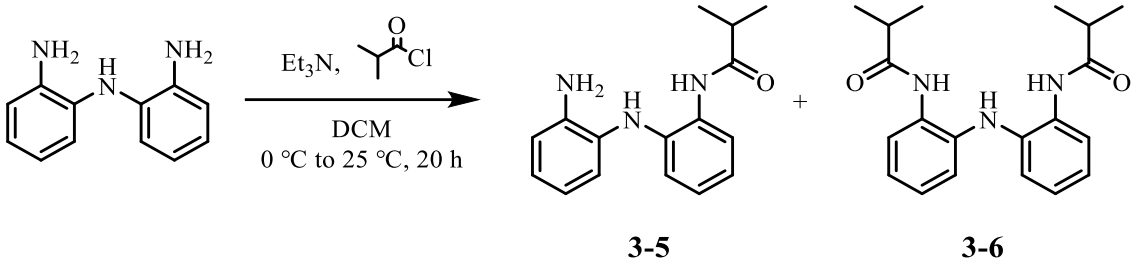

3-5 **3-6**

Scheme 3-13. Synthesis of **3-5** and **3-6** through acylation reactions.

Recrystallizations were performed to purify the desired monosubstituted ligand **3-5**. The product mixture was dissolved in minimum amount of dichloromethane in a crystallization jar and then carefully layered with hexane and was left overnight. Then the crystals/powder formed was filtered out from the solution, and the filtrate was concentrated under vacuum and reused for the following recrystallizations (Table 3-2). At the third time of recrystallization, the molar ratio of **3-5** and **3-6** in the filtrate turned to 1: 0.16, however, the crystal/powder that formed after the third recrystallization was found to be a mixture of **3-5** and **3-6** instead of pure **3-6**, as in the cases of previous recrystallizations. Bulkier bases such as *N*,*N*-diisopropylethylamine were used instead of triethylamine in the hope of promoting the formation of mono-substituted product, but this approach was not successful. Intense studies on adjusting the equivalents of base and acyl chloride used in the reaction, as well as lowering temperature or using of syringe pump for slow addition were carried out; however, none of these methods were able to eliminate the formation of di-substituted product **3-6**.

Table 3-2. Recrystallization trials after first acylation reaction.

Recrystallization round	Molar ratio in filtrate mono **3-5** : di **3-6**	Crystal/powder formed
1st	1: 0.33	**3-6**
2nd	1: 0.28	**3-6**
3rd	1: 0.16	**3-5** and **3-6**

Since the aforementioned method did not successfully yield the desired mono-substituted ligand with high purity, column chromatography was applied to the reaction mixture using 3:1 hexane: ethyl acetate as eluent. The reaction mixture contained the desired mono-substituted one arm ligand **3-5**, di-substituted two arm ligand **3-6** and the unreacted stating material. Since they all contained free amine in their structures, the interaction between free amine and acidic silica gel created difficulty in complete separation of the product on the column. In addition, the structural similarity between mono- and di-substituted ligands caused overlap between fractions and resulted in a 30% maximum yield of the final isolated product **3-5**.

The alkynyl acyl chloride was synthesized by reacting 5-hexynoic acid with excess amount of thionyl chloride in dry dichloromethane (DCM) under nitrogen atmosphere (Scheme 3-14).[36] The product 5-hexynoyl chloride was obtained with full conversion as light-yellow colored liquid.

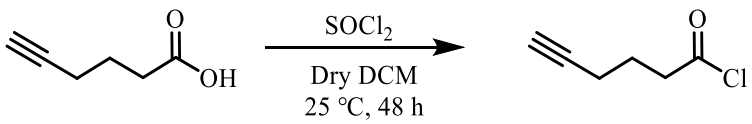

Scheme 3-14. Synthesis of 5-hexynoyl chloride.

Then, a second acylation reaction was carried out between the purified mono-substituted isopropyl ligand **3-5** and 5-hexynoyl chloride to yield the desired terminal alkyne

functionalized ligand $H_3L^{ipr}L^{alkyne}$ in 94% of yield (Scheme 3-15). A crystal of $H_3L^{ipr}L^{alkyne}$ was obtained from a concentrated dichloromethane solution of $H_3L^{ipr}L^{alkyne}$ layered with hexane, and its solid-state structure is shown in Figure 3-5.

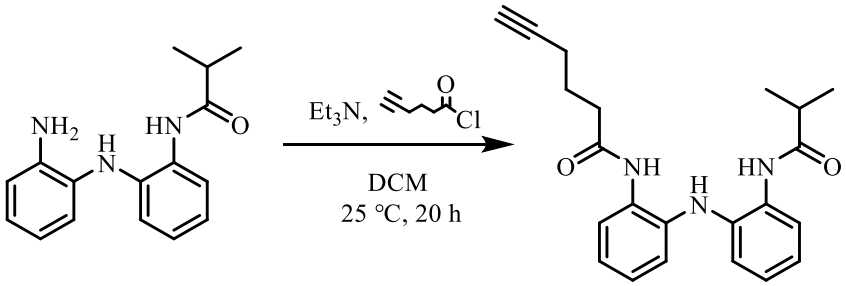

Scheme 3-15. Synthesis of $H_3L^{ipr}L^{alkyne}$.

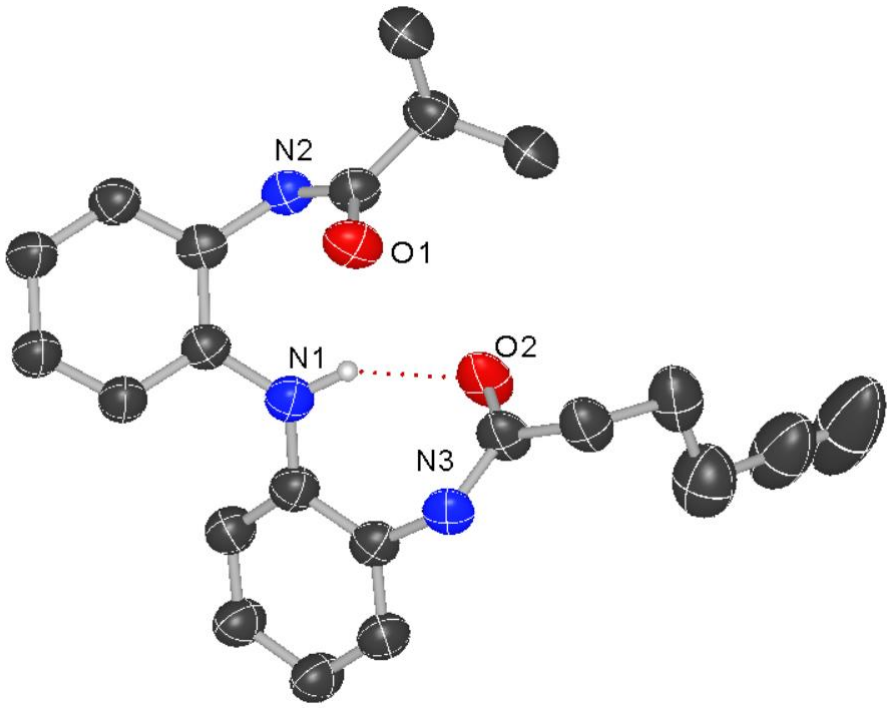

Figure 3-5. Solid-state structure of $H_3L^{ipr}L^{alkyne}$ as determined by single X-ray crystallography. Most hydrogen atoms are omitted for clarity.

The 2,4,6-trisopropyl phenyl group was then proposed as a bulkier amide substituent that could help increase the yield of mono-substituted product (Scheme 3-16). The mono-substituted product with 2,4,6-trisopropyl phenyl group was purified by column chromatography with 9:1 hexane:ethyl acetate as eluent in a yield of 44%.

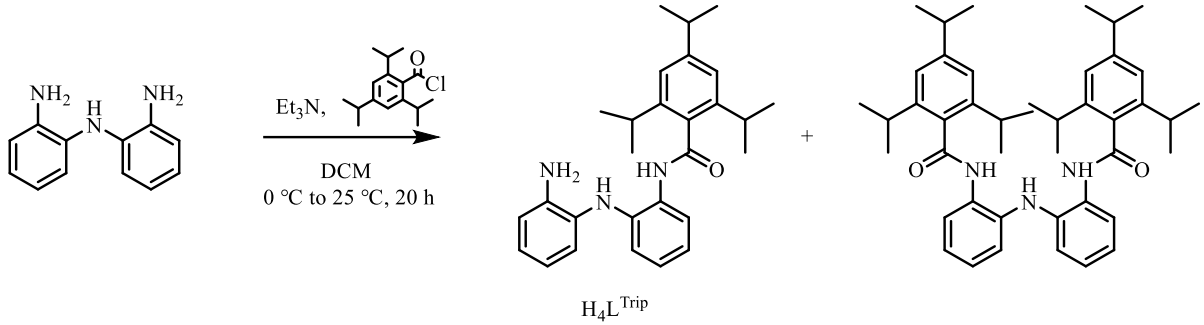

H_4L^{Trip}

Scheme 3-16. Synthesis of ligand H_4L^{Trip}.

Since the H_4L^{Trip} ligand is more sterically hindered for the second substitution, excess amount of base (2.5 equiv.) and acyl chloride (1.2 equiv.) was required for a full consumption of starting material H_4L^{Trip} ligand during the second acylation reaction (Scheme 3-17).

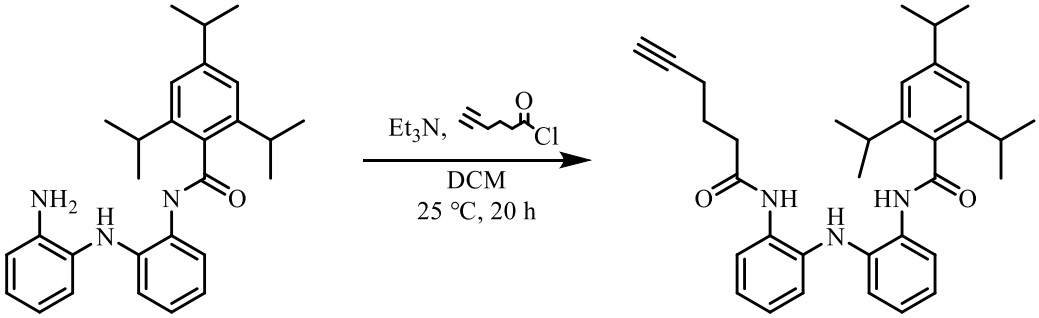

Scheme 3-17. Synthesis of $H_3L^{Trip}L^{alkyne}$.

A crystal of the ligand $H_3L^{Trip}L^{alkyne}$ was obtained by slow evaporation in ethanol and methanol solution (Figure 3-6).

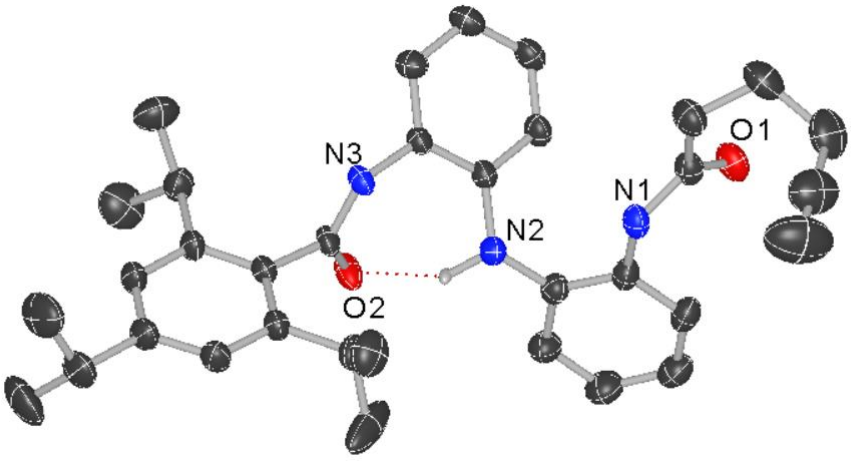

Figure 3-6. Solid-state structure of $H_3L^{Trip}L^{alkyne}$ as determined by single X-ray

crystallography. Most hydrogen atoms are omitted for clarity.

Ligand syntheses–Approach B: Route 4

Since the separation of mono-substituted ligand precursor in route 3 bore the limitations of low yield, small scale, and tedious manual column chromatography, route 4 was proposed where only one primary amine moiety was available for acylation reaction each time, thus eliminating the formation of di-substituted ligands. Ligand precursor N^1-(2-nitrophenyl)benzene-1,2-diamine **3-7** only has one primary amine available for the following acylation reaction. Ligand precursor **3-7** was first synthesized and purified via column chromatography using 94:6 hexane:ethyl acetate eluent with a yield of 57% (Scheme 3-18).

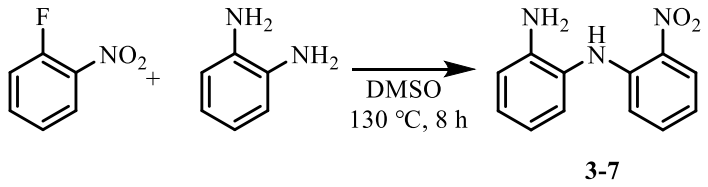

Scheme 3-18. Synthesis of **3-7** N^1-(2-nitrophenyl)benzene-1,2-diamine.

Then the first acylation reaction was carried out by adding base and isobutyryl chloride into the dichloromethane (DCM) solution of **3-7**, affording **3-8** in 98% yield (Scheme 3-19).

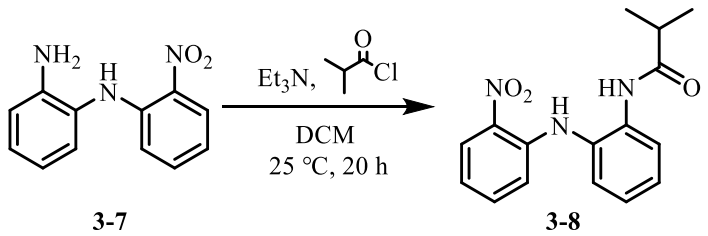

Scheme 3-19. Synthesis of **3-8**.

The nitro group in the ligand precursor **3-8** was then reduced to the primary amine via a Pd/C catalyzed hydrogenation and the resulting product was then used for the second

acylation reaction that installs the terminal alkyne onto the ligand framework (Scheme 3-20). The hydrogeneration afforded **3-9** *N*-(2-((2-aminophenyl)amino)phenyl)isobutyramide product in 92% yield. The following second acylation reaction was carried out by reacting **3-9** with 5-hexynoyl chloride, same as discussed in route 3. These ligands were isolated and fully characterized by ^{1}H NMR, ^{13}C NMR, and mass spectrometry. Detailed procedures and characterization information are described in the experimental section.

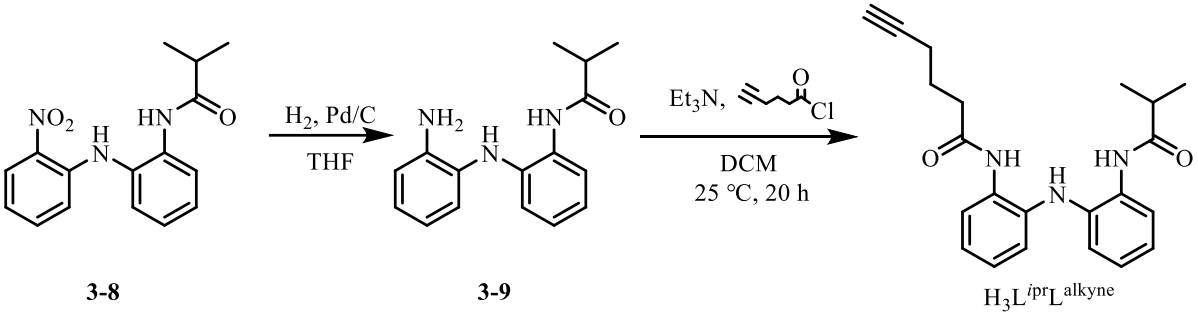

3-8 **3-9** $H_3L^{ipr}L^{alkyne}$

Scheme 3-20. Synthesis of ligand $H_3L^{ipr}L^{alkyne}$ through hydrogenation and second acylation reaction in route 4.

Syntheses of cobalt complexes

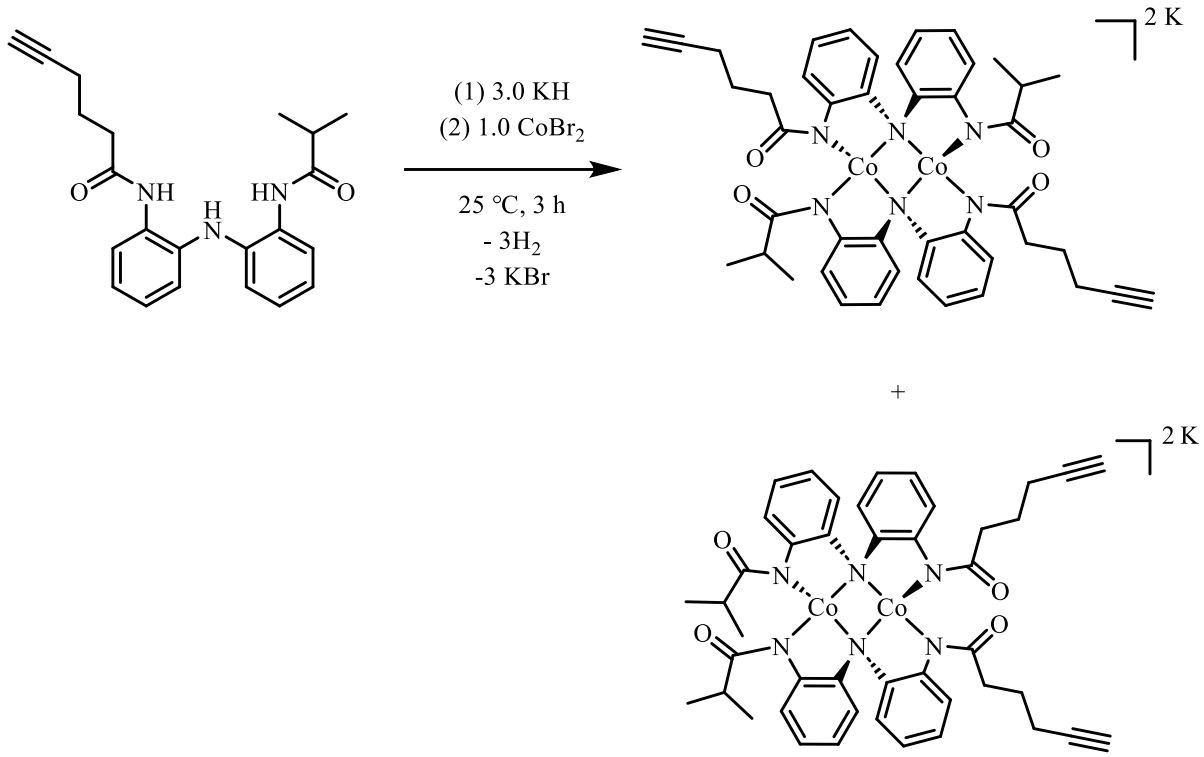

Scheme 3-21. Synthesis of $[Co_2(L^{ipr}L^{alkyne})_2]^{2-}$, $[\mathbf{1}]^{2-}$.

Cobalt dimer complex was synthesized by deprotonating ligand $H_3L^{ipr}L^{alkyne}$ thrice with KH, followed by the addition of cobalt(II) bromide under an inert atmosphere. The deprotonation was stopped when the release of H_2 gas ceased, and then cobalt(II) bromide was added to the reaction. The reaction mixture was left stirring for 3 hours before it was dried under vacuum and redissolved in acetonitrile (MeCN). A filtration was then performed to remove KBr. The resulting filtrate was dried under vacuum and used for recrystallization. Powdered products were obtained and isolated after recrystallization or by washing the dried product with hexane overnight. It is worth mentioning that there are two possible structures for the dimeric cobalt complexes. As shown in Scheme 3-21, the first cobalt complex has two identical Co centers that are each coordinated to one $NPh(COL^{ipr})$, one $NPh(COL^{alkyne})$, and two $N(Ph)_2$ moieties. The second possibility is that two cobalt centers are different where Co1

is coordinated to two NPh(COL^{ipr}) and two $N(Ph)_2$ moieties, while Co2 is coordinated to two NPh(COL^{alkyne}) and two $N(Ph)_2$ moieties. X-ray crystallography studies suggested that the isolated cobalt complexes were of the first structure where two cobalt centers in the complex shared the same chemical environment.

Results and discussions

Mass spectroscopy was applied to the $[\mathbf{1}]^{2-}$ powder isolated from crystallization immediately after it was taken outside of glovebox. The peak with largest intensity in the negative ion spectrum (found *m/z*: 419.11) aligns well with the desired dimeric cobalt complex with a 2 minus charge (*m/z* Calcd: 838.78/2=419.39). A single crystal of $[\mathbf{1}]^{2-}$ suitable for X-ray diffraction was obtained by diffusing diethyl ether into a concentrated acetonitrile solution of $[\mathbf{1}]^{2-}$ in the glovebox (Figure 3-7). The bond lengths and bond angles around the metal centers are shown in Table 3-3.

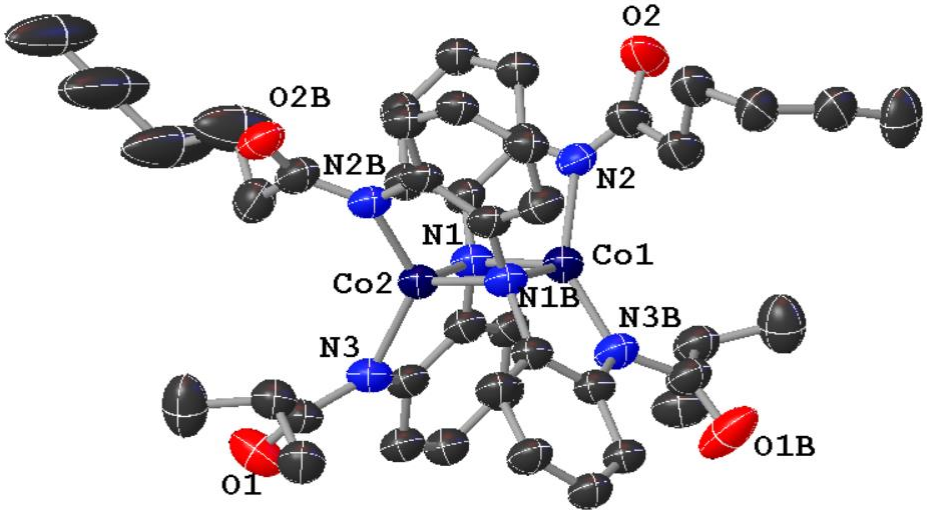

Figure 3-7. Solid-state structure of $(PPh_4)_2[\mathbf{1}]$ as determined by single X-ray crystallography. Hydrogen atoms are omitted for clarity.

Table 3-3. Select bond lengths and bond angles for $(PPh_4)_2$[**1**].

Atom	Atom	length/Å	Atom	Atom	Atom	Angle/°
Co1	N1	1.958	N1	Co1	N3B	130.238
Co1	N1B	2.037	N2	Co1	N3B	130.900
Co1	N2	1.925	N1B	Co1	N3B	81.209
Co1	N3B	2.165	N1	Co1	N2	89.668
Co1	Co2	2.558				

It is worth mentioning that alkyne walking phenomenon was observed when slightly excess of base KH (3.2 equiv) was used in the deprotonation step (Scheme 3-22).[37] The crystal suitable for X-ray diffraction of dimeric cobalt complex with internal alkyne ligand was obtained by diffusing diethyl ether into a concentrated acetonitrile solution of $[Co_2(L^{ipr}L^{internal\text{-}alkyne})_2]^{2-}$, [**3**]$^{2-}$ in the glovebox. The [**3**]$^{2-}$ crystals were able to be obtained with three different countercations as K_2[**3**], $(Et_4N)_2$[**3**] and $(PPh_4)_2$[**3**]. A comparison of Co–Co and Co–N distance is summarized in Table 3-4.

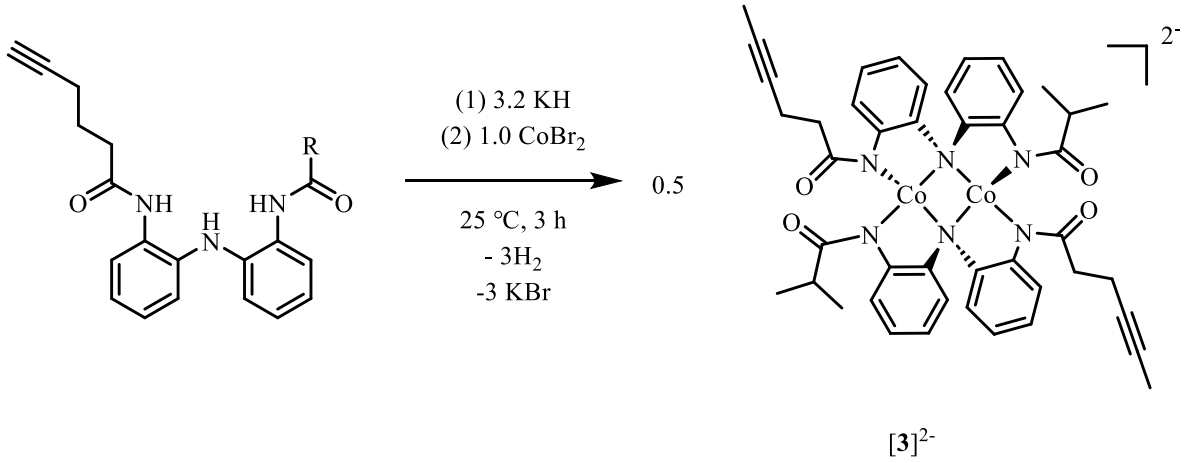

[**3**]$^{2-}$

Scheme 3-22. Formation of $[Co_2(L^{ipr}L^{internal\text{-}alkyne})_2]^{2-}$, [**3**]$^{2-}$.

Table 3-4. Co–Co and Co–N distances in K_2[**3**], $(Et_4N)_2$[**3**] and $(PPh_4)_2$[**3**].

Distance/ Å	K_2[**3**]		$(Et_4N)_2$[**3**]		$(PPh_4)_2$[**3**]	
Co–Co	2.617		2.592		2.610	
$Co–N^{alkyne}$	1.942	1.965	1.976	1.976	1.977	1.963
$Co–N^{iPr}$	1.949	1.954	1.944	1.944	1.972	1.974
$Co–N^{Ph\text{-}Ph}$	2.049	2.045	2.053	2.053	2.064	2.052
	2.025	2.036	2.041	2.041	2.038	2.024

Figure 3-8 shows the C–C bond length of the terminal three carbons on the alkyne chain in ligand $H_3L^{ipr}L^{alkyne}$ itself and cobalt complex $[\mathbf{3}]^{2-}$. Figure 3-8(a) shows the solid-state structure of $H_3L^{ipr}L^{alkyne}$ ligand and the C–C bond distances around the triple bond in the alkyne moiety. The length of C22–C21 bond is 1.207 Å, which is typical for a triple bond. The length of C21–C20 is 1.511 Å, and the length of C20–C19 is 1.504 Å. This confirmed that the alkyne moiety in the synthesized ligand was terminal. However, it rearranged to an internal alkyne after the metalation as shown in Figure 3-8(b). In the cobalt complex $[\mathbf{3}]^{2-}$, the length of terminal C17–C18 bond is 1.456 Å, and C16–C15 bond length is 1.466 Å which are typical for a C–C single bond. Surprisingly, the internal C17–C16 bond is the shortest among all three with the value of 1.179 Å, suggesting an internal triple bond. With the shortest C–C bond being in the middle of the chain, this proves that the terminal alkyne moiety rearranged to internal during the metalation process when excess amount of base existed. The alkyne walking case can be avoided by using exactly 3 equivalents of base KH. Without the excess amount of base, alkyne moiety can remain terminal in the cobalt complexes.

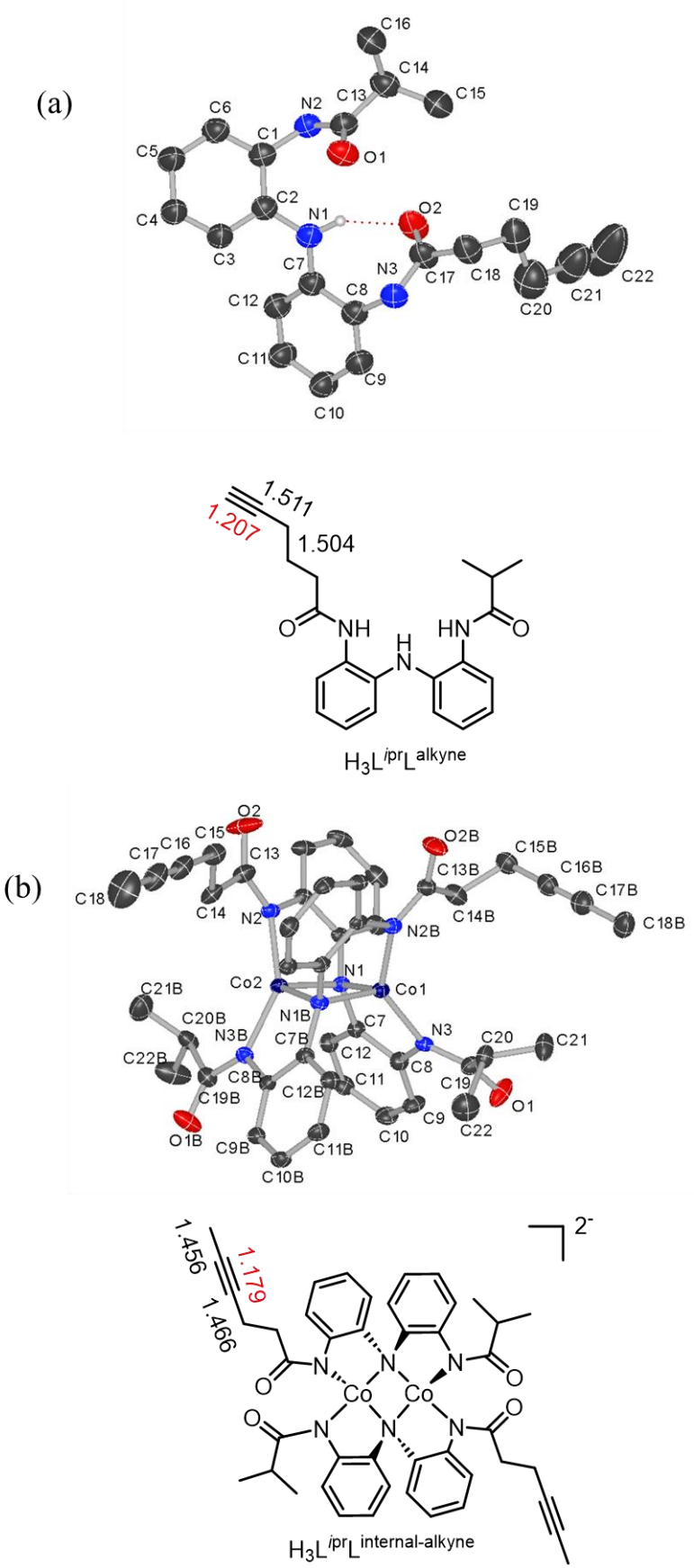

Figure 3-8. Solid-state structures of (a) $H_3L^{ipr}L^{alkyne}$ (b) $[\mathbf{3}]^{2-}$ as determined by single X-ray crystallography and select C–C bond lengths.

After cobalt complexes $[\mathbf{1}]^{2-}$ and $[\mathbf{3}]^{2-}$ were structurally characterized, their electrochemical properties were studied by cyclic voltammetry. Both $[\mathbf{1}]^{2-}$ and $[\mathbf{3}]^{2-}$ showed electron-rich electrochemical profile (Figure 3-9). The cyclic voltammetry studies indicate that these two complexes have the potential to catalyze multi-electron chemical processes, such as catalytic oxidations.

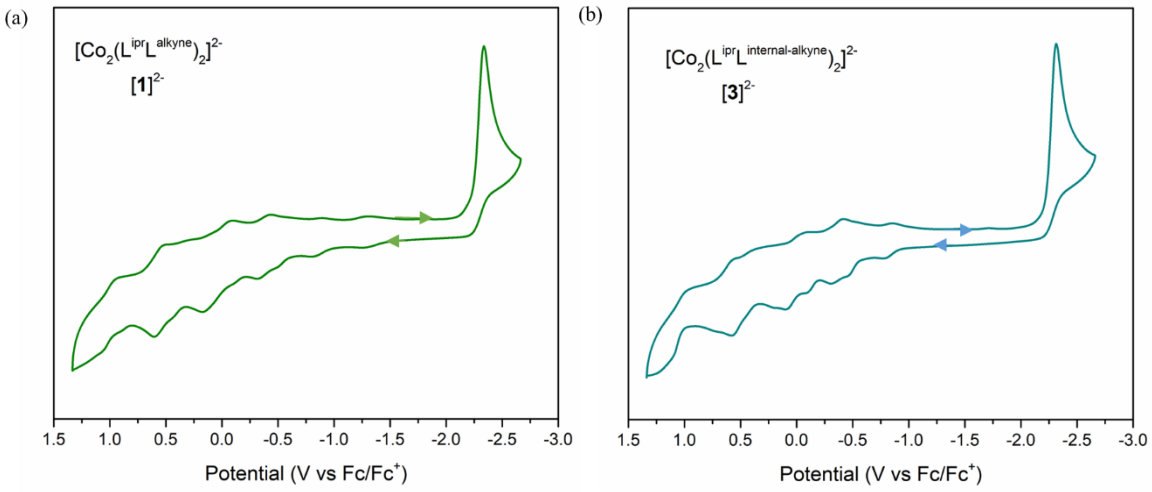

Figure 3-9. Cyclic voltammetry of 0.5 mM (a) $(PPh_4)_2$[**1**] (b) $(PPh_4)_2$[**3**] in 10 mL of 0.1 M $TBAPF_6$ in acetonitrile at v =100 mV/s.

Cyclic voltammetry was also performed on the $H_3L^{ipr}L^{alkyne}$ ligand in acetonitrile, which also showed electron-rich electrochemical profile but with fewer events than cobalt complexes (Figure 3-10). This further demonstrated that electrochemical events could happen between the cobalt metal center and redox-active ligand, and as a result, contributing together to the catalysis of multi-electron reactions.

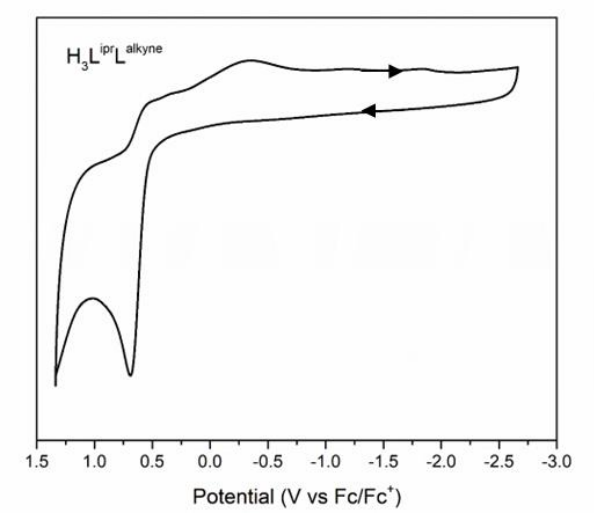

Figure 3-10. Cyclic voltammetry of 1.5 mM $H_3L^{ipr}L^{alkyne}$ in 10 mL of 0.1 M $TBAPF_6$ in acetonitrile at v = 100 mV/s.

Aerobic oxidation

The oxidation of the cobalt complexes by excess amount of dioxygen was monitored by UV-vis spectrometry. Shown in Figure 3-11 is the oxidation of $(PPh_4)_2$[**1**] cobalt dimer complex with terminal alkyne functionalized redox-active ligand by dioxygen. The green trace represents the complex before oxidation, showing two absorptions at 636 nm and 810 nm. Then the excess amount of dioxygen was injected into the cuvette and the reaction was continuously monitored by UV-vis spectroscopy. In the first 40 minutes after being exposed to dioxygen, the intensity of both absorptions kept increasing and reached maximum at the end of the 40 minutes as shown in purple trace. The absorption at 636 nm shifted to 631 nm and a new absorption at 524 nm appeared. The broad absorption at 810 nm shifted to 789 nm 40 minutes after the oxidation. Later, the intensity of the absorptions began to decrease and eventually reached the black trace after an overnight oxidation, which is likely due to decomposition of the cobalt complex.

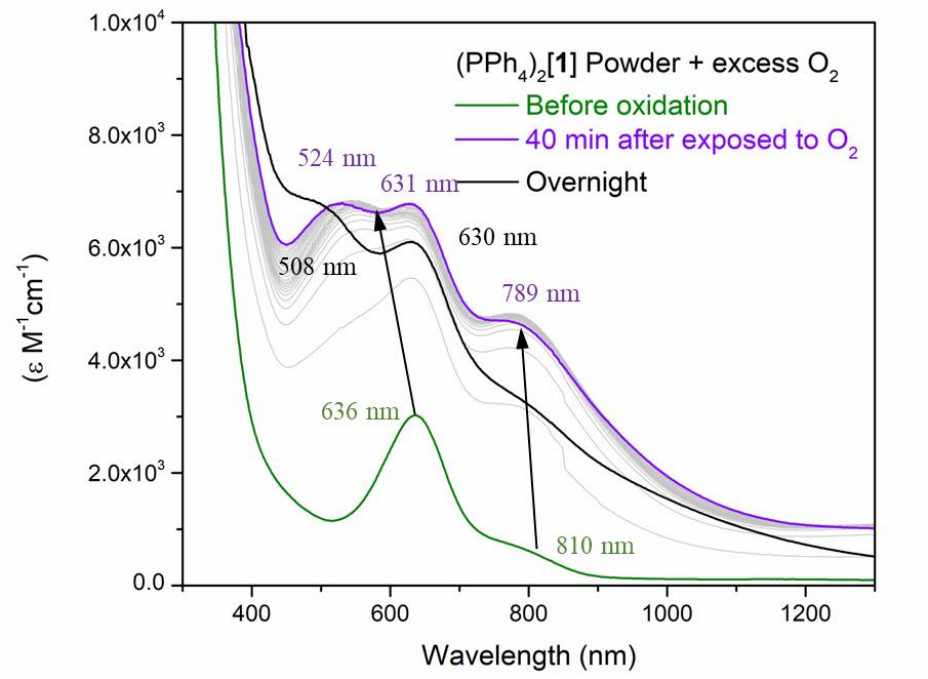

Figure 3-11. Oxidation of $(PPh_4)_2$[**1**] by excess dioxygen monitored by UV-vis spectroscopy in acetonitrile.

A similar aerobic oxidation reaction was performed on [**3**]$^{2-}$, and the result is shown in Figure 3-12. Similarly, there are two absorptions at 611 nm and 926 nm before oxidation as shown in the green trace. With the addition of excess dioxygen to [**3**]$^{2-}$, the intensity of absorptions kept increasing, the wavelength shifted to lower value, and the intensity of absorptions reached maximum 40 minutes after being exposed to dioxygen. The decomposition of cobalt complex was also observed when [**3**]$^{2-}$ was exposed to dioxygen for prolonged time.

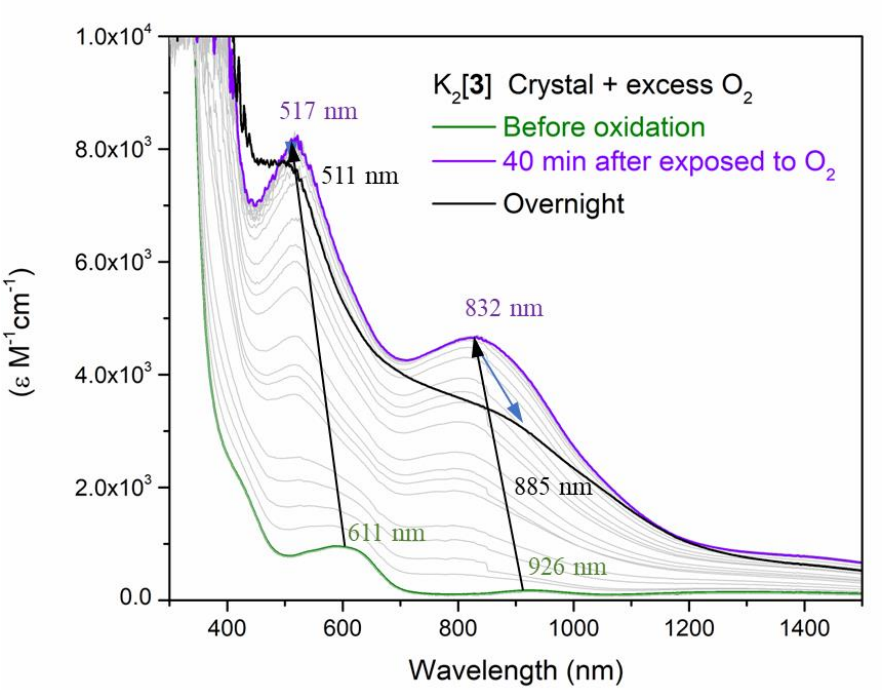

Figure 3-12. Oxidation of K_2[**3**] by excess dioxygen monitored by UV-vis spectroscopy in acetonitrile.

A comparison of using crystal or powder sample K_2[**3**] for the UV-vis study is shown in Figure 3-13. The overall patterns of the spectrum were similar; however, it took longer for the powder sample to finish the oxidation process (60 min vs 40 min), and the intensity of absorptions over the whole spectrum were lower for the powder sample. These indicate that the purity of the powder samples may be lower. Since the powder samples were obtained by washing samples with hexane, the purity issue is likely due to the contamination of some inorganic salt like KBr or organic salt like PPh_4Br or Et_4NBr from the metalation step that was carried to the powdered sample.

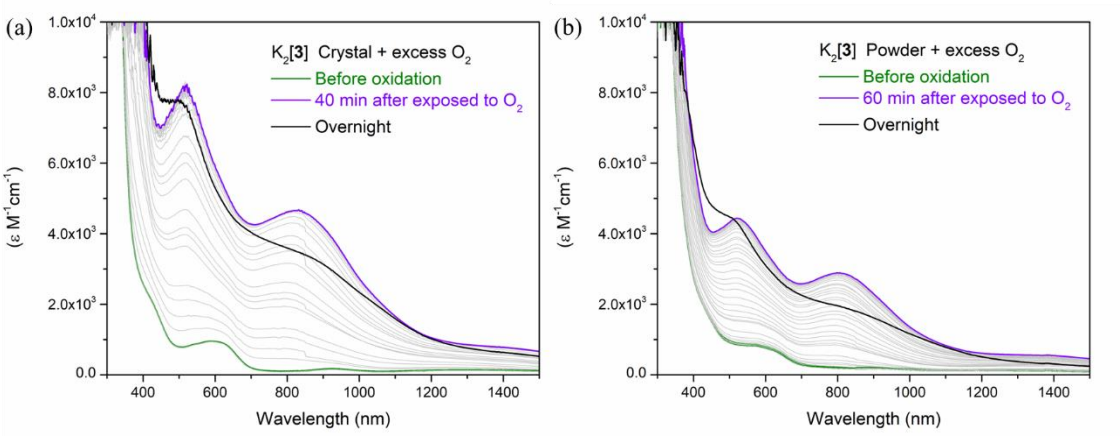

Figure 3-13. A comparison of K_2[**3**] aerobic oxidation between (a) crystal (b) powder sample monitored by UV-vis spectroscopy in acetonitrile.

Catalytic O-atom transfer reaction

To further explore the oxygen activation reactivity of Co complexes supported by terminal alkyne modified redox-active ligands, catalytic O-atom transfer reaction was performed using triphenylphosphine as model substrate, oxygen as terminal oxidant, and 5 mol% of Co complex as catalysts (Scheme 3-23).

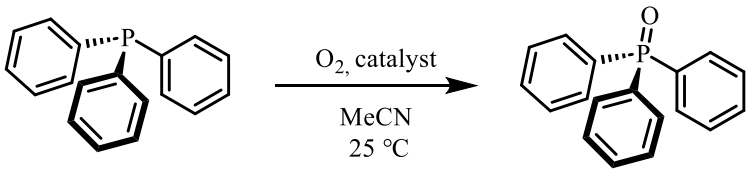

Scheme 3-23. Catalytic O-atom transfer reaction.

As shown in Table 3-5, when 5 mol% of $[PPh_4]_2$[**1**] was used as the catalyst in the reaction of oxidizing triphenyl phosphine into triphenyl phosphine oxide, a yield of 23% was achieved 1 min after mixing the reactants based on ^{31}P NMR. Increasing the reaction time led to a higher yield at a relatively fast increase rate within the first 60 minutes. The yield reached 61% after a reaction time of 60 minutes. Afterwards, the reaction rate slowed down significantly, and the yield was 70% at 2 hour, 72% at 3 hour, 77% at 4 hour and 79% at 5 hour. This slowdown was possibly due to the decomposition of the catalyst as also observed

in the UV-vis studies. $[Co_2(L^{TRIP}L^{hexyne})_2]^{2-}$ $[\mathbf{2}]^{2-}$ and $[Co_2(L^{ipr}L^{internal\text{-}hexyne})_2]^{2-}$ $[\mathbf{3}]^{2-}$ showed less favorable catalytic reactivity towards O-atom transfer reaction with a yield of 25% and 42% after a reaction time of 60 minutes respectively.

Table 3-5. Yield of catalytic O-atom transfer reaction with $[\mathbf{1}]^{2-}$, $[\mathbf{2}]^{2-}$ and $[\mathbf{3}]^{2-}$ as catalysts; triphenylphosphine as model substrate and oxygen as terminal oxidant.

$[PPh_4]_2[\mathbf{1}]$ catalyst								
Reaction Time	1 min	15 min	40 min	60 min	2 h	3 h	4 h	5 h
Yield % $(O)PPh_3$[a]	23%	44%	56%	61%	70%	72%	77%	79%

$K_2[\mathbf{2}]$ catalyst								
Reaction Time	25 min	40 min	60 min	70 min	3 h	6 h	27 h	46 h
Yield % $(O)PPh_3$[a]	13%	23%	25%	27%	38%	48%	66%	72%

$K_2[\mathbf{3}]$ catalyst					
Reaction Time	1 min	30 min	60 min	5 h	21 h
Yield % $(O)PPh_3$[a]	28%	39%	42%	54%	67%

[a] Yield determined by ^{31}P NMR

Aerobic catalytic hydrazone oxidation reaction

In addition to the O-atom transfer reaction, the catalytic reactivity of $[\mathbf{1}]^{2-}$ and $[\mathbf{3}]^{2-}$ was also studied in aerobic catalytic hydrazone oxidation reaction. Oxidation of benzophenone hydrazone to diphenyldiazomethane was chosen as the model reaction due to the commercial availability of the reactant and the relative stability of the product (Scheme 3-24).

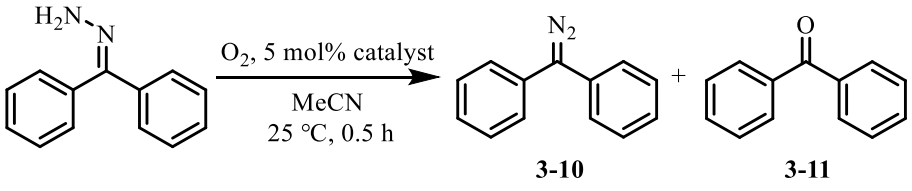

Scheme 3-24. Aerobic catalytic hydrazone oxidation reaction using benzophenone hydrazone.

Studies showed that with 5 mol% of $[\mathbf{1}]^{2-}$ as catalyst, 32% of hydrazone was

converted to diazo product **3-10** after 30-minute reaction time with 65% of starting material recovered. When $[\mathbf{3}]^{2-}$ is used as the catalyst, the yield of diazo product **3-10** after 30-minute reaction time was 40% and the remaining start material was 56%. It is worth mentioning that in both entries, over-oxidized product **3-11** was also observed with a yield that is 10% with respect to the yield of diazo product (Table 3-6).

Table 3-6. Catalytic hydrazone oxidation with $[\mathbf{1}]^{2-}$ or $[\mathbf{3}]^{2-}$ as catalyst, diphenyl hydrazone as substrate and oxygen as the terminal oxidant.

Entry	Catalyst	Yield **3-10**%[a]	Yield **3-11**%[a]	SM%[a]
1	$(PPh_4)_2$**[1]**	32%	3%	65%
2	$(PPh_4)_2$**[3]**	40%	4%	56%

[a] Yield determined by ^{1}H NMR

Conclusions and future directions

In this study, two asymmetric alkyne modified redox-active ligands $H_3L^{ipr}L^{alkyne}$ and $H_3L^{TRIP}L^{alkyne}$ were successfully synthesized and metalated to form the dimeric cobalt(II) complexes $[Co_2(L^{ipr}L^{hexyne})_2]^{2-}$ $[\mathbf{1}]^{2-}$, $[Co_2(L^{TRIP}L^{hexyne})_2]^{2-}$ $[\mathbf{2}]^{2-}$ and $[Co_2(L^{ipr}L^{internal\text{-}hexyne})_2]^{2-}$ $[\mathbf{3}]^{2-}$. The aerobic oxidation of the cobalt complexes was studied by UV-vis spectroscopy, and major change of absorptions were detected within the first 40 minutes of the reaction. Catalytic O-atom transfer and hydrazone oxidation reactions were achieved with the synthesized catalysts in good to moderate yields. The synthetic routes for asymmetric ligands shown in this report could be adapted for other asymmetric ligand systems and provide guidance for future ligand designs. Collaborators can further immobilize these catalysts that are ready with terminal alkyne moiety for heterogeneous catalysis and eventually achieve a reusable, recyclable, and more environmentally benign catalysis.

Experimental section

General considerations

Manipulations under inert atmosphere were carried out using standard Schlenk techniques or conducted in an MBRAUN LabMaster 130 drybox under a nitrogen atmosphere. All reagents used were purchased from commercial vendors and used as received unless otherwise noted. Anhydrous solvents were purchased from Sigma-Aldrich with a Sure/Seal^{TM} bottle or were further purified by sparging with Argon gas followed by passaging through activated alumina columns. NMR experiments were performed on INOVA 400, 500, 600 and Bruker 400, 600 MHz instruments at ambient temperature. Chemical shifts are referenced to the residual solvent. Mass spectra were recorded in the mass spectroscopy center at Emory university on a Thermo LTQ-FTMS mass spectrometer. Infrared spectra were recorded as KBr pellets on a Nicolet iS10 Series FT-IR spectrophotometer. UV-visible absorption spectra were recorded on a Shimadzu UV-3600 (UV-vis/NIR) spectrophotometer using 1.0 cm quartz cuvettes at room temperature. X-ray diffraction studies were carried out in the X-ray crystallography laboratory at Emory university on a XtaLAB Synergy, Dualflex, HyPix diffractometer. Cyclic voltammetry experiments were carried out using a CH instrument (Austin, TX) Model 660C potentiostat. All experiments were conducted in acetonitrile (MeCN) with 0.10 M tetrabutylammonium hexafluorophosphate as the supporting electrolyte. Electrochemical experiments were conducted in a three-component cell consisting of a Pt-wire auxiliary electrode, a non-aqueous reference electrode ($Ag/AgNO_3$), and a glassy-carbon working electrode. All electrochemical measurements are referenced and reported versus the ferrocene/ferrocenium couple.

Ligand syntheses

4-methyl-2-nitro-*N*-(2-nitrophenyl)aniline

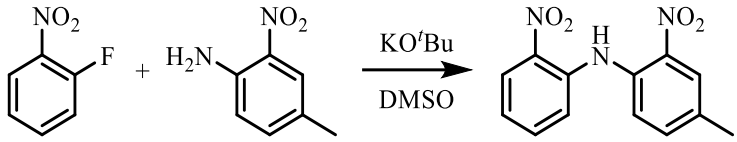

A mixture of 4-methyl-2-nitroaniline (1.5215g, 0.01 mol) and 1-fluoro-2-nitrobenzene (1.05 mL, 0.01 mol) was stirred in dimethyl sulfoxide (DMSO, 20 mL) at 25 ℃. KO^{t}Bu (2.2442 g, 0.02 mol) was slowly added to the reaction, which was stirred at 25 ℃ for 24 hours. The reaction mixture was then quenched with DI water (60 mL) overnight and then filtered to yield a bright orange solid. This bright orange solid was washed with DI water 3 times (3 × 15 mL) followed by ice cold diethyl ether (3 × 15 mL) three times and then dried under vacuum to yield the bright orange powder. (2.4167 g, 88%) ^{1}H NMR (400 MHz, $CDCl_3$) δ: 10.92 (s, 1H, NH), 8.24 (m, 1H, ArH), 8.02 (dd, *J* = 2.1, 1.0 Hz, 1H, ArH), 7.53 (m, 3H, ArH), 7.39 (m, 1H, ArH), 7.05 (ddd, *J* = 8.4, 6.2, 2.2 Hz, 1H, ArH), 2.42 (s, 3H, CH_3). ^{13}C NMR (151 MHz, $CDCl_3$) δ 139.08, 138.09, 137.83, 135.70, 134.89, 134.35, 132.65, 126.80, 126.40, 121.10, 120.62, 119.02, 20.50.

***N*^{1}-(2-aminophenyl)-4-methylbenzene-1,2-diamine**

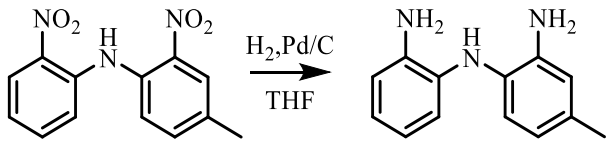

10 wt.% Pd/C (0.6 g) was added to 4-methyl-2-nitro-*N*-(2-nitrophenyl)aniline (2.4167 g, 8.84 mmol) in a THF (150.0 mL) solution. The resulting reaction mixture was placed in a pressure-safe reaction vessel and shaken under H_2 at 50 psi for 1 hour until no more H_2 was consumed. The reaction mixture was then filtered through a pad of celite, and the filtrate was concentrated under vacuum to generate thick, colorless oil. Washing the oil with hexane

yielded the product as a solid. This solid was then filtered and dried under vacuum to yield white powder (1.5227 g, 81%). ^{1}H NMR (400 MHz, $CDCl_3$) δ 6.89–6.81 (m, 2H, ArH), 6.77 (td, *J* = 7.3, 6.8, 2.0 Hz, 1H, ArH), 6.74–6.65 (m, 3H, ArH), 6.60 (dd, *J* = 8.0, 1.9 Hz, 1H, ArH), 3.91 (s, 4H, NH), 2.28 (s, 3H, CH_3). ^{13}C NMR (151 MHz, $CDCl_3$) δ 138.14, 136.09, 133.87, 132.77, 128.13, 122.35, 121.96, 120.90, 120.72, 118.82, 117.61, 117.19, 20.92.

***N*-(2-((2-isobutyramido-4-methylphenyl)amino)phenyl)isobutyramide**

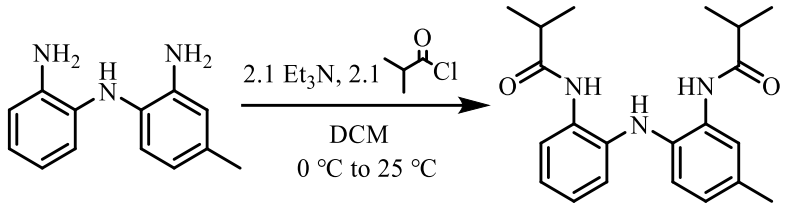

To a dichloromethane (25 mL) solution of N^1-(2-aminophenyl)-4-methylbenzene-1,2-diamine (1.0664g, 5.0 mmol) was added triethylamine (1.0625 g, 10.5 mmol). The solution was then lowered to 0 ℃ followed by an addition of isobutyryl chloride (1.1188g, 10.5 mmol). The reaction mixture was left slowly warmed up to room temperature and stirred for 20 hours. The resulting orange colored solution was extracted with saturated aqueous $NaHCO_3$ (3 × 15 mL) solution and saturated aqueous NaCl solution (1 × 15 mL), dried over $MgSO_4$, and then concentrated under vacuum to yield *N*-(2-((2-isobutyramido-4-methylphenyl)amino)phenyl)isobutyramide as an orange powder. (1.6 g, 91%) ^{1}H NMR (600 MHz, $CDCl_3$) δ 8.10 (s, 1H), 7.84 (s, 1H), 7.74 (s, 1H), 7.48 (dd, *J* = 7.9, 1.5 Hz, 1H), 7.08–7.02 (m, 1H), 6.95–6.87 (m, 3H), 6.76 (dd, *J* = 8.1, 1.4 Hz, 1H), 2.62 (hept, 1H), 2.56 (hept, 1H), 2.32 (s, 3H), 1.21 (d, *J* = 6.9 Hz, 6H), 1.11 (d, *J* = 6.9 Hz, 6H). ^{13}C NMR (151 MHz, $CDCl_3$) δ 176.42, 176.34, 137.69, 134.17, 131.23, 130.96, 127.22, 126.68, 126.11, 124.64, 123.89, 123.12, 121.61, 118.84, 36.02, 35.93, 21.01, 19.64, 19.49. MS-ESI: $C_{21}H_{27}N_3O_2$, *m/z* Calcd. 353.2103, Found: 354.2169$[M+1]^+$.

***N*-(5-bromo-2-((2-isobutyramido-4-methylphenyl)amino)phenyl)isobutyramide**

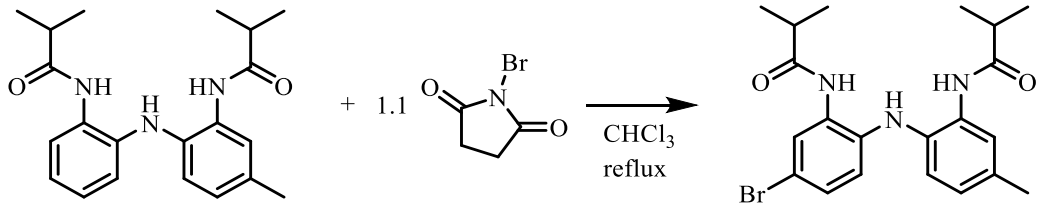

A mixture of *N*-(2-((2-isobutyramido-4-methylphenyl)amino)phenyl)isobutyramide (1.7674 g, 5.0 mmol) and *N*-bromosuccinimide (0.9789 g, 5.5 mmol) was stirred in chloroform ($CHCl_3$, 30 mL) and heated under reflux at 62 ℃ for 24 hours. Dichloromethane (DCM, 30 mL) was added to the resulting dark blue colored solution, and then the solution was extracted with saturated NaCl solution (3 × 50 mL), dried over $MgSO_4$, and then concentrated under vacuum to yield a dark blue oil. The oil was then washed with hexane overnight to afford the grey-blue colored powder. (2.1619 g, 83%) ^{1}H NMR (600 MHz, $CDCl_3$) δ 7.95 (d, *J* = 10.7 Hz, 2H), 7.81 (s, 1H), 7.58 (s, 1H), 7.14 (dd, *J* = 8.6, 2.3 Hz, 1H), 6.89 (dd, *J* = 8.1, 2.0 Hz, 1H), 6.80 (d, *J* = 8.0 Hz, 1H), 6.68 (d, *J* = 8.6 Hz, 1H), 2.66–2.54 (m, 2H), 2.30 (s, 3H), 1.17 (t, *J* = 6.9 Hz, 12H). ^{13}C NMR (151 MHz, $CDCl_3$) δ 176.48, 176.42, 136.06, 133.67, 132.06, 129.89, 129.33, 128.95, 126.91, 126.60, 124.32, 121.97, 121.04, 113.77, 35.99, 35.91, 20.90, 19.57, 19.52. MS-ESI: $C_{21}H_{26}BrN_3O_2$, *m/z* Calcd. 431.1208 (100%), 433.1188 (97.3%), Found: 430.1139 (99%), 432.1117 (100%) $[M-1]^-$.

***N*-(2-((2-aminophenyl)amino)phenyl)isobutyramide**

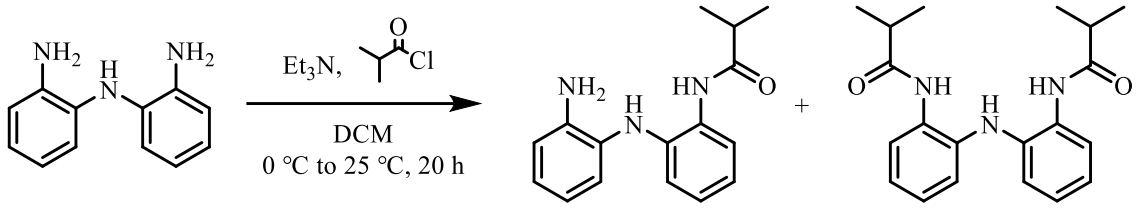

To a dichloromethane (5 mL) solution of bis(2-aminophenyl)amine (199.0 mg, 1.0

mmol) was added triethylamine (116.2 mg, 1.15 mmol). The reaction mixture was stirred at room temperature for 30 minutes. Then the solution was placed in an ice bath, and the temperature was lowered to 0 ℃ before isobutyryl chloride (122.4 mg, 1.15 mmol) was slowly added into the reaction. The reaction mixture was slowly warmed to room temperature and stirred for an additional 20 hours. The resulting burgundy colored solution was extracted with saturated $NaHCO_3$ (3 × 10 mL) solution, saturated NaCl solution (2 × 10 mL) and DI water (1 × 10 mL), dried over $MgSO_4$, concentrated under vacuum, and purified through silica gel chromatography (EtOAc/Hexane 1:3) to give the product *N*-(2-((2-aminophenyl)amino)phenyl)isobutyramide as a white powder. (40.4 mg, 15% yield). ^{1}H NMR (400 MHz, $CDCl_3$) δ 7.53 (d, 2H), 7.37 (s, 1H), 7.10 (t, 1H), 6.97 (m, 2H), 6.90 (d, 1H), 6.82 (m, 2H), 6.75 (d, 1H), 5.52 (s, 1H), 3.83 (s, 2H), 2.54 (septet, 1H), 1.22 (d, 6H). ^{13}C NMR (151 MHz, $CDCl_3$) δ 175.98, 140.14, 137.92, 129.33, 126.91, 126.63, 124.80, 124.32, 123.13, 121.35, 119.27, 118.43, 116.33, 36.26, 19.64.

Hex-5-ynoyl chloride

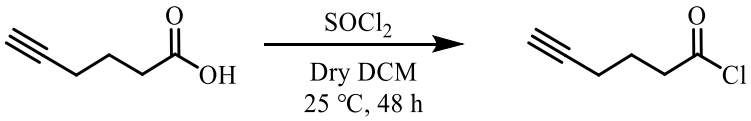

Dry dichloromethane (DCM, 5 mL) was transferred into a 25 mL round bottom flask in the glovebox under nitrogen atmosphere. The round bottom flask was charged with a stir bar and sealed with a septum with electrical tape around the neck before it was taken outside of the glovebox. Then 5-hexynoic acid (0.5 g, 0.5 mL, 4.45 mmol) was injected into the round bottom flask by a syringe followed by addition of thionyl chloride (2.7 g, 1.7 mL, 23.4 mmol) through another syringe. The round bottom flask was then charged with a nitrogen

balloon, and the reaction was left stirred for 48 hours. Afterwards, the excess amount of thionyl and solvent was removed under vacuum with a base trap filled with K_2CO_3. Product 5-hexynoyl chloride was isolated as a light-yellow colored liquid. (0.58 g, 100% yield) ^{1}H NMR (400 MHz, $CDCl_3$) δ 3.08 (t, *J* = 7.2 Hz, 2H), 2.32 (td, *J* = 6.8, 2.7 Hz, 2H), 2.04 (t, *J* = 2.7 Hz, 1H), 1.93 (p, *J* = 7.0 Hz, 2H). ^{13}C NMR (151 MHz, $CDCl_3$) δ 173.41, 82.17, 70.00, 45.55, 23.62, 17.20.

$H_3L^{ipr}L^{alkyne}$ *N*-(2-((2-isobutyramidophenyl)amino)phenyl)hex-5-ynamide

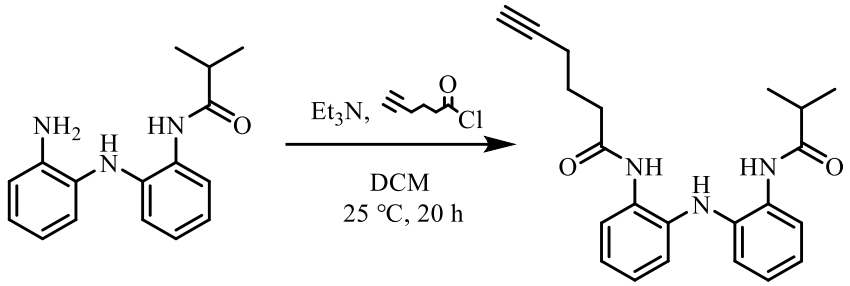

To a dichloromethane (20 mL) solution of *N*-(2-((2-aminophenyl)amino)phenyl)isobutyramide (100.0 mg, 0.3573 mmol) was added triethylamine (36.16 mg, 0.3573 mmol). The reaction mixture was stirred at room temperature for 30 minutes. Then the solution was placed in an ice bath, and the temperature was lowered to 0 ℃ before 5-hexynoyl chloride (46.7 mg, 0.3573 mmol) was slowly added into the reaction. The reaction mixture was slowly warmed to room temperature and stirred for an additional 20 hours. The resulting light-yellow colored solution was extracted with saturated $NaHCO_3$ (3 × 15 mL) solution, saturated NaCl solution (1 × 15 mL) and DI water (1 × 15 mL), dried over $MgSO_4$, concentrated under vacuum, and yielded the product as off-white powder. (121.9 mg, 94%) ^{1}H NMR (600 MHz, $CDCl_3$) δ 7.87 (s, 1H), 7.73 (s, 1H), 7.68 (dd, *J* = 7.8, 2.6 Hz, 2H), 7.10 (tt, *J* = 7.9, 2.2 Hz, 2H), 7.04 (t, *J* = 7.6 Hz, 2H), 6.91 (d, *J* = 7.9 Hz, 2H), 2.62–2.56 (m, 1H), 2.54 (t, *J* = 7.3 Hz, 2H), 2.27 (tdd, *J* = 6.9, 2.7, 0.8 Hz,

2H), 2.00–1.96 (m, 1H), 1.89 (p, *J* = 7.1 Hz, 2H), 1.17 (d, *J* = 6. 9Hz, 6H). ^{13}C NMR (151 MHz, $CDCl_3$) δ 176.20, 171.55, 135.86, 128.98, 126.31, 126.22, 124.14, 124.09, 122.92, 121.14, 120.85, 83.55, 69.24, 36.05, 35.51, 24.04, 19.55, 17.84.

***N*-(2-((2-aminophenyl)amino)phenyl)-2,4,6-triisopropylbenzamide**

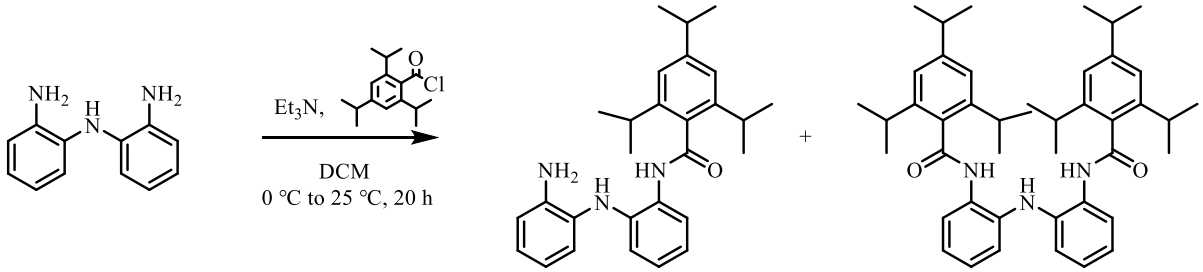

To a dichloromethane (25 mL) solution of bis(2-aminophenyl)amine (797.0 mg, 4.0 mmol) was added triethylamine (526.2 mg, 5.2 mmol). The reaction mixture was stirred at room temperature for 30 minutes. Then the solution was placed in an ice bath and the temperature was lowered to 0 ℃ before 2,4,6-triisopropylbenzoyl chloride (1387.4 mg, 5.2 mmol) was slowly added into the reaction. The reaction mixture was slowly warmed to room temperature and stirred for an additional 20 hours. The resulting solution was extracted with saturated $NaHCO_3$ (3 × 15 mL) solution, saturated NaCl solution (2 × 15 mL) and DI water (1 × 15 mL), dried over $MgSO_4$, concentrated under vacuum, and purified through silica gel chromatography (EtOAc/Hexane 1:9) to give *N*-(2-((2-aminophenyl)amino)phenyl)-2,4,6-triisopropylbenzamide as white powder. (752.9 mg, 44%). ^{1}H NMR (600 MHz, $CDCl_3$) δ 7.60 (s, 1H), 7.57 (dd, *J* = 7.9, 1.5 Hz, 1H), 7.28 (s, 1H), 7.15 (td, *J* = 7.7, 1.5 Hz, 1H), 7.03–6.94 (m, 3H), 6.89 (dd, *J* = 8.1, 1.4 Hz, 1H), 6.82 (dd, *J* = 7.9, 1.4 Hz, 1H), 6.78 (td, *J* = 7.6, 1.4 Hz, 1H), 5.83 (s, 1H), 3.16 (hept, *J* = 6.8 Hz, 2H), 2.93 (hept, *J* = 6.9 Hz, 1H), 1.28 (dd, *J* = 6.9, 2.3 Hz, 18H). ^{13}C NMR (151 MHz, $CDCl_3$) δ 170.11, 150.36, 145.04, 138.46, 133.07, 129.74, 127.12, 126.96, 124.64, 124.19, 123.08, 121.38, 121.17, 119.44, 118.65, 116.54,

34.46, 31.29, 24.63, 24.44, 23.99.

_N_-(2-((2-(hex-5-ynamido)phenyl)amino)phenyl)-2,4,6-triisopropylbenzamide

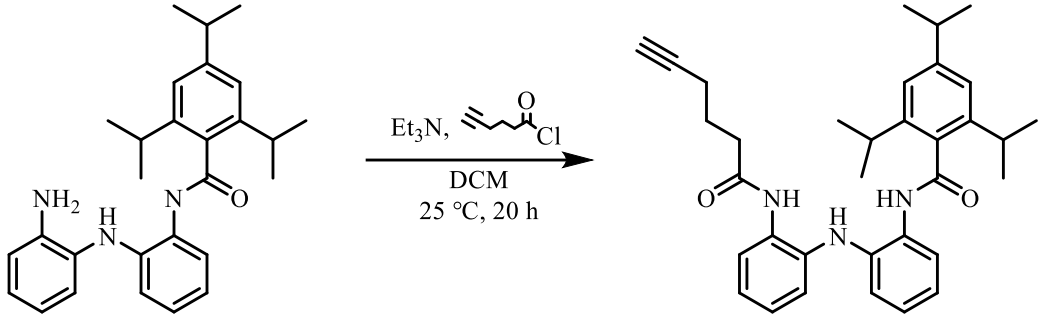

To a dichloromethane (20 mL) solution of *N*-(2-((2-aminophenyl)amino)phenyl)-2,4,6-triisopropylbenzamide (100.0 mg, 0.2328 mmol) was added triethylamine (58.9 mg, 0. 5820 mmol). The reaction mixture was stirred at room temperature for 30 minutes before 5-hexynoyl chloride (36.5 mg, 0.2794 mmol) was added into the reaction. The reaction mixture was stirred for an additional 20 hours. The resulting solution was extracted with saturated $NaHCO_3$ (3 × 15 mL) solution, saturated NaCl solution (1 × 15 mL) and DI water (1 × 15 mL), dried over $MgSO_4$, concentrated, dried under vacuum, and yielded the product as off-white powder (111.3 mg, 91%). ^{1}H NMR (400 MHz, $CDCl_3$) δ 8.06 (s, 1H), 8.02–7.95 (m, 1H), 7.74 (s, 1H), 7.56–7.49 (m, 1H), 7.20–7.08 (m, 3H), 7.08–6.99 (m, 4H), 6.86 (d, *J* = 8.1 Hz, 1H), 6.04 (s, 1H), 3.09 (h, *J* = 6.8 Hz, 2H), 2.94 (dq, *J* = 13.8, 6.7 Hz, 1H), 2.46 (t, *J* = 7.4 Hz, 2H), 2.16 (td, *J* = 7.0, 2.7 Hz, 2H), 1.86 – 1.81 (m, 1H), 1.77 (q, *J* = 7.2 Hz, 2H), 1.27 (dd, *J* = 6.9, 5.3 Hz, 18H). ^{13}C NMR (151 MHz, $CDCl_3$) δ 171.33, 170.17, 150.44, 144.99, 138.33, 133.75, 132.93, 131.34, 127.39, 127.31, 125.33, 124.43, 124.11, 123.51, 123.09, 122.06, 121.15, 119.26, 83.53, 68.99, 35.75, 34.44, 31.39, 24.66, 24.25, 24.08, 23.98, 17.77.

N^1-(2-nitrophenyl)benzene-1,2-diamine

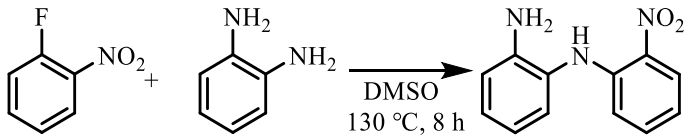

A reaction mixture of 1-fluoro-2-nitrobenzene (776 mg, 5.5 mmol) and 1,2-diaminobenzene (542 mg, 5 mmol) in DMSO (10 mL) was stirred at 130 ℃ for 8 hours. After cooling to room temperature, it was quenched with H_2O (10 mL) and extracted with ethyl acetate (EtOAc) (3 × 20 mL). The combined organic layer was washed with saturated NaCl solution (3 × 10 mL), dried over anhydrous Mg_2SO_4, concentrated, and purified through silica gel chromatography (EtOAc/hexane 6:94) to give N^1-(2-nitrophenyl)benzene-1,2-diamine as a bright orange solid. (652.4 mg, 57%) ^{1}H NMR (400 MHz, $CDCl_3$) δ 9.10 (s, 1H), 8.28–8.22 (m, 1H), 7.37 (dddd, *J* = 8.5, 7.1, 1.6, 0.6 Hz, 1H), 7.23–7.13 (m, 2H), 6.92–6.72 (m, 4H). ^{13}C NMR (151 MHz, $CDCl_3$) δ 144.16, 143.42, 136.04, 132.80, 128.51, 128.39, 126.55, 123.64, 119.11, 117.15, 116.26, 116.15. MS-ESI: $C_{12}H_{11}N_3O_2$ *m/z* Calcd: 229.0851, Found: 228.08 $[M-1]^-$.

***N*-(2-((2-nitrophenyl)amino)phenyl)isobutyramide**

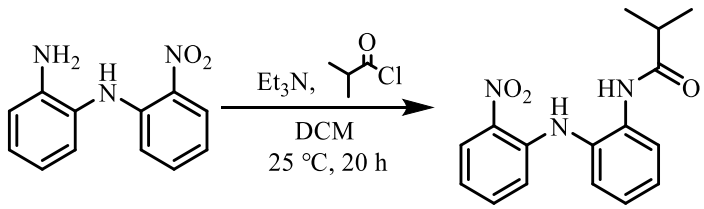

To a dichloromethane (20 mL) solution of N^1-(2-nitrophenyl)benzene-1,2-diamine (411.4 mg, 1.8 mmol) was added triethylamine (181.6 mg, 1.8 mmol). The reaction mixture was stirred under room temperature for 30 minutes before isobutyryl chloride (191.2 mg, 1.8 mmol) was added to the solution and stirred for an additional 20 hours. The resulting orange

colored solution was extracted with saturated $NaHCO_3$ (2 × 20 mL) solution, saturated NaCl solution (2 × 20 mL), and DI water (1 × 10 mL), dried over $MgSO_4$, and then concentrated under vacuum to yield *N*-(2-((2-nitrophenyl)amino)phenyl)isobutyramide as an orange powder (525.6 mg, 98%). ^{1}H NMR (600 MHz, $CDCl_3$) δ 9.10 (s, 1H), 8.29 (d, *J* = 8.2 Hz, 1H), 8.26 (dd, *J* = 8.6, 1.6 Hz, 1H), 7.46 (s, 1H), 7.42–7.34 (m, 2H), 7.21 (td, *J* = 7.6, 1.5 Hz, 1H), 6.85 (ddd, *J* = 8.4, 7.0, 1.3 Hz, 1H), 6.73 (dd, *J* = 8.6, 1.3 Hz, 1H), 2.44 (hept, *J* = 6.9 Hz, 1H), 1.13 (d, *J* = 6.9 Hz, 6H). ^{13}C NMR (151 MHz, $CDCl_3$) δ 175.34, 143.41, 136.18, 134.77, 133.46, 128.21, 127.40, 126.65, 125.12, 122.48, 118.20, 116.18, 36.62, 19.43, 1.03. MS-ESI: $C_{16}H_{17}N_3O_3$ *m/z* Calcd: 299.1270, Found: 298.12 $[M-1]^-$.

_N_-(2-((2-aminophenyl)amino)phenyl)isobutyramide

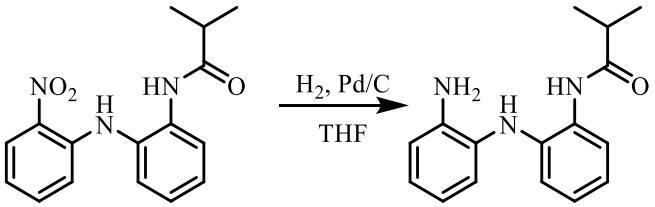

To a THF (10 mL) solution of *N*-(2-((2-nitrophenyl)amino)phenyl)isobutyramide (559.8 mg, 1.87 mmol) was added 5 wt.% Pd/C (52.5 mg, 3 mol%). The reaction mixture was placed in a pressure-safe reaction vessel and shaken under H_2 at 50 psi for 45 minutes. The reaction mixture was filtered through a pad of celite, and the filtrate was concentrated under vacuum to yield a thick, colorless oil. Washing the oil with hexane yielded the product as white powder. (464.5 mg, 92%) ^{1}H NMR (400 MHz, $CDCl_3$): δ 7.53 (d, 2H, ArH), 7.37 (s, 1H, ArNHCOR), 7.10 (t, 1H, ArH), 6.97 (m, 2H, ArH), 6.90 (d, 1H, ArH), 6.82 (m, 2H, ArH), 6.75 (d, 1H, ArH), 5.52 (s, 1H, ArNHAr), 3.83 (s, 2H, NH_2Ar), 2.54 (septet, 1H, Me_2CHCOR), 1.22 (d, 6H, CH_3R). ^{13}C NMR (151 MHz, $CDCl_3$): δ 175.98, 140.14, 137.92, 129.33, 126.91, 126.63, 124.80, 124.32, 123.13, 121.35, 119.27, 118.43, 116.33, 36.26, 19.64.

Catalytic O-atom transfer reaction procedure

In a 25 mL round bottom flask, 0.1 mmol PPh_3 and 0.005 mmol catalyst (5 mol%) was dissolved in 5 mL acetonitrile (MeCN) in the glovebox. Then the round bottom flask was sealed with a septum, and the neck was taped with electrical tape before taking out of the glovebox. The O_2 line was charged with a needle, and O_2 flow was introduced to the reaction mixture by injecting through the septum of the round bottom flask. Another open needle was injected through the septum for ventilation. ^{31}P NMR was performed to determine the yield for triphenylphosphine oxide.

Catalytic hydrazone oxidation reaction procedure

In a 25 mL round bottom flask, 0.1 mmol benzophenone hydrazone and 0.005 mmol catalyst (5 mol%) was dissolved in 5 mL acetonitrile (MeCN) in the glovebox. Then the round bottom flask was sealed with a septum, and the neck was taped with electrical tape before taking out of the glovebox. The O_2 line was charged with a needle, and O_2 flow was introduced to the reaction mixture by injecting through the septum of the round bottom flask. Another open needle was injected through the septum for ventilation. The reaction mixture was left under O_2 flow for 30 minutes. The solvent was then removed under vacuum, and the residue was redissolved in diethyl ether (Et_2O). The diethyl ether solution was filtered through a short plug of silica, and the collected filtrated was dried under vacuum. ^{1}H NMR was performed to determine the yield of diphenyldiazomethane.

References

(1) Kolb, H. C.; Finn, M.; Sharpless, K. B. Click chemistry: diverse chemical function from a few good reactions. *Angewandte Chemie International Edition* **2001**, *40* (11), 2004-2021.

(2) Binder, W. H.; Sachsenhofer, R. 'Click'chemistry in polymer and materials science. *Macromolecular Rapid Communications* **2007**, *28* (1), 15-54.

(3) Davies, H. M.; Morton, D. Recent advances in C–H functionalization. *Journal of Organic Chemistry Research* **2016**, *81* (2), 343-350.

(4) Roudesly, F.; Oble, J.; Poli, G. Metal-catalyzed CH activation/functionalization: The fundamentals. *Journal of Molecular Catalysis A: Chemical* **2017**, *426*, 275-296.

(5) Ferreira, V. F. Synthesis of heterocyclic compounds by carbenoid transfer reactions. *Current Organic Chemistry* **2007**, *11* (2), 177-193.

(6) Gillingham, D.; Fei, N. Catalytic X–H insertion reactions based on carbenoids. *Chemical Society Reviews* **2013**, *42* (12), 4918-4931.

(7) Regitz, M. Diazo compounds: properties and synthesis; *Elsevier*, **2012**.

(8) Singh, G. Reactions of organic nitrogen compounds with carbenoids and diarylketenes from diazoalkanes and diazocarbonyls. *Current Organic Synthesis* **2005**, *2* (3), 377-391.

(9) Ye, T.; McKervey, M. A. Organic synthesis with alpha-diazo carbonyl compounds. *Chemical Reviews* **1994**, *94* (4), 1091-1160.

(10) Doyle, M. P.; McKervey, M. A.; Ye, T. Modern catalytic methods for organic synthesis with diazo compounds: from cyclopropanes to ylides.**1998**.

(11) Davies, H. M.; Manning, J. R. Catalytic C–H functionalization by metal carbenoid and nitrenoid insertion. *Nature* **2008**, *451* (7177), 417-424.

(12) Mix, K. A.; Aronoff, M. R.; Raines, R. T. Diazo compounds: Versatile tools for chemical biology. *ACS Chemical Biology* **2016**, *11* (12), 3233-3244.

(13) Green, S. P.; Wheelhouse, K. M.; Payne, A. D.; Hallett, J. P.; Miller, P. W.; Bull, J. A. Thermal stability and explosive hazard assessment of diazo compounds and diazo transfer reagents. *Organic Process Research & Development* **2020**, *24* (1), 67-84.

(14) Tran, D. N.; Battilocchio, C.; Lou, S.-B.; Hawkins, J. M.; Ley, S. V. Flow chemistry as a discovery tool to access sp^2–sp^3 cross-coupling reactions via diazo compounds. *Chemical Science* **2015**, *6* (2), 1120-1125.

(15) Deadman, B. J.; Collins, S. G.; Maguire, A. R. Taming hazardous chemistry in flow: the continuous processing of diazo and diazonium compounds. *Chemistry–A European Journal* **2015**, *21* (6), 2298-2308.

(16) Curtius, T. Ueber die Einwirkung von salpetriger Säure auf salzsauren Glycocolläther. *Berichte der Deutschen Chemischen Gesellschaft* **1883**, *16* (2), 2230-2231.

(17) Regitz, M.; Menz, F.; Rüter, J. Synthese von α-diazo-carbonylverbindungen durch entformylierende diazogruppenübertragung. *Tetrahedron Letters* **1967**, *8* (8), 739-742.

(18) Baum, J. S.; Shook, D. A.; Davies, H. M.; Smith, H. D. Diazotransfer reactions with *p*-acetamidobenzenesulfonyl azide. *Synthetic communications* **1987**, *17* (14), 1709-1716.

(19) Goddard-Borger, E. D.; Stick, R. V. An efficient, inexpensive, and shelf-stable diazotransfer reagent: Imidazole-1-sulfonyl azide hydrochloride. *Organic Letters* **2011**, *13* (9), 2514-2514.

(20) Ye, H.; Liu, R.; Li, D.; Liu, Y.; Yuan, H.; Guo, W.; Zhou, L.; Cao, X.; Tian, H.; Shen, J. A safe and facile route to imidazole-1-sulfonyl azide as a diazotransfer reagent. *Organic*

Letters **2013**, *15* (1), 18-21.

(21) Holton, T. L.; Schechter, H. Advantageous syntheses of diazo compounds by oxidation of hydrazones with lead tetraacetate in basic environments. *The Journal of Organic Chemistry* **1995**, *60* (15), 4725-4729.

(22) Curtius, T. Ersatz von Ketosauerstoff durch die Azogruppe (N_2). *Berichte der Deutschen Chemischen Gesellschaft* **1889**, *22* (2), 2161-2164.

(23) Andrews, S.; Day, A. P_Ra-mondand MC Whiting. *Organic Synthesis* **1970**, *50*, 27.

(24) Schroeder, W.; Katz, L. The use of silver oxide in the preparation of diaryldiazomethanes. *The Journal of Organic Chemistry* **1954**, *19* (5), 718-720.

(25) Morrison, H.; Danishefsky, S.; Yates, P. Communications-preparation of α-diazo ketones. *The Journal of Organic Chemistry* **1961**, *26* (7), 2617-2618.

(26) Lee, K.-H.; Ko, K.-Y. Catalytic oxidation of benzophenone hydrazone with alumina-supported $KMnO_4$ under oxygen atmosphere. *Bulletin of the Korean Chemical Society* **2006**, *27* (2), 185-186.

(27) Jones, M. B.; MacBeth, C. E. Tripodal phenylamine-based ligands and their Co^{II} complexes. *Inorganic Chemistry* **2007**, *46* (20), 8117-8119.

(28) Corcos, A. R.; Villanueva, O.; Walroth, R. C.; Sharma, S. K.; Bacsa, J.; Lancaster, K. M.; MacBeth, C. E.; Berry, J. F. Oxygen activation by Co(II) and a redox non-innocent ligand: spectroscopic characterization of a radical–Co(II)–superoxide complex with divergent catalytic reactivity. *Journal of the American Chemical Society* **2016**, *138* (6), 1796-1799.

(29) Villanueva, O.; Weldy, N. M.; Blakey, S. B.; MacBeth, C. E. Cobalt catalyzed sp^3 C–H amination utilizing aryl azides. *Chemical Science* **2015**, *6* (11), 6672-6675.

(30) Collins, T. J. Designing ligands for oxidizing complexes. *Accounts of Chemical Research* **1994**, *27* (9), 279-285.

(31) Reynolds, W. R.; Plucinski, P.; Frost, C. G. Robust and reusable supported palladium catalysts for cross-coupling reactions in flow. *Catalysis Science & Technology* **2014**, *4* (4), 948-954.

(32) Pan, S.; Yan, S.; Osako, T.; Uozumi, Y. Batch and continuous-flow Huisgen 1,3-dipolar cycloadditions with an amphiphilic resin-supported triazine-based polyethyleneamine dendrimer copper catalyst. *ACS Sustainable Chemistry & Engineering* **2017**, *5* (11), 10722-10734.

(33) Chen, X.; Jiang, H.; Hou, B.; Gong, W.; Liu, Y.; Cui, Y. Boosting chemical stability, catalytic activity, and enantioselectivity of metal–organic frameworks for batch and flow reactions. *Journal of the American Chemical Society* **2017**, *139* (38), 13476-13482.

(34) Govindarajan, R.; Deolka, S.; Khusnutdinova, J. R. Heterometallic bond activation enabled by unsymmetrical ligand scaffolds: bridging the opposites. *Chemical Science* **2022**, *13* (47), 14008-14031.

(35) Gorvin, J. H. The synthesis of di-and tri-arylamines through halogen displacement by base-activated arylamines: comparison with the Ullmann condensation. *Journal of the Chemical Society, Perkin Transactions 1* **1988**, (6), 1331-1335.

(36) Van Den Broeck, E.; Verbraeken, B.; Dedecker, K.; Cnudde, P.; Vanduyfhuys, L.; Verstraelen, T.; Van Hecke, K.; Jerca, V. V.; Catak, S.; Hoogenboom, R. Cation−π interactions accelerate the living cationic ring-opening polymerization of unsaturated 2-alkyl-2-oxazolines. *Macromolecules* **2020**, *53* (10), 3832-3846.

(37) Liu, X.; Liu, B.; Liu, Q. Migratory hydrogenation of terminal alkynes by base/cobalt relay catalysis. *Angewandte Chemie International Edition* **2020**, *59* (17), 6750-6755.